The Thermohaline Circulation and its Impacts on the European Storm Tracks

Master's Thesis in Meteorology and Climate Physics
by

Juliane Voigt

November 2023

INSTITUTE FOR METEOROLOGY AND CLIMATE RESEARCH
KARLSRUHE INSTITUTE OF TECHNOLOGY (KIT)

Advisor:	Prof. Dr. Joaquim Pinto
Second Advisor:	Prof. Dr. Andreas Fink

Abstract

The Thermohaline Circulation (THC) is an oceanic circulation, important for global heat transport and long-term storage of atmospheric gases and chemicals. With its global extent, the THC can impact the whole planet and regulate its climate system. The circulation has its strongest branch in the Atlantic, which is also the more climate-sensitive part. As a consequence, this thesis will focus on the Atlantic Meridional Overturning Circulation (AMOC) and investigate its characteristics and links to the atmosphere.

Through interconnections, the AMOC can exert an influence on the European storm tracks. A large heat import by the AMOC from the tropics changes the Sea Surface Temperatures (SSTs) and the meridional temperature gradient over the North Atlantic ocean, both of which influence the low-level baroclinicity and the position and strength of the storm track over the North Atlantic and Europe.

Previous studies suggested that a change in the climate will impact the AMOC and alter its characteristics. The expected future warming and increased ice melting will most likely lead to a weakening of the global ocean circulation and reduce its climate mitigation abilities. With a reduced northward heat transport, the lower-troposphere warming over the high latitudes due to polar amplification is locally offset. This effect causes a strengthening of the meridional temperature gradient, while the general atmospheric response to climate change exhibits a weakening in the equator-pole temperature gradient. Under such an AMOC impact, the local low-level baroclinicity in the central mid-latitude North Atlantic is expected to increase, leading to an enhancement and a shift of storm tracks northeastward toward the European continent.

The above-described physical relationship has been examined for historical and future climate scenarios but has not yet been analysed under past climate conditions. Understanding whether this physical relationship also holds in varied climate conditions can be helpful in correctly projecting future changes and gauging the effects of these new climatic conditions.

During paleoclimate periods very specific climate conditions developed, with distinct solar insolations, Greenhouse Gas (GHG) concentrations, and global Surface Air Temperature (SAT). As an example of these past periods, the mid-Holocene and the Last Glacial Maximum (LGM) are analyzed. The LGM was chronologically the first period approximately 21,000 ka BP and during a glacial age in our earth's history. Climatologically the GHG-concentrations were lower and the SAT cooler than our current conditions. Extensive ice sheet over North America and northern Europe modulated the storm track path and the salinity and SST changes had an impact on the AMOC. The other investigated period is the mid-Holocene, a period starting approximately 8 ka BP after solar insolation changes had led to large-scale melting of the LGM ice sheets. This period has similar climate conditions to the pre-industrial times (1850-1880), with similar albeit still slightly lower GHG concentrations and SATs.

Under these different climatic situations, both the AMOC and the storm tracks exhibit different characteristics. The here used model depicts a greater strength during the LGM and a very similar strength of the mid-Holocene compared to the pre-industrial time. Here-found results of the storm tracks suggest that during the LGM a strengthening and southeastward shift.For the mid-Holocene, the current analysis indicates a slight strengthening of the storm track. Altogether, the here plotted climatic conditions and changes to the AMOC and storm tracks are in agreement with other studies, indicating them as a good physical basis to investigate the connection between the oceanic circulation and the European storm tracks during the paleoclimate.

To study the relationship between the two climate components, both a linear regression (for the future period) and a composite analysis were performed. The composite analysis compares the difference of storm track features between weak- and strong-AMOC years, and the result shows a qualitative consistent trend over the central North Atlantic in past, present, and future climates. A weakening of the AMOC led to a strengthening and eastward shift of the storm tracks, an outcome also supported by the linear regression. This result has been found in all four (historical, future under the Shared Socioeconomic Pathway (SSP) 5-8.5, mid-Holocene, and LGM) analyzed time periods and is an indication of the robustness of the relationship between the AMOC and the European storm tracks in the North Atlantic region under contrasting climate conditions.

Zusammenfassung

Die Thermohaline Zirkulation (THC) ist eine ozeanische Zirkulation, die für weltweiten Wärmetransport und die Speicherung von atmosphärischen Gasen und Chemikalien sorgt. Da die THC vier der fünf (Atlantik, Pazifik, Antartik und Indik) Ozeanbecken miteinander verbindet, hat sie einen globalen Einfluss und reguliert das Klima des ganzen Planeten. Der intensivste Zweig der Zirkulation befindet sich im Atlantik, welcher auch am empfindlichsten auf die Änderungen aufgrund des Klimawandels reagiert. Aufgrund dessen konzentriert sich diese Masterarbeit auf die Atlantische Meridionale Durchmischende Zirkulation (Atlantic Meridional Overturning Circulation (AMOC)) und untersucht genauer deren Charakteristiken und ihre Verbindung zur Atmosphäre.

Die verschiedenen Teile des Klimasystems beeinflussen sich gegenseitig und ermöglicht es der AMOC eine Wirkung auf die europäischen Storm Tracks auszuüben. Wärme, die durch die AMOC von den Tropen in die höheren Breiten transportiert wird, erhöht die Oberflächentemperaturen (Sea Surface Temperature (SST)) und ändert den meridionalen Temperaturgradient über dem Nordatlantik. Beide Faktoren sind relevant für die oberflächennahe Baroklinität und beeinflussen die Position und Stärke des Storm Tracks über dem Nordatlantik und Europa.

Vorangehende Studien legen nahe, dass der Klimawandel die AMOC beeinträchtigen wird und sich deren Charakteristiken ändern werden. Die erwartete globale Temperaturerhöhung und die Zunahme der Eisabschmelzung werden sehr wahrscheinlich die Ozeanzirkulation abschwächen und ihren Einfluss auf das Klima reduzieren. Mit einem verringerten Wärmetransport nach Norden wird die starke Erwärmung der nördlichen Gebiete aufgrund der polaren Verstärkung (polar amplification) lokal schwächer. Dieser Effekt führt zu einer Verstärkung des meridionalen Temperaturgradienten, während die globale atmosphärische Reaktion eine Verringerung des Temperaturgradienten zwischen dem Äquator und den Polen aufweist. Aufgrund dieses Einflusses der AMOC nimmt die oberflächennahe Baroklinität im zentralen Nordatlantik der mittleren Breiten zu, was dazu führt, dass der Storm Track sich intensiviert und nach Nordosten Richtung Europa verlagert.

Das beschriebene physikalische Verhältnis wurde bereits für historische Zeiten und verschiedene zukünftige Szenario untersucht, wurde aber bisher noch nicht gründlich für die Paläoklimatologie getestet. Ein besseres Verständnis dafür, ob die Verhältnisse auch für die vergangenen Zeitperioden gültig sind, kann helfen, die Zukunft mit größerer Genauigkeit vorherzusagen und die Effekte der Klimaänderungen besser einschätzen.

Während der paläoklimatologischen Perioden sind sehr spezifischen Klimabedingungen entstanden, mit einer bestimmten solaren Einstrahlung, Treibhausgaskonzentrationen und globale Oberflächentemperaturen. Als Beispiel für diese vergangenen Zeiten werden das Mittelholozän und das letzte glaziale Maximum (Last Glacial Maximum (LGM)) analysiert. Das LGM war chronologisch die frühere Periode, war vor ungefähr 21 000 Jahren und fand während einer glazialen Eiszeit

unserer erdgeschichtlichen Zeit statt. Klimatologisch betrachtet war die Treibhausgaskonzentration niedriger und die Oberflächentemperaturen geringer als heutzutage. Erheblichen Eisschilde über Nordamerika und Nordeuropa veränderten die Bahn der Storm Tracks und Änderungen in der Salinität und den Meeresoberflächentemperaturen beeinflussten die AMOC. Die andere analysierte Zeitperiode ist das Mittelholozän, das vor ungefähr 8 000 Jahren begann, nachdem eine Änderung der solaren Einstrahlung zu einem großskaligen Abschmelzen der Eisschilde des LGM geführt hatten. Diese Periode hatte ähnliche Klimacharakteristiken wie die vor-industrielle Zeit (1850-1880), mit leicht niedrigeren Treibhausgaskonzentrationen und Oberflächentemperaturen.

Aufgrund dieser anderen klimatischen Bedingungen wiesen sowohl die AMOC wie auch die Storm Tracks andere Charakteristiken auf. Das hier verwendete Model hat eine stärkere AMOC während des LGM und eine Zirkulation ähnlich der vorindustriellen Zeit während des Mittelholozän. Erhaltene Befunde des Storm Tracks legen eine Intensivierung und Südwärtsbewegung während des LGM nahe. Für das Mittelholozän deutet die aktuelle Analyse eine leichte Intensivierung der Storm Tracks an. Insgesamt sind die hier dargestellten Klimabedingungen und Änderungen der AMOC und Storm Tracks übereinstimmend mit anderen Studien. Dies deutet darauf hin, dass sie eine gute physikalische Basis sind, um das Verhältnis zwischen der ozeanischen Zirkulation und den europäischen Storm Tracks zu untersuchen.

Um die Verhältnisse zwischen der AMOC und den Storm Tracks untersuchen zu können, wurden eine lineare Regression (nur für die Zukunft) und eine Composite Analyse durchgeführt. Bei einem Composite werden die verschiedenen Storm Track-Eigenschaften zwischen starken und schwachen AMOC Jahren verglichen. Das Ergebnis zeigt einen konsistenten Trend im zentralen Nordatlantik für die Vergangenheit, Gegenwart und Zukunft. Eine Abschwächung der AMOC führt zu einer Intensivierung und Verschiebung Richtung Nordost des Storm Tracks, ein Resultat welches von der linearen Regression bestätigt wird. Diese Änderung wurde bei allen vier analysierten Zeitperioden (historisch, Zukunft unter dem gemeinsam genutzter sozioökonomischer Pfad 5-8.5 (Shared Socioeconomic Pathway (SSP) 5-8.5) Szenario, Mittelholozän und dem letzten glazialen Maximum (LGM)) gefunden.

Contents

List of Figures

List of Tables

Abbreviations

AABW Antarctic Bottom Water

ACC Antarctic Circumpolar Current

AMO Atlantic Multidecadal Oscillation

AMOC Atlantic Meridional Overturning Circulation

AO Artic Ocean

AR Assessment report

CMIP Coupled Model Intercomparison Project

DJF December-January-February

DKRZ Deutsche Klimarechenzentrum

FSIS Fennoscandinavian Ice Sheet

GCM Global Climate Model

GHG Greenhouse Gas

IPCC Intergovernmental Panel on Climate Change

ITCZ Intertropical Convergence Zone

LGM Last Glacial Maximum

LIS Laurentide Ice Sheet

MSLP Mean Sea Level Pressure

NADW North Atlantic Deep Water

NH Northern Hemisphere

NAO North Atlantic oscillation

NAWH North Atlantic Warming Hole

PMIP Paleoclimate Modelling Intercomparison Project

PSU Practical Salinity Unit

RCP Representative Concentration Pathway

SAT Surface Air Temperature

ScenarioMIP Scenario Model Intercomparison Project

SH Southern Hemisphere

SPA Shared Climate Policy Assumption

SPG Subpolar Gyre

SSP Shared Socioeconomic Pathway

SSS Sea Surface Salinity

SST Sea Surface Temperature

STG Subtropical Gyre

THC Thermohaline Circulation

1 Introduction

The global climate system has many subsystems, all interlinked with each other. Oceanic processes for example are influenced by and influence the atmosphere, which is in turn nudged by the ground and the ice cover. Analyzing just one component, while neglecting the entire rest provides an incomplete picture, and potentially important feedback is ignored. It is therefore instrumental to consider multiple pieces of the climate system and investigate their effects on each other. With different predictabilities, understanding the inter-connections can be instrumental in improving the seasonal/inter-annual/inter-decadal predictions and climate projections.

The ocean is an important part of the climate system, storing heat and gases for millions of years and playing a vital part in the global energy distribution (Clark et al., 2002). It is a climate regulator, influencing the more short-lived atmosphere and moderating daily, seasonal, and interannual temperature fluctuations. Differences in surface warming, vertical stratification, and wind forcings lead to diverse types of currents, and circulations at all longitudes, latitudes, and depths. An important circulation in the ocean is the THC, connecting the Arctic with the Antarctic and reaching from the surface levels to the deep ocean, transporting large water volumes through all ocean basins. Sinking in the high latitudes and dense water flowing to the Antarctic at the bottom are balanced by warm and saline surface currents reaching the polar regions (Stouffer et al., 2006).

An effect of this circulation is the balance of the global insolation difference and the warming of polar regions. The THC also affects the sequestering of air and heat in the ocean. Especially the deep water formation (for more information, see 2.2) in the polar regions (**N**, **L**, **W** and **R** in Figure 2.2) is important for the long-term storage of dissolved gases (both anthropogenic and natural greenhouse gases (GHG), (Weaver et al., 1999)), nutrients, and heat (Kostov et al., 2014) in the deep ocean. Additional impacts of the THC are on the marine ecosystem, surface winds, precipitation, evaporation, and soil moisture (Garcia-Soto et al. (2021), Vellinga und Wood (2002)).

As for the impacts in the North Atlantic-European area, the surface currents of the circulation flow through the tropical regions and are heated because of the stronger solar warming. This means that the ocean water transports heat of approximately 1 PW[1] (Hu et al. (2007), Stouffer et al. (2006), Clark et al. (2002)) from the Southern Hemisphere into the Northern part. This leads to a change in Sea Surface Temperature (SST) and air temperature, which can be seen best in the North Atlantic and the climate of Europe. If considering the zonal mean of the near-surface air temperature, then the Atlantic Meridional Overturning Circulation (AMOC) causes a warming of 5 K (see Figure 1.1) over the north-eastern ocean and the northern parts of Europe. Because of the warmer temperatures, there is a decrease in the sea ice extent. This leads to an ice-albedo-feedback resulting in an additional warming of 5 K over parts of the Atlantic Ocean (Rahmstorf, 2006). Therefore, the climate in Europe is milder compared to the rest of the latitudes.

[1] 1 PW = 1 Petawatt = 10^{15} W

The interconnection of the different climate components implicates an impact of the THC on the

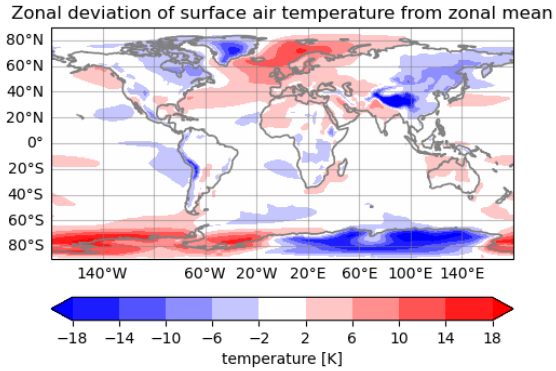

Figure 1.1: Deviation of the surface air temperature from the zonal mean in °C based on Rahmstorf (2006) their Figure 11

atmospheric circulation. Here the focus will be on the oceanic influence on the mid-latitude storm tracks in the North Atlantic. These tracks depict the mean path taken by extratropical cyclones through their respective region. During their lifetime, cyclonic systems are associated with strong wind gusts, heavy precipitation, and storm surges. The passing of a storm influences the air temperature and the cloud cover. For the climate system, cyclones are important as heat, momentum, and moisture transport from the tropics northward and a general mixing of the atmosphere (Priestley et al. (2020), Bengtsson et al. (2006)).

In the last two decades, several strong storms have hit Germany, Kyrill in 2007, and Lothar and Martin in 1999 among the most memorable. In January 2007, Kyrill caused damage of 1 billion € and the storm season in December 1999 created damage of 18.5 billion € (Catto et al., 2011). This shows that cyclones have a great socioeconomic impact and that there is a need for accurate forecasts and characterization.

While the properties of the North Atlantic THC and the storm tracks are mostly well understood under present-day conditions, the consequences of the changing climate are still not fully understood. Additionally, a change in the THC will influence the strength of its connection to the North Atlantic storm tracks, and their detailed development in response to climate change could benefit from further investigation.

A different approach to increase the understanding of climatic impacts on components of the climate system is to investigate the paleoclimate. During these past time periods, the orbital positioning, earth's surface configurations, and atmospheric gas compositions (Ludwig et al., 2016) were very specific and occasionally highly dissimilar to today's climate conditions. The influence of the individual past climates on the THC, storm tracks, and on their relationship has not yet been intensively investigated. Understanding the changes in past climates could provide important insights into their potential variability under different climate conditions, which can benefit future projection studies. This analysis will be performed for the two available paleoclimate periods of the mid-Holocene and the LGM.

The specific goals of this thesis are

- to depict the large-scale climate conditions for the paleoclimate and the future relative to the pre-industrial time,
- to investigate the link between the Thermohaline Circulation and the storm tracks in the future SSP 5-8.5 (SSP5-8.5) scenario, and
- to asses if the relationship is also valid for the paleoclimatic time slices of the mid-Holocene and the LGM.

The thesis continues with the second chapter, containing the fundamental descriptions of the THC and the storm tracks, their link, and the paleoclimatology. Next are the utilized methods, followed by a presentation of the results. The subsequent discussion will put the findings into a larger context and the summary will conclude the thesis.

2 Background Information on the Thermohaline Circulation and the Storm Tracks

This chapter will begin with a description of the global climate system. Next the Thermohaline Circulation and the European storm tracks will be introduced and their connection will be explained. Afterwards, the paleoclimate conditions and the states of the oceanic circulation and the storm tracks will be summarized.

2.1 General Climate System

The climate system consists of five major components all interconnected with each other: the atmosphere, biosphere, hydrosphere, cryosphere, and lithosphere. A representation of the five spheres is shown in Figure 2.1. Observing one subsystem of an individual sphere separately from the others is almost impossible because each element is influenced by multiple others.

- The atmosphere is the fastest sphere with temporal scales down to seconds and minutes. It encompasses the air above the earth's surface and reaches a height of approximately 10,000 kilometers (Society, 2023), containing next to trace gases liquid droplets, and solid particles. In the atmosphere (mostly in the troposphere or the lowest 8-18 km) all the weather regimes like wind, precipitation, clouds, and storms take place. This climate part is, for example, influenced by the lithosphere's ground through friction, and by the hydrosphere with moisture availability. The precipitation from the atmosphere, in turn, affects volcanic eruptions from the lithosphere or creates changes to the cryo- and hydrosphere.

- The biosphere includes the plant life of the earth like trees, flowers, and grass, and can be found on land, as part of the cryosphere in the form of permafrost, or in the ocean as phytoplankton. This widespread implies the dependants of this section, for instance, to atmospheric precipitation and snow cover by the cryosphere. With evapotranspiration, albedo, and friction can this sphere influence the other parts of the climate system. The biosphere has temporal scales from the stomata response time (less than 30 minutes) to the tree growth (hundreds of years).

- The hydrosphere encompasses all bodies of water on our planet like the oceans, lakes, and rivers, and has a larger area than the continents. An important role of the ocean is to store atmospheric heat and gases and regulate continental warming. For the cryosphere, it is a reservoir of water that can be frozen. At the surface, the water exchange can be much more quickly with evaporation and precipitation moving the water from the hydrosphere to the

atmosphere and back respectively. In contrast to this rather quick time scale is the water transport through the deep ocean, which can take thousands of years.

- The cryosphere describes the frozen water in the climate system and applies to the sea ice, glaciers, and permafrost. Because of the solid state of water, this climate component needs low temperatures. Therefore heat transport by the hydro- and atmosphere can lead to ice melting and lithospheric earthquakes can break ice sheets apart. Normally the temporal scale of this climate component is slow, but with fast warming, for example, due to climate change, the ice melting process has been greatly accelerated.

- The final sphere is the lithosphere, encompassing the earth's crust and the upper earth's mantle where earthquakes and volcanic activities originate. Volcanic eruptions release large amounts of ash, gases, and magma into the atmosphere and onto the biosphere. The particles are a basis for cloud droplets, gases like sulfur influence the incoming solar radiation[1], and the magma can both destroy the biosphere but is also responsible for one of the most fertile soils. On a temporal scale, this part of the climate system is very slow with processes taking millions to billions of years.

From all these interacting climate system components, this thesis will focus on the hydrosphere's ocean and the North Atlantic mid-latitudes in the atmosphere.

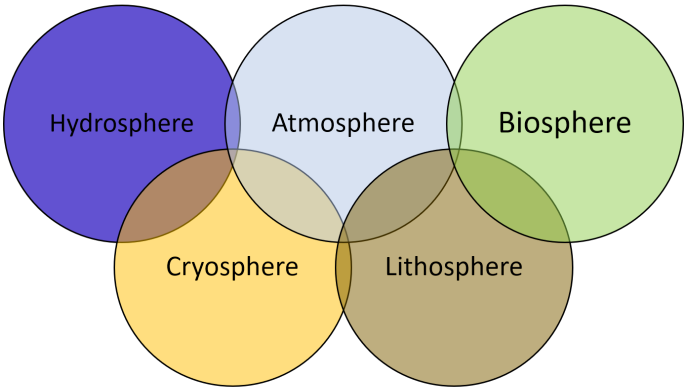

Figure 2.1: Overview over the different subsystems of the climate

2.2 The Thermohaline Circulation

The Thermohaline Circulation (THC) is, as the name suggests, an oceanic circulation driven both by temperature and salinity gradients. It stretches over both hemispheres and has currents in almost all the basins of the ocean.

2.2.1 Path of the Circulation through the Global Ocean

A sketch of this circulation can be found in Figure 2.2 where the red and blue lines depict the path of the currents. The yellow circles show deep water formation regions and are located in

[1] Gas emissions from strong volcanic eruptions can lead to a global cooling of 0.5-1 °C (Disasters, 2021)

the high latitudes of the Northern Hemispheres (NHs) and Southern Hemispheres (SHs) where the densest water can be found. Ocean density is influenced by both salinity and temperature and water becomes denser with a decrease in temperature and an increase in salinity (Rahmstorf, 2003). In the ocean, salinity has a great spatial variance, depicted in the sketch (Figure 2.2), where salty regions with salinity above 36‰ are in green and fresh regions (S < 34‰) colored in blue. The densest waters are in the subtropical regions, linked to the trade winds and evaporation. Fresher ocean waters can be found in the global polar regions, the tropics, and the Oceanic warm pool. These lower salinity values are caused by freshwater run-off from the (Ant-) Arctic ice and rivers in the high latitudes and precipitation by the Intertropical Convergence Zone (ITCZ). Salinity therefore decreases the density in the high and low latitudes, while the density increases in the subtropical regions. The temperature, on the other hand, has its highest values in the tropics and cools down poleward. Since lower temperatures mean denser water, the cold high latitudes create the densest water at the poles. This means that the salinity produces the densest water in the subtropics, the cool temperatures of the high latitudes generate a higher density there. With the conditions of our planet, the temperature effect is stronger, and therefore the dense water formations can be found in the cold and fresher polar areas below the ice-free oceanic surface. These deep water formation regions are located in the Greenland-Norwegian (**N** in Figure 2.2) and the Labrador Sea (**L**) in the NH, and the Ross (**R**) and the Weddell Sea (**W**) in the SH (Rahmstorf, 2006).

After the very dense water is formed in the NH, it convectively sinks down (Wunsch, 2002). This water is then transported through western boundary currents to the Antarctic (Stouffer et al., 2006), which is depicted in Figure 2.2 with the light blue lines for deep water flows. When reaching the Antarctic, the dense water becomes part of the Antarctic Circumpolar Current (**ACC**) which encircles the Antarctic continent. The circulation is (partly or entirely) wind-driven, has a vertical extend from the surface to the bottom, and acts as a natural boundary against warm tropical currents to the southern pole (Barker und Thomas, 2004). The driving atmospheric winds blow clockwise around the Antarctic and are, next to maintaining the ACC, also an important forcing for the THC. These winds create Ekman currents which are directed towards the left[2] of the wind directions, generating ocean surface currents towards the equator and away from the poles. This creates a strong wind-driven upwelling (circles with a point in Figure 2.2), that leads to a resurfacing of the deep ocean currents.

But not all Antarctic bottom water returns to the surface through this upwelling. Another portion of the dense water leaves the ACC as deep or bottom (purple lines in Figure 2.2) water into one of the three big ocean basins (Atlantic, Pacific, and Indian Ocean). In the North Atlantic, the Antarctic Bottom Water (AABW) rejoins the deep currents from the Northern Pole to the Antarctic. The bottom water flowing into the Pacific mostly stays in the deep ocean and returns to the Southern Ocean as deep water. In the Indian Ocean, the dense ocean water experiences mixing-driven upwelling (red circle with a dot in Figure 2.2), bringing the bottom water to the surface. This mixing takes place mostly in the low latitudes where the water is the warmest.

The water can also leave the Antarctic Circumpolar Current (ACC) at the surface. An exemplary path could be water traveling first to the Eastern Pacific then through Oceania to the Indian Ocean,

[2] Because of the SH

where the current merges with the upwelled water from the Indian Ocean. The water flows as a surface current past the Cape of Hope in South Africa as a part of the Agulhas Current. Then the water crosses the southern Atlantic and moves past northern South America as the Brazil current. Next, from the tropical insolation strongly heated water travels along the eastern North American coastline as the Gulf Stream. Afterwards, the warm water flows to Europe and influences the climate there greatly. Finally, the water returns to the northern high latitudes to become once again part of the deep water formation and sink as dense water to the ocean bottom.

This cycle takes multiple thousand years to be completed. In reality, there are of course many different routes a water package can take and it can always leave this circulation due to hard-to-predict small-scale turbulence. Additionally, is the circulation not an enclosed system, but the ocean water experiences mixing with the surrounding water, changing its properties. However, the Figure 2.2 gives a good overview of the main characteristics of the THC and the global span of this circulation.

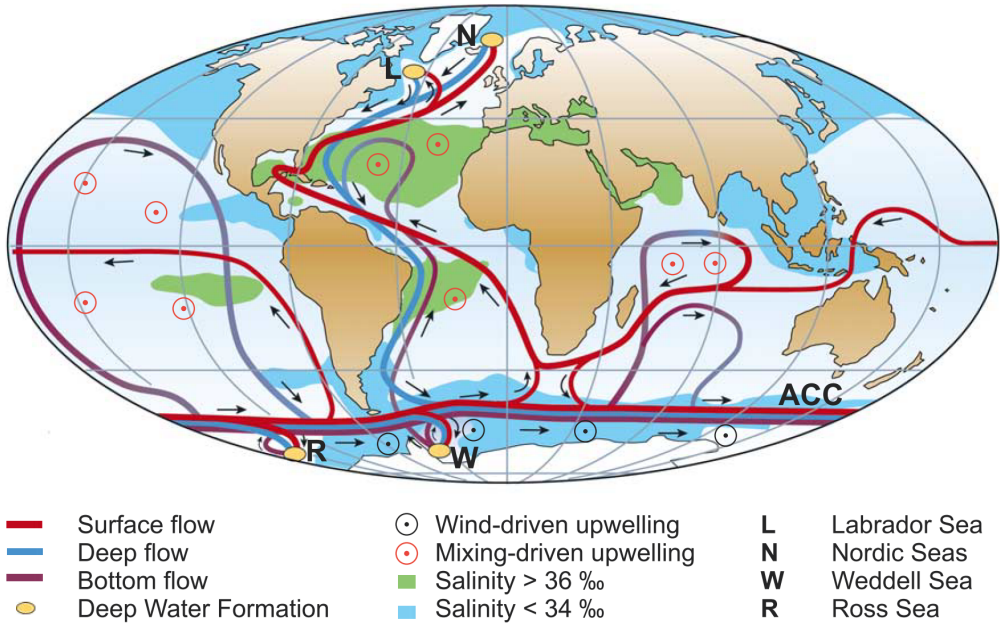

Figure 2.2: Simplified sketch of the path of the Thermohaline Circulation with the abbreviation **ACC** standing for Antarctic Circumpolar Current from Rahmstorf (2006)

2.2.2 Definition of the Thermohaline Circulation

The THC is a long and branched circulation throughout the ocean making reliable observations describing it rather limited. Additionally, the definition poses another problem. Up to this day, there is not one clear definition of the term “Thermohaline Circulation“ but at least seven different ones (Wunsch, 2002) that are used in papers. These describe the THC as:

1. a circulation of mass, heat, and salt,
2. the abyssal circulation,
3. the meridional overturning circulation (MOC) of mass,

4. the net export of chemical substances (e.g. protactinium) by the North Atlantic,
5. a global conveyor belt carrying heat and moisture from low to polar latitudes,
6. a circulation driven by surface buoyancy forcing, and
7. a circulation driven by pressure and/or density differences in the deep ocean.

The first definition is the broadest one while the other definitions are all only partial descriptions of the Figure 2.2. For example, the second, third, and fourth items suggest that the circulation only takes place in parts of the ocean either only at a certain depth (second) or a specific ocean basin (third and fourth), here for instance in the North Atlantic. In addition, the third item omits the zonal component of the circulation, only focusing on the meridional flows. The fifth definition only describes a transport from the tropics to the poles but neglects the cross-equatorial part of this circulation. Finally, the last two descriptions name either surface buoyancy or internal pressure/density differences as the sole driver for the THC. But the circulation, as described by Rahmstorf (2006), has both a surface wind forcing and a thermohaline forcing moving the ocean masses. To sum up, the concept of the thermohaline circulation has no uniform definition.

The reason is that the THC is more of a conceptual idea and is very hard to measure. On the one hand, the vertical motions are too slow to accurately ascertain. On the other hand, the surface currents are a part of the wind-driven horizontal circulation, making it difficult to separate out the THC.

The path of the THC depicted in Figure 2.2 shows that two out of the four deep water formation regions and the largest part of the circulation outside of the Antarctic region can both be found in the North Atlantic Ocean. In the polar Pacific Ocean, virtually no deep water formation is taking place and no vigorous and narrow meridional circulation can be found. Instead, the oceanic circulation reaches only up to 60°N and has a broad and weak flow (Weaver et al., 1999).

There are multiple reasons for the missing deep water formation. For example, the Sea Surface Salinity (SSS) in the Pacific is significantly lower than in the Atlantic (see Figure 2.2), leading to a more stable stratification. The salinity difference is caused by the northward heat transport of the THC resulting in higher Sea Surface Temperature (SST) values in the North Atlantic. These warmer surface waters produce more evaporation and therefore a higher salt content. Because of the existing THC circulation in the Atlantic, more saline waters are transported faster from the subtropics northwards and these waters spend less time in strong-precipitation areas. Instead, the salty waters are transferred directly to the deep water formation regions, where they sink to the deep ocean (Weaver et al., 1999).

The above-mentioned factors all at least partly depend on an existing overturning circulation. Other, independent of the AMOC, elements are the further northward extension of the North Atlantic Ocean, influencing the waters by the cold Arctic Ocean. The smaller east-west width of the Atlantic Ocean makes the waters subject to continental climates, meaning evaporated moisture loss and advection of dry continental air. Additionally, atmospheric water vapor transport takes place from the Atlantic to the Pacific Ocean across the American and Afro-Eurasian continents. This can lead to a total freshwater export of 0.66 Sv in the low latitudes to the east and in the

mid-latitudes to the west (Dey und Döös, 2020). A final difference is the influence of inland seas. These, almost completely enclosed, basins experience stronger warming, and more evaporation and have therefore a greater salinity content. Through outflows, these salty waters influence the salt content of the neighboring oceans. With the Mediterranean and the Gulf of Mexico, the Atlantic is impacted by more saline water mixing from the inland seas.

Not only has the Atlantic THC a greater overturning, but atmospheric temperature changes caused by climate warming are more prominent in higher latitudes. Since the Pacific Ocean reaches only up to 60°N, the greatest SAT and SST changes do not affect the Pacific THC. The Indian Ocean is only in the (sub-) tropical regions, which are less affected by temperature change overall. This means that the THC branches in the Indian and Pacific Oceans are less climate-sensitive (Wang und Mysak, 2000).

Given its predominant role in the entire THC and the potentially high sensitivity to climate change, this thesis will focus on the analysis of the THC in the Northern Atlantic, also known as the AMOC.

2.2.3 Forcing of the Thermohaline Circulation

The oceanic circulation has two main drivers, the turbulent downward mixing of heat and salt (the thermohaline forcing) and wind-created Ekman divergence (wind-driven forcing). Model experiments have shown that both mechanisms are relevant and that a circulation without one would be much weaker (Rahmstorf, 2006).

Thermohaline Forcing

The thermohaline forcing consists of a haline and a thermal part. Higher latitudes receive on average weaker heating than tropical regions and therefore, the thermal circulation at the surface flows from low latitudes into polar regions. The haline part is on the one hand controlled by the freshwater input in high-latitude regions because of river run-off, precipitation, and glacial and ice-sheet melting. On the other hand, the stronger evaporation in lower latitudes creates saline waters there. This means that the haline surface circulation would flow from the polar to the tropical regions, opposite the thermal surface flow. In Earth's oceans, the thermal forcing is stronger and dominates over the haline drive, thus the flow is thermally moved polewards with a haline limiting factor (Clark et al. (2002), Caesar et al. (2021)).

Heating and cooling of the ocean are realized through solar insolation and radiative cooling, both processes taking place only in the upper hundreds of meters if the lower geothermal heating is neglected. This creates a problem, addressed by the Sandström theorem (by Johan Sandström in 1908) (Kuhlbrodt et al., 2007) in regards to the continuation of circulations. If the heating and cooling of a system take place at the same depth, then after approximately 1000 years the densest water would be at the bottom, which would in turn terminate the entire circulation. This prerequisite is fulfilled for this ocean circulation because the thermal heating and cooling only take place at the surface. To avoid a cessation of circulation, the heating of the ocean needs to take place at a greater depth than the cooling to create a stable circulation. This effect can be achieved by turbulent downward mixing of heat.

The case of the sole thermohaline forcing can be seen in the sketch in Figure 2.3 on the left side. Here, deep water formation on the right leads to a sinking of the dense water with the density ρ_1 below the lighter water with ρ_2. The wavy arrow shows the downward mixing of warmer surface waters, creating heating below the surface and cooling in the high latitudes. With this, the thermohaline forcing can partly maintain the THC.

Wind-driven Forcing

Effects of the wind-driven forcing are most clearly evident in the Southern Ocean. The sketch on the right side in Figure 2.3 represents an example of the wind-driven forcing in a latitude-depth cross section (left-right reaching from the Northern to the Southern Pole). In the SH, strong westerly winds flow around the Antarctic continent, denoted by the circle with the dot in the sketch. These near-surface winds create an Ekman spiral in the ocean waters, meaning a divergence of the surface currents towards the tropics[3]. This northward flow leads to an upwelling (the upward arrow in the sketch) to maintain the mass balance. The wind-driven forcing pulls up deep water by moving the surface water toward the tropics. For the THC, the wind-driven forcing is also influenced by tidal forcing, but the wind component is a greater source of energy.

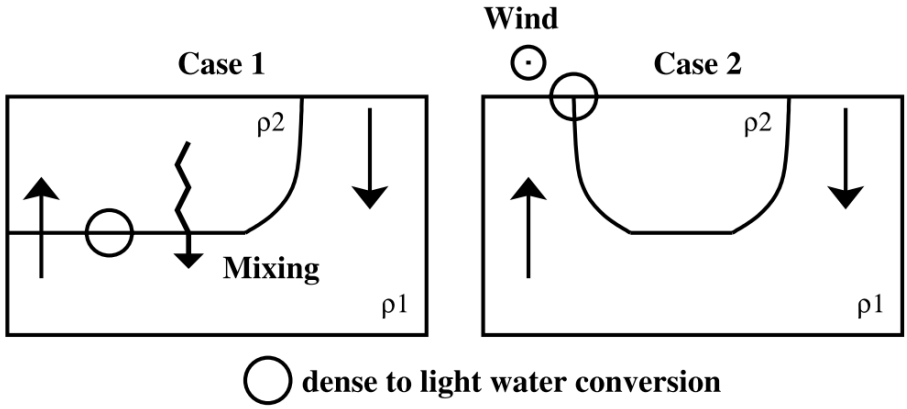

Figure 2.3: Sketch of extreme cases with only thermohaline mixing (case 1 on the left) and only wind-driven upwelling (case 2 on the right). On the right side of each case, the deep water formation takes place, creating the denser water (ρ_1) compared to the lighter water (ρ_2). The line depicts the thermocline[4] separating the differently dense waters from each other. Straight arrows describe volume transports and wavy arrows heat fluxes due to mixing from Rahmstorf (2006)

2.2.4 Projected Impacts by the Climate Change on the Thermohaline Circulation

In historical times, the North Atlantic oceanic circulation transported warm and salty subtropical waters into the high latitudes and exported fresh and cold waters in the deep to the SH (Stouffer et al., 2006). The most current Intergovernmental Panel on Climate Change (IPCC) Assessment report (AR) (AR6) shows a broad probable circulation strength in the Atlantic between 15 to 30 Sv ($1\,\mathrm{Sv} = 10^6\,\mathrm{m^3\,s^{-1}}$) for the historical experiment of the models in Coupled Model Intercomparison Project 6 (Coupled Model Intercomparison Project (CMIP)6) (with a slightly higher spread than

[3] Because in the SH, the Ekman divergence is directed to the left. On the NH, it would be to the right

for the CMIP5) (Fox-Kemper et al., 2021b). In the Antarctic circumpolar currents, the transport has a volume of approximately 15 Sv (Rahmstorf, 2006), meaning a total THC transport of 25 to 45 Sv for the historical period.

In the past, the THC has experienced changes both from natural variability as well as due to climate change. Estimates in the AR6 predicts a likely reduction in the Atlantic part of the circulation by approximately 25 % to 40 % by 2100 depending on the scenario (Fox-Kemper et al., 2021b), but has little confidence in the timing and exact magnitude of the reduction (see Figure 2.4). Such a slowdown is unprecedented in the past thousand years (Caesar et al., 2021).

The low confidence in the prognosis is caused by the difficulties in measuring the THC, the

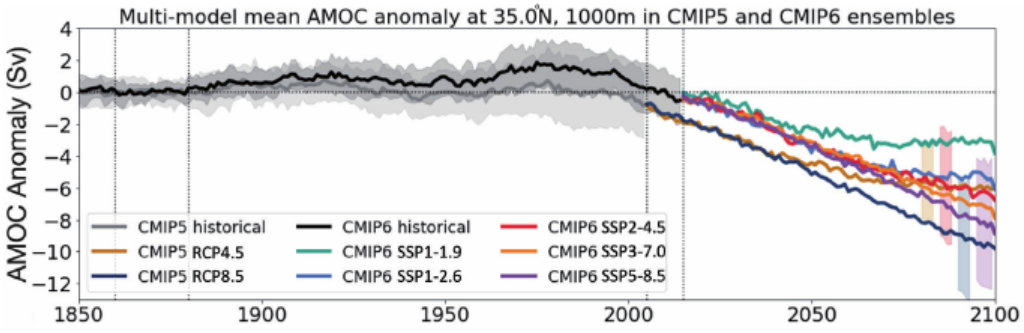

Figure 2.4: Multi-model time series of Atlantic Meridional Overturning Circulation anomaly relative to 1850–1880 at 35°N of CMIP5 and CMIP6 ensembles from Fox-Kemper et al. (2021b)

lack of an available long time series needed for a reliable prediction, and the high uncertainty in models. Two different approaches are generally used to investigate the climate change effect on the oceanic circulation (Stouffer et al., 2006).

One approach to investigating the THC changes in response to global warming is through idealized simulations by adding larger than natural freshwater inputs into the Arctic regions, also called hosing experiments (see Stouffer et al. (2006), Vellinga und Wood (2002), Kuhlbrodt et al. (2009), Woollings et al. (2012)). For these "perturbation experiments" (Stouffer et al., 2006) different freshwater amounts (mostly 0.1 to 1 Sv) are pumped into parts of the ocean (mostly the North Atlantic) over different time periods (usually between 100 and 500 years). This way, it is possible to observe the likely reaction of the ocean circulation to large-scale ice sheets and glacier melting.

The other approach is to analyze Global Climate Model (GCM) simulations under varied GHG-forcings either with those assumed in different SSP scenarios or with prescribed CO_2 forcings (e.g. doubled CO_2 concentration) (Vellinga (2008), Thomas F. Stocker (1997), R. J. Stouffer (2003)). Due to the non-linearity and complex, coupled physics in GCMs, the simulated THC change in the second approach is usually weaker as its response can be affected/counteracted by changes in other components of the model and therefore shows less clear signals of change.

Both methods exert changes in the density of the deep water formation regions in the high latitudes. The hosing experiment means a reduction in the surface density because of the freshwater input. In the SSP scenario, the world experiences a warming resulting in a strong SST increase in the high-latitude NH because of the polar amplification. In addition, there will be an increased

input of freshwater due to the melting of glaciers and ice sheets, both effects leading to a density reduction at the surface in high latitudes. The change in density near the surface results in an increase in vertical stratification in the ocean. Since the THC strongly depends on vertical mixing, freshwater hosing or climate warming both lead to a reduction in circulation strength. The right plots in Figure 2.5 depict vertical cuts of the AMOC during a control and hosed experiment. In the lower plot, the weakened circulation features a reduced depth and an approximately halved overturning strength in the mid-to-high latitudes. In all papers where a realistic freshwater input was used (e.g., Bellomo et al. (2023) and Vellinga und Wood (2002)), the geographical origin of the freshwater pulse is important for the magnitude and duration of AMOC reaction (Clark et al., 2002).

However, there was no permanent collapse of the oceanic circulation reported in any of those studies. The models all showed a (partly strong) reduction of its strength, but the ocean always recovered after the cessation of the freshwater forcing. In the left plot in Figure 2.5, the hosing was terminated after 100 years and almost immediately afterwards, a recovery of strength can be observed. A complete shutdown of the circulation would require a freshwater input of at least 1 Sv which is unrealistic with the current climate projections (Stouffer et al., 2006).

But even a short-term slow-down (for a few hundred years) of the THC can have a large impact on

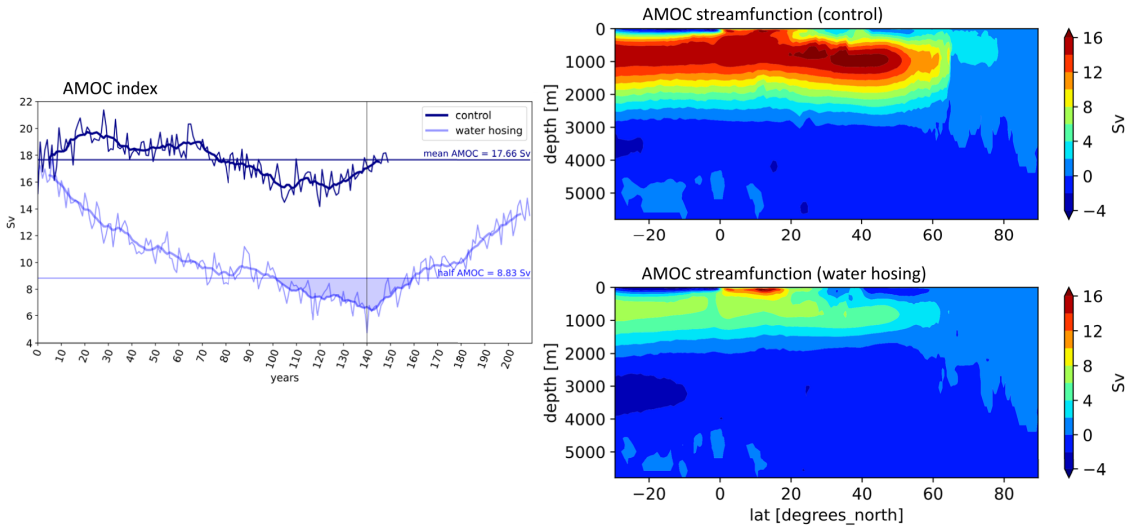

Figure 2.5: Example of the development of the AMOC strength for both a control run (preindustrial conditions of 1850) and a hosing experiment (0.3 Sv added uniformly for 140 years poleward of 50 °N in Atlantic and Arctic Ocean). The dark purple lines show the control experiment and the lighter blue shows the perturbed run. Both time series are superimposed with the 10-year running averages. The two vertical cuts on the right side show the AMOC strength during the control (top) and hosed experiment (bottom) during the grey-shaded time in the left plot from Bellomo et al. (2023)

the global climate. The slowdown of the THC, caused by surface freshening or warming, would weaken global water transport and impact both the ocean and the atmosphere. A consequence for the North Atlantic Ocean would be the reduced northward transport of heat and salinity. Estimates expect a reduction of poleward heat transport in the Atlantic to be almost halved until the end of the century (Fox-Kemper et al., 2021b). The weaker cross-equator heat transport means increasing temperatures in the SH and cooling, especially in the North Atlantic. Figure 2.6 shows

in the left plot the resulting SST changes under strong hosing[5] and depicts the warming of the SH and the cooling in the Northern Atlantic. The strongest reduction takes place near the deep water formation regions in the high latitudes, the prior final location of the warm surface waters. Lower SSTs favor the sea-ice formation and can lead to local SSS increases. However, the reduced northward salinity transport caused by the weakened THC and the increased freshwater input by ice melting have a stronger and more large-scale effect. The right plot in Figure 2.6 depicts the SSS changes under the same forcing as the SST and shows a freshening, especially in the high latitudes in addition to the hosing freshening.

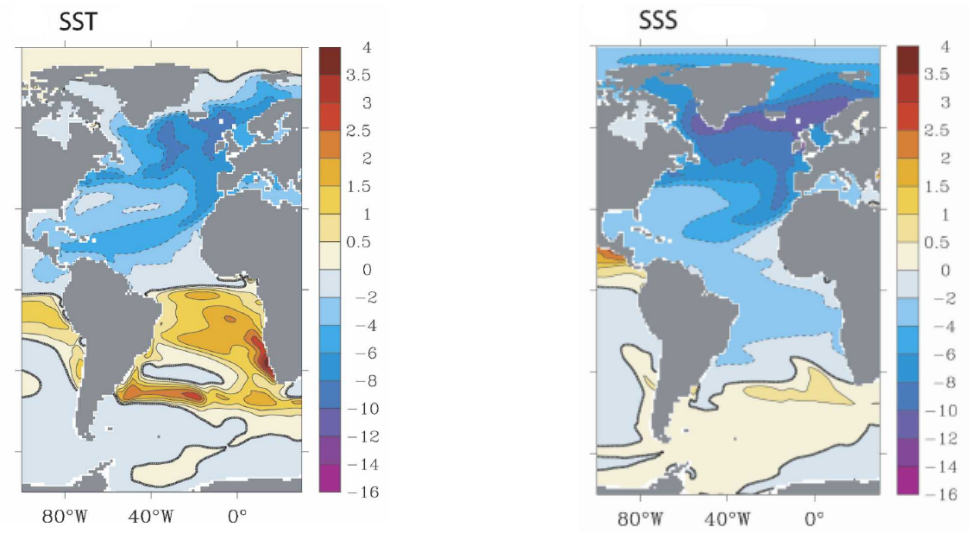

Figure 2.6: The response of the Sea Surface Temperature (left plot in °C) and Sea Surface Salinity (right plot in Practical Salinity Unit (PSU)) to a hosing of 1 Sv for 100 years for the model years 81 to 100 from Yin und Stouffer (2007)

Furthermore, the weakened deep convection in addition to the ocean-atmosphere interaction leads to subsurface warming which impacts the recovery of the circulation (Shi und Lohmann (2016), Umling et al. (2019)). Subsurface transports are relevant because they are an indicator for the STG/Subpolar Gyre (SPG) inter-gyre dynamics, which can stabilize not only the climate but also compensate for high latitude freshening and might even be able to restart halted AMOC circulations. A weakening or shutdown of the AMOC would lead to a reduced SPG, an increased STG strength, and an increased inflow of saline Atlantic waters into the Nordic Sea. The Figure 2.7 shows the further northward extension of the STG and the greater northward water transport.

Through the East Greenland Currents, these saline waters would be transported into the Labrador Sea, where deep-water convection would be strengthened or restarted on the one hand (Repschläger et al. (2017), Zhu et al. (2014), Thornalley et al. (2009)). On the other hand, the warm Atlantic waters can flow under the ice sheets and melt them from below, re-enabling the heat exchange between ocean and atmosphere and further helping the restart of the overturning (Repschläger et al., 2015). These strengthening effects probably happened in the past after an AMOC weakening for example at 6-5 and 2.8 ka BP (Thornalley et al., 2009).

[5] Hosed for 100 years with 1 Sv at 50°-70°N.

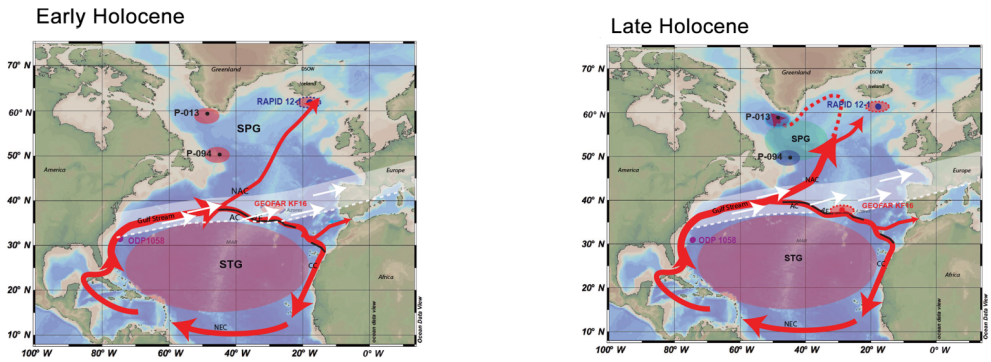

Figure 2.7: Conceptual model of the STG and related ocean currents during the early Holocene, dominated by meltwater from the glaciers and ice sheets (left), and late modern Holocene (right). The abbreviation AC stand for Azores Current from Repschläger et al. (2017)

2.3 The Storm Tracks

Storm tracks describe the paths that midlatitude cyclones take over the ocean and continental areas. In this thesis, the main focus will be on the tracks of extratropical cyclones over the North Atlantic Ocean and the European continent.

2.3.1 Placement of the Storm Tracks in the Global Climate System

The main atmospheric driver is the incoming solar radiation or rather the differences between the tropics and the polar latitudes. In the tropical regions, more energy from the sun reaches the atmosphere than in the high latitudes leading to a stronger warming in lower latitudes. The atmosphere tries to balance this disequilibrium with northward heat transport through the ocean and the atmosphere. Oceanic northward heat transport in the Atlantic is mostly covered by the aforementioned THC dominating the (sub-) tropics. In the atmosphere, storms and the meridional circulation are strongly responsible for moving heat to the poles. The meridional circulation (see Figure 2.8) can be divided into three cells, the Hadley, the Ferrell, and the polar cell.

Because of the strong solar insolation in the tropics, the SATs are heated and the air rises. During the ascent, the air parcels cool down and, if saturation is reached, leads to cloud formation and possibly precipitation. This is known as the near-equatorial trough or ITCZ. The ascending air rises to the top of the troposphere, where it is redirected to the north and south. Because of the Coriolis force the winds are diverted to the right in the NH and the left in the SH. At approximately 30°N/S the winds at the tropopause blow parallel to the ITCZ, creating the subtropical jet stream (the right green circles in the left sketch in Figure 2.8). At the same latitude, the air sinks down to the ground creating a high-pressure belt. It either returns as the dry trade winds to the equator, completing the Hadley cell, or flows polewards as part of the Ferrell cell.

In the polar regions, the small incoming radiation creates low temperatures, leading to a sinking of the air and a high-pressure system at the ground. This surface air flows to the south and is redirected by the Coriolis force to the right (left) in the northern (southern) hemisphere. At approximately 60°N/S the polar air meets the northward flowing air from the Ferrell cell. The lighter subtropical air from the Ferrell cell rises while being mixed with the polar air, is advected, and returns at the top of the troposphere partly back to the subtropical region. Because of mixing with

the warmer air, the polar air is lifted as well and flows below the tropopause back to the poles.

Where the warm subtropical meets the cooler polar air, the boundary is called the polar front, and this interaction between different air masses drives the unstable mid-latitude weather. At the surface, a low-pressure trough develops. Meanwhile, the greater temperature gradient leads to an increasing westerly wind with heights (due to the so-called "thermal wind balance"), leading to a polar jet stream at the upper troposphere (BBC, 2023).

The cells can be categorized into thermally direct (Hadley and polar) and indirect (Ferrell) ones. The Ferrell cell is thermally indirect because the air experiences sinking in the warm subtropics and lifting in the subpolar. In the thermally direct cell, the air rises in the warmer areas and moves downward in the colder regions.

The other possibility of transport next to the meridional circulation is with transient eddies, which

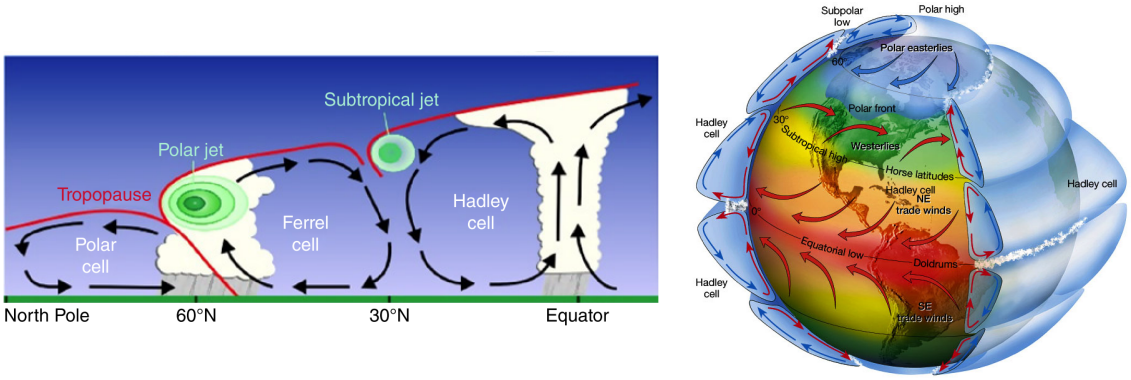

Figure 2.8: Left plot: Horizontal cut of the global wind circulation pattern. Red lines show the troposphere height and fronts, black arrows indicate the flow direction, and green circles show the wind strengths of the jets from Griffin et al. (2017). Right Plot: Global wind circulation pattern. The red arrows denote the warm trade winds and westerlies, while the blue ones show the polar easterlies. The blue areas around the globe show the meridional cells from Society (2020)

are deviations from the zonal mean state, important for moving heat and momentum northward (Priestley et al., 2020). Examples are tropical and extratropical cyclones. In the following subsections, the development and impacts of extratropical cyclones are depicted.

2.3.2 Life Cycle of Cyclones

Extratropical cyclones are rotating (counterclockwise on the NH) air masses characterized by a low central pressure and, unlike their tropical counterparts, a cold core. Over the North Atlantic, extratropical cyclones are particularly active along the Gulf Stream, and they generally travel from the eastern coast of North America toward Europe. The main driver for extratropical cyclone generation and maintenance is the baroclinicity of the atmosphere, which is tied closely to the SST gradient and the position of the jet stream. Other influencing factors include the orographic effect (for example the Rocky Mountains in America and Canada), heat fluxes from the underlying surface, and diabatic processes (Brayshaw et al., 2009a).

There are two conceptual models describing the life cycle of extratropical cyclones. One is the Norwegian model and the other is called the Shapiro-Keyser model.

For a storm to form, a disturbance in the lower layers of the polar jet stream is first caused by

atmospheric waves or surface obstacles. The more common Norwegian model has an early disturbance spreading vertically through the entire atmosphere with the wave-like formation starting to rotate anti-clockwise. This creates a low-pressure system with the surface manifestation ahead (more eastward) compared to the upper level (around 300 hPa) low-pressure region, also described by a slanted vertical axis. The cyclone intensifies with diabatic heating (solar irradiation, latent heat) and other large-scale processes creating stronger baroclinicity. During this intensification, it creates fronts and sectors (see Figure 2.9 on the left, Step II). First, the warm sector is on the equatorward side with the warm front on the eastward side as a separation from the cold sector. Likewise, there is a cold front on the western side between the different sectors. Behind the fronts air masses are transported, meaning that the cold polar air moves southward and the warm tropical air is shifted towards the poles. With time, the steeper and faster cold front comes closer to the other front, leading to a horizontal shrinking of the warm sector. When the cold front catches up with the warm front, the warm air is lifted on top of the colder air and a so-called occlusion front is created. At this time, the low-pressure system at jet stream height has also caught up with the surface pressure depression, meaning that the upper low-pressure system is above the ground low-pressure system and the vertical axis of the cyclone is no longer slanted. This means that virtually no further intensification of the cyclone is possible and the weather system will either dissipate or be reintegrated into the jet. It is also possible that a cyclone at the end of its life cycle experiences a re-intensification if it encounters strong baroclinicity and gains strength again.

The other cyclone model, describing a Shapiro-Keyser cyclone, has a frontal fracture, where the normally linked cold and warm front break apart in the center of the storm (see Figure 2.9 on the right, Step II). This leads thereto that the warm front wraps around the low-pressure center, the orientation of the cold front becomes nearly perpendicular to the orientation of the warm front, and phenomena like the sting jets can be observed.

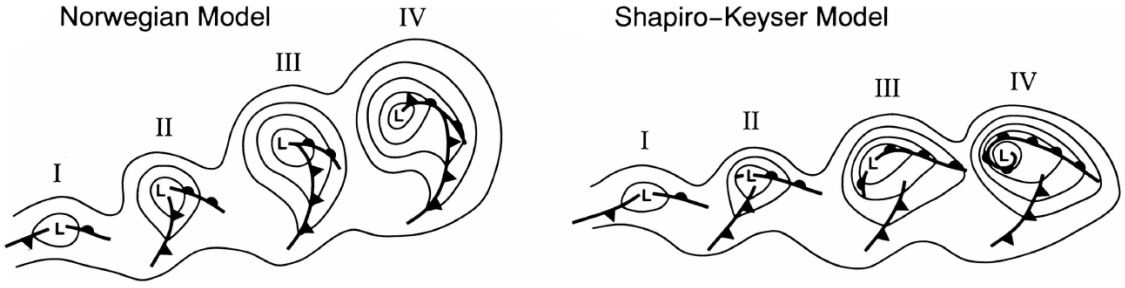

Figure 2.9: Conceptual models of cyclone evolution in the lower-tropospheric geopotential height and frontal systems for the Norwegian model (a) and the Shapiro-Keyser model (b) from Schultz et al. (1998)

2.3.3 Definition of the Storm Tracks

Storm tracks are the prevailing paths of the cyclonic systems and represents a collective quantity. They are helpful to investigate the mean behaviour of cyclones in a region, without having to analyze each individual storm.

For the initial formation, the cyclones need either a large orography, the land-sea contrast, or SST anomalies (Bengtsson et al., 2006). These requirements lead to the main genesis for the NH re-

gions being found on the lee side of the Rocky Mountains and the Tibetan Plateau and over the Mediterranean. Secondary storm formation regions are over the ocean, where moisture availability leads to instability and baroclinicity increase. Here, the Gulf Stream region is the most prominent one (Catto et al., 2011).

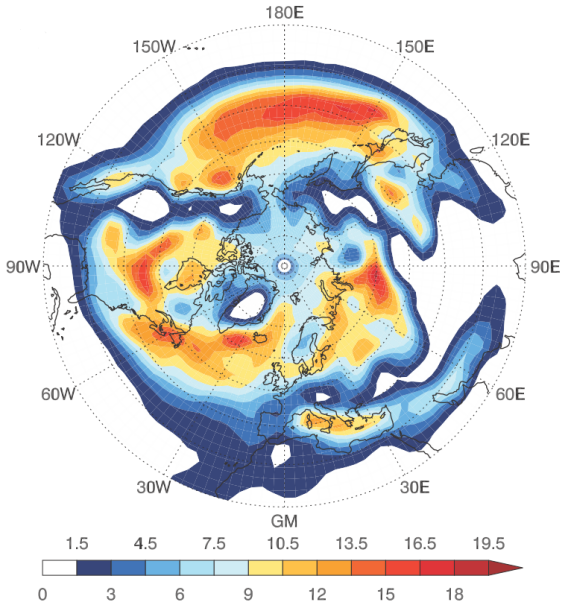

Figure 2.10: Track density (number of cyclones in a certain area) for the NH DJF for ERA-40 from Catto et al. (2011)

After the formation, the cyclone develops and generally travels eastward. Over the northern Atlantic Ocean, the tracks are more uniformly spread compared to over the continent with a slight tendency to follow the Northern American and Greenlandic coast. But over the Eurasian continent, there are two preferred tracks (see Figure 2.10): One denser track over the Norwegian Sea bringing strong precipitation and mild weather over northwestern Europe. And another smaller southern track starting over the Mediterranean, bringing precipitation to South Europe and cold weather to the northern parts of Europe (Bengtsson et al., 2006). Next to the generation area, the large-scale atmospheric oscillations like the phase of the North Atlantic oscillation (NAO), Artic Ocean (AO) and even ENSO (El-Niño Southern Oscillation), can lead to some inter-annual and inter-decadal variabilities of the climatological picture and influence the preference for the different tracks (Bengtsson et al. (2006), Ulbrich et al. (2009)).

2.3.4 Projected Impacts by the Climate Change on the Extratropical Cyclones

Theoretically, the future warmer climate and the polar amplification will lead to a weaker large-scale meridional temperature gradient (Raible et al., 2021), which will decrease the low-level baroclinicity, and reduce the number and intensity of cyclones over the Atlantic. On the other hand, higher temperatures will increase the atmospheric water vapor content by 7%/K according to the Clausius Clapeyron equation, which could potentially strengthen the intensity of the storms via latent heat release (Brayshaw et al. (2010), Raible et al. (2021)). Another consideration should

be that an increase in atmospheric moisture means that more effective heat transport is possible. Therefore, fewer cyclones could transport the same heat amount as in the current climate with more storms (Catto et al. (2011), Bengtsson et al. (2006), and Bengtsson et al. (2009)).

Multiple studies investigated the future developments of extratropical cyclones, but different experimental and model setups led to partly contrasting results. Most papers projected a reduction for the number of cyclones by approximately 4 % from the end of the 20th to the end of the 21st century (Ulbrich et al. (2009), Bengtsson et al. (2006)). However, some found this decrease only to be relevant for weaker storms, while they predict a weaker reduction of stronger storms (Bengtsson et al., 2006) or sometimes even an increase in intense cyclones (Ulbrich et al. (2009), Catto et al. (2011), Raible et al. (2021)). Bengtsson et al. (2009) reported an increase in precipitation along the tracks by up to 11 %, which could mean local precipitation increases by 40-50 % because of the higher atmospheric moisture content in a warmer climate. Other sometimes projected changes of extratropical cyclones are the increase in cyclone radius and the reduction in wind speed (Ulbrich et al. (2009), Bengtsson et al. (2009)) by some studies. The above-shown results suggest that the changes in storms are heterogeneous in space and characteristics. Different predicted changes in for example path, strength, and horizontal extent make a general and consistent statement about the development of the extratropical cyclones not possible.

2.3.5 Projected Impacts by the Climate Change on the Storm Tracks

The majority of the studies agree on an eastward shift of the storm track with a further intrusion into the European continent (Ulbrich et al. (2009), Harvey et al. (2020), Brayshaw et al. (2009b)). Especially over the British Isles, the strengthening of the storm tracks is predicted. This shift of the track can be seen in Figure 2.11, where storm tracks are intensified more strongly over the central and eastern than the western North Atlantic.

The left plot in Figure 2.12 shows the eastward wind changes in 850 hPa (colors) in the high

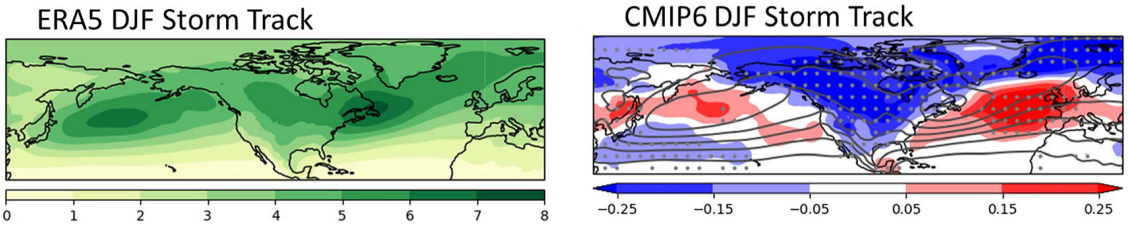

Figure 2.11: The left plot shows the DJF present-day storm tracks (root-mean-square error of 2-6 day band-pass filtered mean sea level data) from ERA5 in hPa. On the right the DJF multi-model mean future (SSP2-4.5) minus present-day storm tracks in hPa is depicted from Harvey et al. (2020)

emission scenario of the CMIP5 models. They indicate stronger low-level winds over northern Europe (Bengtsson et al., 2009), while the south is simulated to have weaker winds resulting in a northward shift. The strengthening of the easterly winds supports the eastward shift of the future storm tracks towards Europe.

The cyclone activity over the Mediterranean area is predicted to be strongly reduced, especially in winter (Ulbrich et al. (2009), Raible et al. (2021)). Figure 2.12 shows in the left plot a significant low-level wind reduction over this inland sea in the future. Another interpretation of the changes in

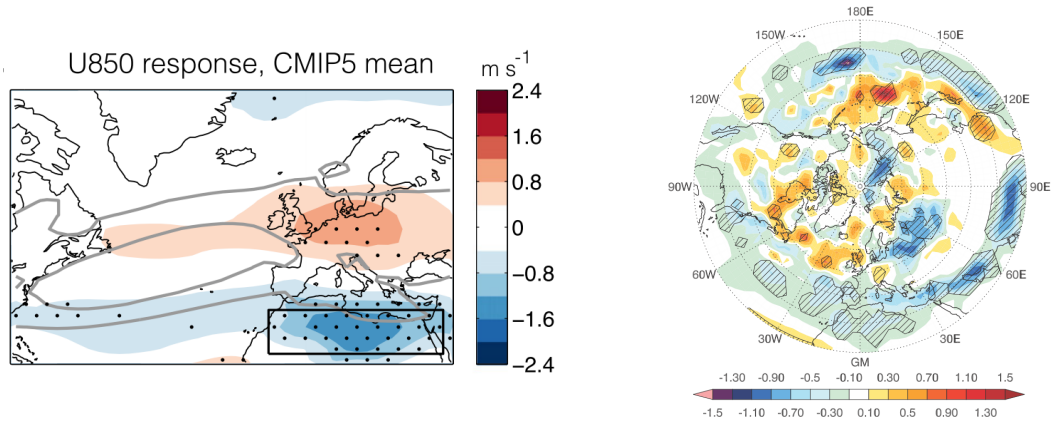

Figure 2.12: Left: Multi-model mean CMIP5 end of century response (Representative Concentration Pathway (RCP)8.5-historical) of the winds in 850 hPa in NDJFMA. The grey contours show the 4 and 8m s^{-1} isotach of the 850 hPa zonal wind of the historical simulation (1976-2005) and stippling indicates a 90 % inter-model sign agreement from Zappa et al. (2015). Right: Track density changes for a doubled CO_2 minus control experiment for the NH in DJF. Cyclone identification based on the maxima in the 850 hPa 6-hourly relative vorticity field from Catto et al. (2011).

the western North Atlantic is the development from two semi-separated tracks over the Norwegian Sea and the Mediterranean to an intermediate track over the British Isles (Bengtsson et al., 2009), meaning more storms in this region.

Many studies also report a poleward shift of the storm tracks (Ulbrich et al. (2009), Bengtsson et al. (2009), Bengtsson et al. (2006), Catto et al. (2011)) more pronounced in the Pacific Ocean. The right plot in Figure 2.12 depicts this shift from eastern North America, across the North Atlantic, all the way to Europe. A possible explanation is the widening of the Hadley cell (Brayshaw et al., 2010) and subsequently, the changed position of the jet stream. Figure 2.13 depicts the impacts of a weakened and widened Hadley cell and the polar amplification. As a consequence the temperature gradient is smaller, the westerlies and jets are weakened and the entire mid-latitude circulation is affected.

However, studies still report that the local response of the storm tracks can exhibit differences in

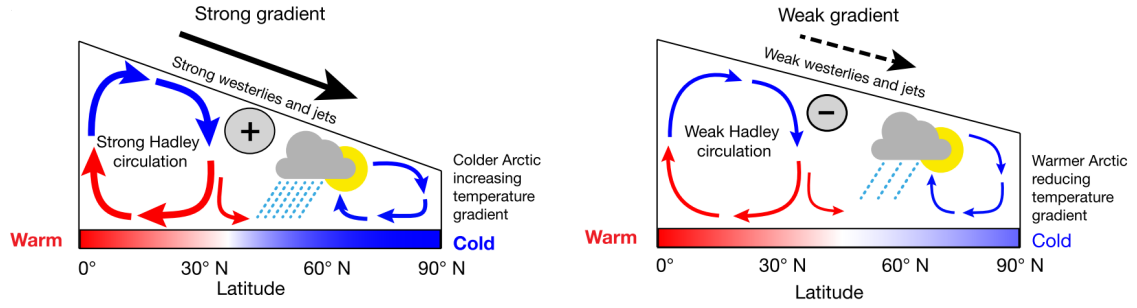

Figure 2.13: Conceptual diagram of impacts of the warming in the high latitudes and a weaker Hadley circulation. The left sketch shows the cold-climate conditions, and the right one depicts the changes after warming from Routson et al. (2019)

the changing characteristics of the future climate. For example, the right plot in Figure 2.11 depicts no weakening signal south of the storm track intensification over the eastern North Atlantic and Europe. Potential factors leading to those mixed results (e.g., the right plots in Figure 2.11 and

Figure 2.12) include disparities in the tracking methods, forcings of future-climate scenarios, and model version in use.

The heterogeneous developments of the storm track in the future suggest that the employment of a different experiment structure can produce contradicting outcomes. This indicates that there is still some uncertainty left in giving accurate and concurring predictions of storm track changes for the future.

2.4 Relationship between the Thermohaline Circulation and the Storm Tracks

2.4.1 Present-Day Relationship between the Thermohaline Circulation and the Storm Tracks

The main aspect of the THC in the North Atlantic is the northward transport of warm and salty water near the surface and a southward export of fresh cold water in the deep ocean. As a result, the SST and SAT are warmer than the latitudinal average.

Higher SSTs mean a stronger evaporation and therefore a greater moisture availability for the latent heating of the cyclone (Brayshaw et al., 2009a). The oceanic heat transport warms the low-level atmosphere, influencing the local SAT gradient, creating baroclinic instability. This instability acts as an important energy source for the initial storm formation and can strengthen the cyclones.

However as the THC transports warm subtropical water northward, it warms up the mid-to-high-latitudes, which subsequently contributes to a weakening of the large-scale SST gradient between low and high latitudes. Since cyclones try to balance the insolation difference between the tropics and the poles, the reduced gradient could weaken storm intensity and frequency.

2.4.2 Projected Changes to the Relationship between the Thermohaline Circulation and the Storm Tracks

In subsection 2.2.4 the projected changes of the THC caused by climate change are described. The interconnection between the different climate system components postulates an impact of the weaker ocean circulation on the atmosphere.

Weakening in heat transport to the higher latitudes will reduce the SAT over the mid-to-high-latitude ocean and potentially the adjacent continents. Figure 2.14 (on the left) shows the predicted surface air temperature changes relative to the control experiment. Here, a hosing with 0.3 Sv for 140 years was applied and the subsequent weakening of the THC led to a strong cooling in the NH, especially over the North Atlantic region. The so-called North Atlantic Warming Hole (NAWH) (Bellomo et al., 2021) shows an even stronger cooling exceeding the surrounding temperature reduction. The strongest temperature changes here show that a cooling of up to 10°C is possible. More extreme hosing or forcing experiments even consider local temperature reductions up to 16°C (Vellinga und Wood, 2002). The earlier mentioned reduction in SST and the possible increase in sea ice would, due to the change in albedo, lead to a further reduction in SAT in the high latitudes. Cooling in turn influences the precipitation, snow cover, and many other climate system components.

Impacts of the weakened Atlantic circulation on precipitation were investigated by Bellomo et al. (2023). They showed that an approximately halved AMOC strength leads to changes in the global precipitation pattern (see Figure 2.14 on the right). Over the northern North Atlantic, a reduction of precipitation is projected. This is most likely caused by the colder SSTs, which reduce the evaporation by the ocean. Also because of a weakened circulation, the air temperatures experience a weaker warming, meaning that the air over the North Atlantic can hold less moisture relatively. This results in the precipitation amount being reduced.

Next to the easy-to-understand temperature and precipitation changes, there are also impacts on the pressure and wind both over the ocean and the continent. However, these exhibit more locally individual patterns: for more information see for example Stouffer et al. (2006) and Vellinga und Wood (2002).

Changes of the THC and its altered impact on the atmosphere influences the storm tracks differ-

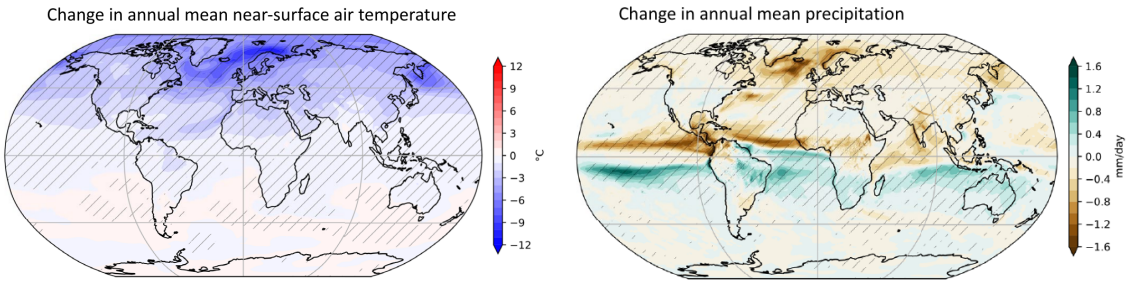

Figure 2.14: Annual mean change in near-surface air temperature (on the left) and precipitation (on the right) (hosed minus control experiment, see Figure 2.5 for more information) with hashing showing statistical significance from Bellomo et al. (2023)

ently in the future climate. The most important consequence of changes in the THC is the SST cooling in the Atlantic Ocean. A weakening of the circulation leads to cooler oceanic surface temperatures in the mid-to-high latitudes, which locally increase the meridional temperature gradient and by impacting the low-level baroclinicity, changes the position of the storm tracks eastward (Catto et al., 2011). Cooler air temperatures, reduce the evaporation and moisture availability in the lower atmospheric levels. Therefore the latent heating will be weaker in the future (Brayshaw et al., 2009a). The hosing experiment from Brayshaw et al. (2009b) showed that the weaker oceanic heat transport was balanced with a stronger atmospheric heat transport. This meant a strong increase in storm density and a strengthening of the North Atlantic storm tracks, with local cyclogenesis increase by 40 %[6].

The connection between the AMOC and the storm tracks was already previously investigated by Woollings et al. (2012). Using the CMIP3 data, they explored the impact of the changing oceanic circulation on the atmospheric circulation. A regression analysis allows us to quantify the storm track response to a change in the AMOC. The resulting plots are in Figure 2.15. Near-surface air temperatures (middle plot in Figure 2.15) show cooling and zonal winds in 850 hPa (right plot in Figure 2.15) depict a strengthening and an eastward shift as a response to the AMOC slowdown.

[6] In this experiment, the THC was forcefully shut down and the results are therefore not a realistic projection for the near future but only an indicator.

With a weaker ocean circulation the resulting storm tracks (left plot in Figure 2.15) are expected to extend further east and also experience an intensification.

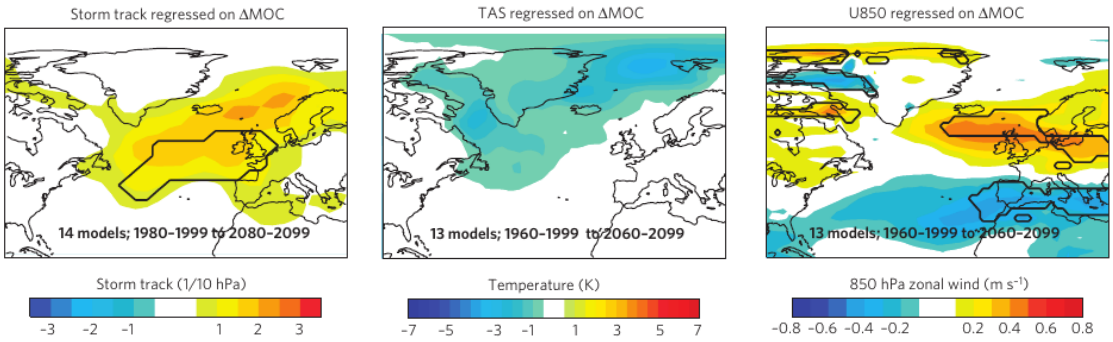

Figure 2.15: Plots of the multi-model regression slope between the AMOC and storm tracks (left), SAT (middle), and U850hPa (right) changes over the North Atlantic and Europe from Woollings et al. (2012)

2.5 Large-Scale Conditions in Paleoclimate Times

The Milankovitch cycle[7] describes the yearly path around the sun, the inclination of the earth, and the distance between the earth and the sun. With different period lengths, these factors change and impact as an external influence the shortwave insolation. This led to the development of partly very contrasting climate conditions compared to the current one.

Despite the fact, that paleoclimates describe bygone time periods, studying those previous climates can help in today's research. For example, understanding the past climate and the reasons for its shifts will most likely enhance our comprehension of the current conditions. Paleoclimates can also be used to test hypotheses about potential mechanisms and drivers of climate change. With climatic time series extending far into the past, the recent and predicted changes can be put in long-term perspective (Raible et al., 2021). Today's climate models usually need to use parameterization and still contain bias and uncertainties, paleo proxies can help validate results and test model skill (Laîné et al., 2009) under different climate conditions.

2.5.1 Climate Proxies

Since there were no measurement instruments during paleoclimate times, paleo proxies are the best way to get information about past climates. These proxies can come from many different sources. Some examples are deep ice (sheets and glaciers) or sediment (oceans and lakes) cores, tree-rings, speleothems, shell organisms, and historical documents (Aken (2007), Raible et al. (2021), Peltier (2007)).

Ice cores store a snapshot of the past air composition in small bubbles: With measurements of the individual gas concentrations they give the possibility to develop a concept of the past atmospheric structure. Additionally, with, for example, an analysis of the oxygen concentration the atmospheric temperature can be inferred (Peltier, 2007). Sediment cores contain multiple types of information. The calcium carbonate concentration helps to identify freshwater pulses (Peltier,

[7] Orbital eccentricity, obliquity, and precession

2007). From cadmium, phosphate, and oxygen the age of the deep water can be dated (Aken, 2007). Planktic and benthic shell organisms (e.g. Foraminifera) build their shells near the surface and incorporate oxygen. During colder periods the heavier ^{18}O concentration in the ocean is higher and lower in the atmosphere, which can be calculated with the creatures remaining shells (Aken (2007), Peltier (2007)). Tree rings show with their width the general growth conditions, like water availability, temperature, and nutrients. Speleothems are for example stalagmites and from the growth amount the availability and composition of water can be determined. Historical documents include for example paintings or contemporary witness accounts, containing volcanic eruptions, very low temperatures, or floods.

For a proper analysis of the storm tracks, 6-hourly pressure data is required, however most proxies only give insight into temperature or precipitation changes and are not sub-daily. Therefore temporal down-scaling is needed and wind and pressure data has to be derived indirectly. This derivation is possible from the available variables or for example from sediment transport (e.g., large sand transport suggesting strong winds) (Raible et al., 2021).

The oceanic circulation faces a similar problem because no proxies are showing its strength directly. Therefore a combination of the ventilation age, the vertical gradient of $^{231}Pa/^{230}Th$ (Menviel et al., 2020) and the amount of ^{14}C (Clark et al., 2002) is being used to infer the circulation strength.

Unfortunately, paleo proxies are only sparsely available and show sometimes contradicting results, which is why a study only based on these climate indicators is impossible (Raible et al., 2021). As a result, models are useful means to fill the gaps. A challenge here, next to the high model uncertainty, is the spatial resolution (Raible et al., 2021). Models have a regular grid and idealized boundary conditions, while the proxies are spatially limited to their point of origin and influenced by the local topography (Brayshaw et al., 2010). For the models, it is also important that proper boundary conditions are applied because the correct representation of the coarseness, albedo, fresh water storage of the ice sheet (Ludwig et al. (2016), Zhu et al. (2014)) or the dynamic of the ocean (Brayshaw et al., 2010) lead to a greater agreement with the paleo-data (Pinto und Ludwig, 2020).

2.5.2 The Holocene

The most recent interglacial period, also known as the Holocene, started approximately 12,000 years ago and is usually divided into three periods with the early- (8.2-11.6 ka BP[8]), mid- (4.3-8.2 ka BP) and the late-Holocene (0-4.3 ka BP) (Repschläger et al., 2017). At the beginning of the Holocene, large parts of the NH were still ice-covered from the last glacial period. The early Holocene was dominated by extensive sea and glacier ice melting caused by a change in insolation and consequently, large sea level increases (Thornalley et al., 2009). The following mid-Holocene period experienced a more stable climate comparable to the pre-industrial conditions. This is the period, on which this thesis will be focusing its study of the recent paleoclimate. Currently, since 4.3 ka BP the earth is in the late Holocene time period.

Due to changes in the Earth's orbit, the solar insolation was different, with more solar radiation reaching the high latitudes during summer and the tropics receiving less incoming sunlight during

[8] Thousand years Before Present

the December-January-February (DJF). This can be seen in the upper part in Figure 2.16. The change was approximately 5 $W m^{-2}$, which translates roughly to 15-20% of the insolation and impacts therefore the global latitudinal insolation gradient (Brayshaw et al., 2010).

The mid-Holocene was characterized by lower than pre-industrial GHG concentrations which

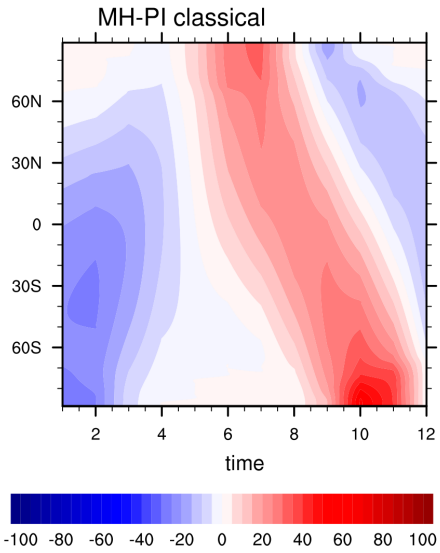

Figure 2.16: Monthly mean insolation difference (in $W m^{-2}$) at the top of the atmosphere between the mid-Holocene and the pre-industrial as a function of time (in months) and latitude (in °) from Shi et al. (2020).

increased with time. For example CO_2 increased from 240 to 280 ppm from the early Holocene to the pre-industrial times, similar increases can be found for CH_4 and N_2O (Brovkin et al., 2019). The global near-surface air temperatures during the mid-Holocene were lower than in the pre-industrial times. Simulations like in Figure 2.17 suggest, that these colder temperatures were more pronounced over the continents like North America but weaker over the oceans. South of Greenland and in the higher latitudes, papers like Kang und Yang (2023) suggest regional warming is caused by the higher polar insolation. Brayshaw et al. (2010) postulated that with an increase in GHGs, the SAT experienced a weak warming of 0.5-1°C over the past 11.6 ka.

Under these different climate conditions, both the ocean and the atmosphere exhibited varied characteristics. In the atmosphere, the stronger boreal summer insolation in the polar regions led to a weaker pressure gradient, suggesting a northward shift of the westerly wind belt and general changes in the atmospheric circulation (Repschläger et al., 2017).

In the ocean, the higher polar insolation in the early Holocene caused warming relative to the glacial period of the SAT and SST in the high latitudes. This caused large parts of the extensive ice sheets from the LGM to melt to reach the pre-industrial state and the sea level to rise by 60 m (Repschläger et al. (2017), Brayshaw et al. (2010)). During the mid-Holocene, the SSTs were mostly constant, with a variability of 2 °C. At the beginning of the Holocene, the SSS had slightly lower values than the present day and experienced additional freshening due to the glacial melting. After 9 ka BP, the SSS probably increased again, caused by the reduction in meltwater and changes in the freshwater export from the Arctic Ocean (Thornalley et al., 2009).

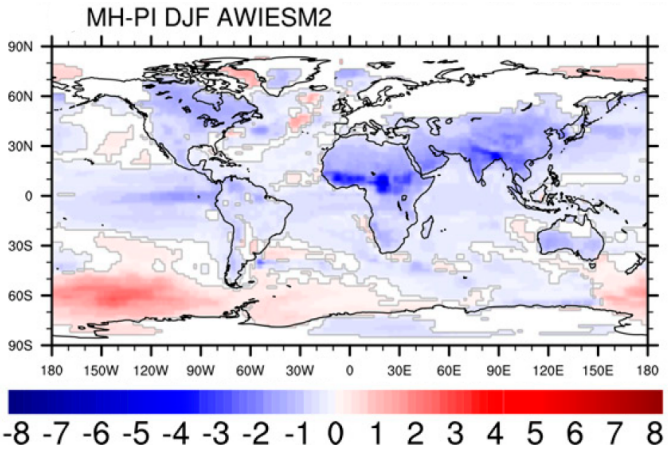

Figure 2.17: Simulated anomalies of the SATs (in K) between the mid-Holocene and the pre-industrial for the winter months from Shi et al. (2020).

The Thermohaline Circulation

The behavior of the THC during the Holocene is hard to characterize. Unfortunately, there are no proxies to directly show the circulation pattern during the paleoclimate, meaning that the presented results are either indirectly linked to the THC or only based on model results. On the one hand, drier conditions over the Baffin Bay, the Nordic Sea, and the western North Atlantic as well as a density increase in the Labrador Sea were suggested by Shi und Lohmann (2016). In addition, a smaller ice export from the Arctic through the Fram Strait, leading to an increase in SSS in the Greenland Sea and stronger deep-water formation, would indicate a stronger THC circulation (Shi und Lohmann, 2016).

Wetter conditions over the northeast of the Atlantic and near the North American coast and general sea ice melting indicate a local density decrease. Warming over the Baffin Bay and the Nordic Sea would also reduce the density, same as an increase in liquid water transport through the Fram Strait. Those characteristics would, however, suggest a weaker THC circulation (Shi und Lohmann, 2016). Zhu et al. (2014) modeled the impact of orographic changes due to large-scale ice sheet retreats and found a northward shift of the westerlies. This led to an eastward transport and local formation of sea ice over the Labrador, Greenland, Iceland, and Norwegian Seas. As a consequence, the ice insulated the ocean against heat loss to the atmosphere, weakening the dense water formation and deep convection. The resulting AMOC weakening (by 41 % if the entire ice sheet is reduced (Zhu et al., 2014)) means a reduced poleward heat transport and therefore the further expansion of the ice cover (Zhu et al., 2014).

Because the aforementioned effects partially offset each other and their intensity depends on the resolution, there is great uncertainty in models at capturing the strength of paleoclimate AMOCs. It is therefore no surprise that studies simulate different oceanic circulation overturnings. Most show only smaller deviations from the pre-industrial situation, with 2 Sv stronger or weaker circulations (Shi und Lohmann (2016), Repschläger et al. (2015)). The Figure 2.18 depicts one simulated AMOC during the mid-Holocene, which is shifted to the south and has a slight intensification of 2 Sv.

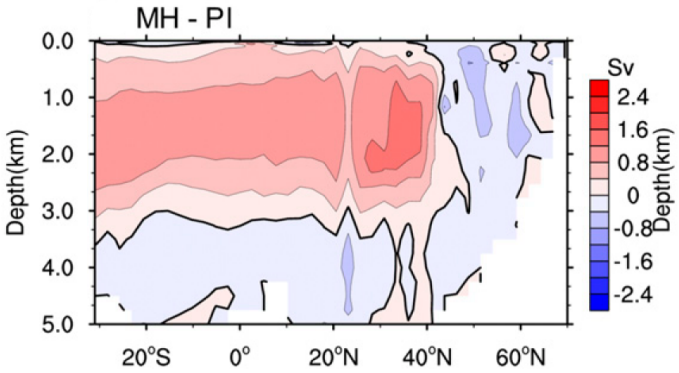

Figure 2.18: Simulated annual mean AMOC difference between the mid-Holocene and the pre-industrial overturning circulation from Zhang et al. (2021)

Storm Track

The different climate state of the Holocene influenced the characteristics of the North Atlantic and Mediterranean storm tracks, causing a change to the position and strength of the tracks. Slightly higher insolation in DJF at the poles and lower solar radiation in the tropics led to a smaller latitudinal insolation gradient during the mid-Holocene period. A consequence is a lower required poleward heat transport, which suggests weaker midlatitude storm tracks (Brayshaw et al., 2010).

The weaker insolation gradient in winter also impacts the SST gradient between low and high latitudes and results in cooler SSTs in lower latitudes compared to the pre-industrial times. These lower temperatures induce a lower atmospheric moisture content, which negatively affects the latent heat release during the storm formation, also implying a reduced storm track intensity (Brayshaw et al., 2010).

However local effects are causing different outcomes. For example, the lower insolation in addition to the different specific heat capacities of land and water led to a greater land-sea contrast, resulting in stronger baroclinicity along the North American coast. In addition, with cold air advection from the remainder of the Laurentide Ice Sheet (LIS), there might have been stronger storm activities along the North American coastline (Raible et al., 2021). A probably stronger and narrower Hadley cell caused an equatorward shift of the subtropical jet, which in turn induced a southward shift of the storm tracks (Brayshaw et al., 2010). This geographical shift meant more cyclones over the Mediterranean regions, where these systems could trigger new cyclogenesis, meaning an even stronger Mediterranean storm track during the mid-Holocene. The stronger seasonal cycle of insolation also generates especially in the northern part of the Mediterranean a stronger land-sea contrast. Models suggest a strengthening of the storm track over the Northern Mediterranean and Southern European region by 5 % compared to the pre-industrial area (Brayshaw et al., 2010).

2.5.3 The Last Glacial Maximum

From 33 ka BP on, a reduction in polar insolation, a cooling in tropical Pacific SSTs, and a decrease of the atmospheric CO_2 led to a large-scale growth of the ice sheets retaining its extent until

the deglaciation around 19 ka BP. During this cold phase, the time around 21,000 years ago is conventionally defined as the LGM when the ice sheet had its maximal extent (Clark et al., 2009).

Despite similar insolation during the LGM to the present climate (Laîné et al. (2009), Raible et al. (2021)), the air temperatures and SST were significantly lower than today. Figure 2.19 depicts this with a global SAT (left plot) decrease of 5-6.5°C (Raible et al., 2021) and local cooling up to 25°C (Clark et al., 2002). The right plot shows the SST differences during the glacial time and illustrates ocean surface temperature reduction of 2 to 12°C in the North Atlantic (Cauquoin et al. (2023), Ludwig et al. (2016))). This caused the formation of large continental and sea ice sheets over Europe (Fennoscandinavian Ice Sheet (FSIS)), North America (LIS), and the North Atlantic. As a consequence, the global sea level was 115-130 cm lower than the current levels (Raible et al., 2021), and the topography of the earth's surface changed significantly (Menviel et al., 2017). In this period, the GHG concentration was also significantly lower. Reduced ventilation of the deep ocean meant a larger amount of aged water and a greater carbon dioxide storage capability compared to today. This suggests for CO_2 a concentration 100 ppm lower than during pre-industrial times (LGM: 185 ppm) and CH_4 and N_2O having also lower atmospheric concentrations (Laîné et al. (2009), Lan et al. (2023)). In all, the LGM climate is mainly modulated by the change of greenhouse gas concentrations and the existence of land ice sheets, along with the associated sea level drop and exposure of the continental shelf (Cao et al., 2019).

The different climate conditions of the LGM impacted the characteristics of the ocean and the

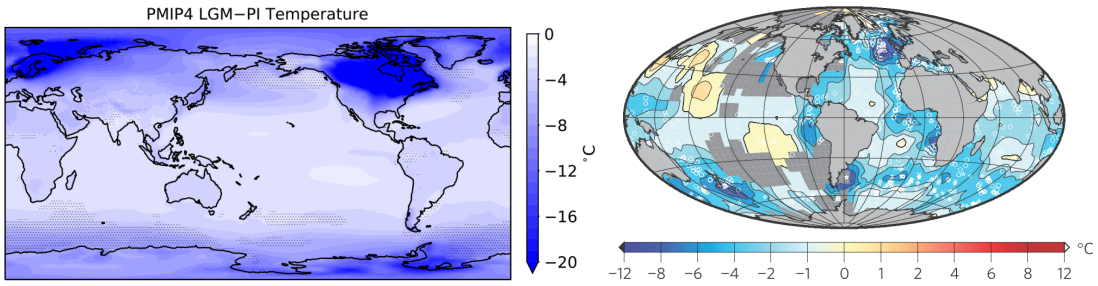

Figure 2.19: Air temperature anomalies in 2 m height (left, from Kageyama et al. (2021)) and the winter SST changes (right, from Waelbroeck und Members (2009)) between the LGM and the pre-industrial.

atmosphere. During this period, the meridional temperature gradient was stronger, which intensified the upper-level jet stream as can be seen in Figure 2.20. Additionally, a southward shift, a latitudinal narrowing, a further extension eastward towards Europe, and a reduction in variability was simulated (Pinto und Ludwig (2020), Ludwig et al. (2016), Raible et al. (2021)). The topographical changes because of the up to 4 km higher ice sheets (Laîné et al., 2009) can also cause the jet to be split, creating two possible paths.

Cooling of the atmosphere leads, according to the Clausius-Clapeyron-Equation, to less atmospheric moisture and caused during the LGM a global precipitation decrease by 0.49 mm/day (Zhang et al., 2022). The large ice sheets (e.g., the LIS and FSIS) created strong high-pressure systems over the continents, which caused the advection of cold and dry polar air into storm formation areas east of them, leading to additional precipitation loss (Laîné et al., 2009).

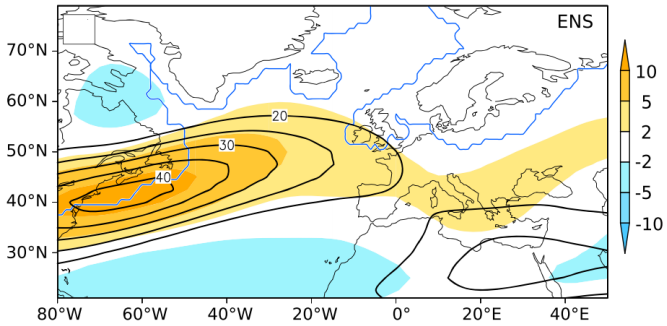

Figure 2.20: Ensemble mean of annual mean jet position and strength (black contour lines) and the difference between the control and the LGM simulation (shading). The LGM ice sheet extent is shown by the blue contour line from Ludwig et al. (2016)

The Thermohaline Circulation

The colder climate also impacted the general ocean and the THC. Indicators for the strength and position of the oceanic circulation can be the North Atlantic Deep Water (NADW) and the AABW. Models and proxies mostly indicate a shallower NADW circulation reaching down to only 3 km, and AABW reaching much further into the North Atlantic (Menviel et al. (2020), Zhang et al. (2022)) compared to pre-industrial times. The shallower circulation in the North Atlantic (Fox-Kemper et al., 2021a) would indicate a weakening of the THC, with a maximum depth of 2500 km and consequently mean a reduced northward heat transport (Fichefet et al., 1994). The changed THC was simulated in Figure 2.21. Here both the further northward reaching (darker) AABW and the shallower overturning circulation can be seen. Because of the ice sheet coverage, the deep convection areas were shifted to 50 °N (Fichefet et al., 1994), which can also be seen in the figure.

However, the lower sea level suggests stronger tides with stronger mixing rates, which would

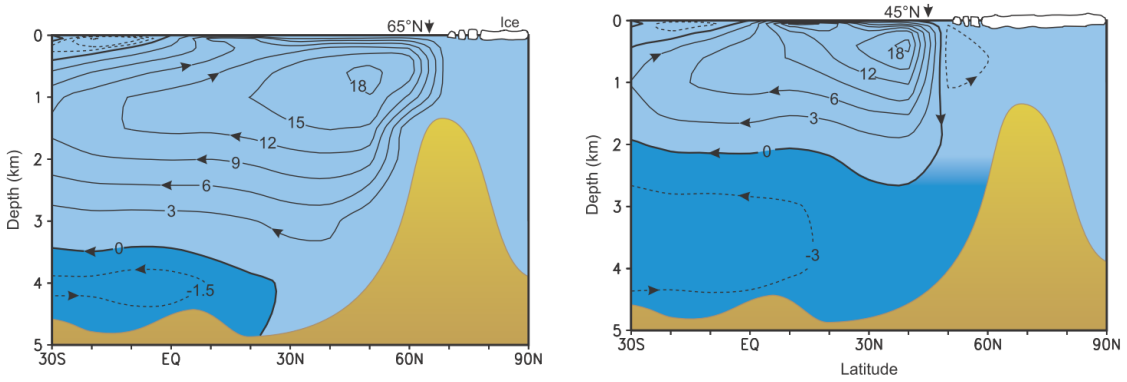

Figure 2.21: Simulated modern (left) and glacial (right) AMOC with the lighter blue depicts the NADW and the darker color means the AABW from Rahmstorf (2006)

indicate a strengthening of the AMOC (Aken, 2007). The stronger temperature gradient causing stronger winds could also support a strengthening of the circulation (Ludwig et al., 2016). Finally, pure model studies (like this thesis) show a stronger AMOC during the LGM (Ludwig et al. (2016), Repschläger et al. (2015)).

Storm Tracks

The above-described variances in the climate have impacts on the storm tracks during the LGM as depicted in the different storm track paths in Figure 2.22. During the glacial maximum, large parts of the continents were covered by up to 4 km high ice sheets. This created a semi-permanent anticyclone over the LIS, which moved both the jet stream and the baroclinic zone southwards and towards Europe(Luetscher et al., 2015). Coinciding with these geographical changes was a south-eastward shift of the storm tracks over the North Atlantic. Because of the blocking of the FSIS, the storm track split near the European continent. Storms either follow the northern path along the ice sheet or move southeastwards towards central Europe and the Mediterranean, intensifying the storm track over the Mediterranean Sea (Ludwig et al. (2016), Raible et al. (2021), Luetscher et al. (2015)).

Cooler temperatures and lower air moisture mean a reduced latent heat release during the cyclone

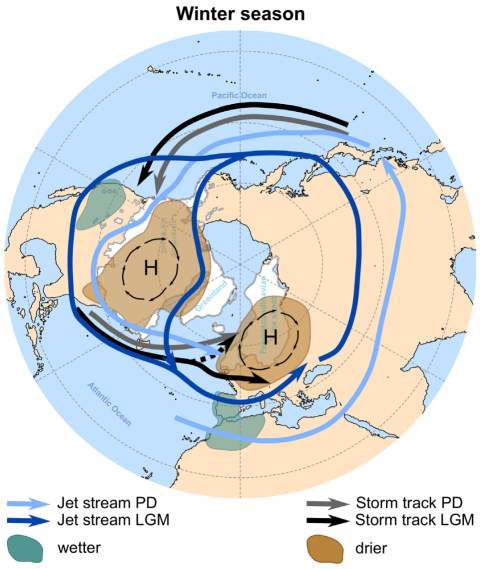

Figure 2.22: Schematic of the storm track and the jet stream for the present day (grey and light blue, respectively) and the LGM (black and dark blue, respectively), with dashed arrows indicating limited model evidence. Additionally are hydrological implications of the LGM cyclones compared to the present day shown. The results are based on modeling studies of the winter months from Raible et al. (2021)

lifetime and would indicate for the LGM weaker cyclone systems (Pinto und Ludwig (2020), Laîné et al. (2009)). However, with an increased meridional temperature gradient in the lower troposphere, the low-level baroclinicity is enhanced. This indicates fewer in total but more strong cyclones in the extratropics (Pinto und Ludwig (2020), Ludwig et al. (2016), Raible et al. (2021)). Additional to the greater strength of LGM-cyclones are indications of a more narrow storm track and an increase of the cyclogenesis off the North American coast (Pinto und Ludwig, 2020). The right plot in Figure 2.23 depicts differences in the mean storm tracks over the Northern Atlantic compared to the pre-industrial and shows an enhanced track along the ice sheets south of Greenland and north of the Mediterranean Sea.

Pinto und Ludwig (2020) summarized changes to the cyclone statistics compared to pre-industrial times and reported the following differences. The total number of cyclones would increase by ap-

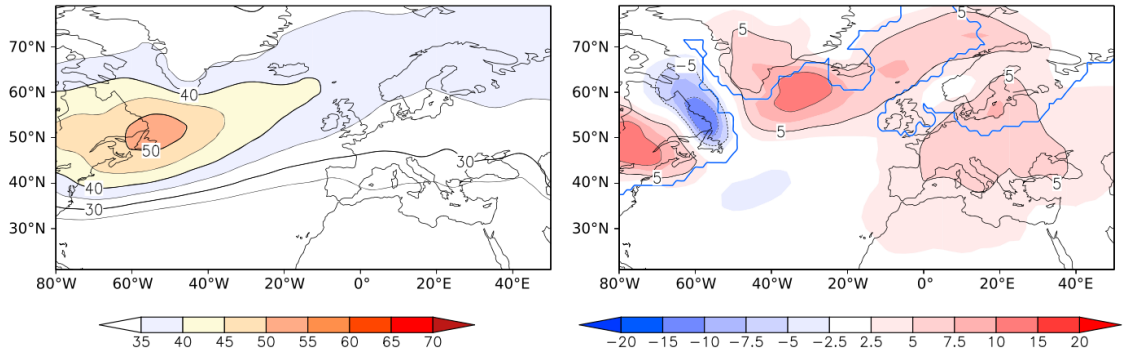

Figure 2.23: Storm track (2.5-6 day bandpass filtered daily mean sea level pressure data) simulation for the control (left, in 1/10 hPa) and the differences to the LGM (right). The LGM ice sheet extent is shown by the blue contour line from Ludwig et al. (2016)

proximately 26 % with an increased cyclone rate per day by 0.4 (2.2 to 1.8 cyclones/day). Because of stronger deepening rates, the storms during the LGM were likely more intense as can be seen in Figure 2.24, where during the LGM the number of weaker systems is reduced, while the number of intense storms increased. With stronger storm enhancements, the cyclones reached higher vorticity values and had wind speeds exceeding the pre-industrial by 10-12 $\mathrm{m\,s^{-1}}$. The core mean sea level pressure is higher during the glacial times (LGM: 982.7 and pre-industrial: 975.2 hPa), but that is only because the lower sea level led to a higher global mean sea level pressure (LGM: 1023 and pre-industrial: 1010 hPa). Taking the different sea level pressure into account, the cyclones exhibit a core pressure 40.3 hPa below the average pressure, while in the pre-industrial times, the reduction is only around 34.8 hPa. The generally colder climate led to less moisture and less precipitation associated with the storms and the advection of the cold and dry polar air caused stronger occlusions near the ice edge. The probably faster developing and decaying cyclones also had stronger wind gusts and a larger temperature gradient between air masses.

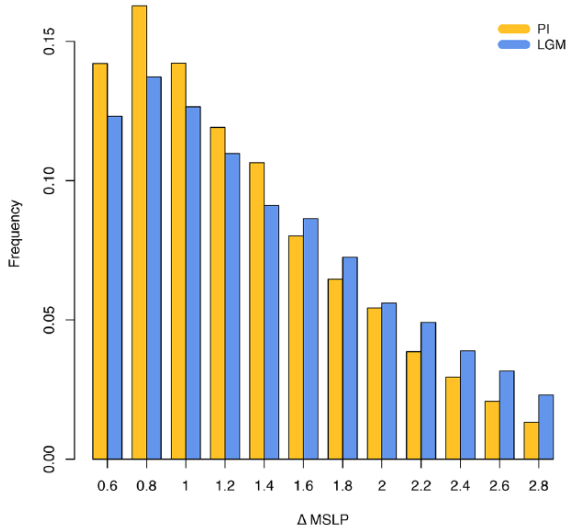

Figure 2.24: Histogram showing the cyclone intensity (Δ Mean Sea Level Pressure (MSLP)) over the North Atlantic (35-70°N, 70-0°W) for the pre-industrial and LGM climate (each containing 30-year slices of 6-hourly MPI data) from Pinto und Ludwig (2020)

3 Data and Methods

In this chapter, the simulation characteristics for the data of the different time periods are described, followed by information on the applied methods for the data analysis.

3.1 Model Data Description

The available data is provided by the Deutsche Klimarechenzentrum, the German Climate Computing Center. Model outputs from the Coupled Model Intercomparison Project are stored with them and have been made accessible for analysis. The ensemble results from the CMIP6 model runs were used to conduct the analysis, the same models which has been used to write the 6th Intergovernmental Panel on Climate Change Assessment report.

The historical data period is part of the core experiment of the CMIP project as it is used to show the basic characteristics of the individual models. This experiment simulates the recent-past climate, from the pre-industrial (1/1/1850) to the present (1/1/2015), with a total duration of 165 years (see Table 3.1 for more information on the individual time periods). During this simulation, the imposed changes are tried to keep as close as possible with the observational data to reduce notable biases in historical experiments compared to observations and reanalyses (Eyring, 2015).

The Scenario Model Intercomparison Project (ScenarioMIP) focuses on the projected future cli-

Table 3.1: Analyzed time periods

Period Name	Time	Length of Available Data	Notes
Historical	1850 - 2014	165 years	
Future SSP5-8.5 Scenario	2015 - 2100	86 years	years 2015 - 2020 were neglected as a spin-up period
Last Glacial Maximum	21,000 - 19,000 ka BP	500 years	
Mid-Holocene	8,200 - 4,300 ka BP	500 years	

mate until the end of the century. A model starts directly after the historical simulation (1/1/2015) and ends after 86 years on 1/1/2101. For the CMIP6 project, the RCPs of the previous CMIPs were updated to the Shared Socioeconomic Pathways (SSPs). These new pathways consist of socioeconomic reasoning for the developments (also called narratives), which describe different possible socioeconomic developments. There are the sustainable SSP1 path, the “Middle of the road” SSP2, the SSP3 with “regional rivalry”, SSP4 with an increase in inter-country inequalities, and finally the fossil-fuel-driven SSP5 pathway (Michael Böttinger, 2015). To additionally improve the application methods of the model results, some Shared Climate Policy Assumptions (SPAs)

can be used. Since most of these pathways violate climate goals, these assumptions allow us to find the right combinations of climate political decisions to stay within the set boundaries.

This thesis focuses on the SSP5 scenario. Such a pathway includes technological and innovative processes based on fossil-fuel resources. High coal use and an energy-intensive lifestyle characterize daily life, as well as a growing world economy. Some local environmental processes are assumed to be solved, like the degrading air quality.

To allow the depiction of multiple possible future scenarios and to increase the available model spread, the individual SSP pathways are combined with different additional radiative forcings until 2100 due to changes in the GHG concentrations (also called forcing levels). The right plot in Figure 3.1 shows the assumed carbon dioxide concentrations for the individual scenarios.

Finally, after combining these factors a scenario matrix (see the left plot in Figure 3.1) is created. Usually the colored combinations in Figure 3.1 (SSP1-2.6, SSP2-4.5, SSP3-7.0, SSP5-8.5) are used, because they are mostly comparable with the RCPs[1].

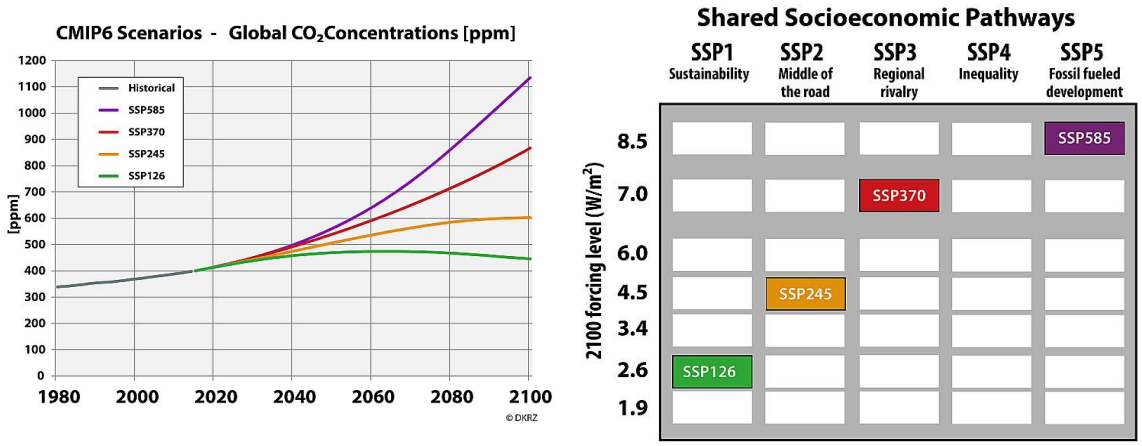

Figure 3.1: Right: Assumed CO_2 concentrations under the most frequently employed scenarios. Left: Scenario Matrix showing the different Shared Socioeconomic Pathways (SSPs) and possible forcing levels by 2100. The colored boxes are the favored combinations because of their comparability to the RCP scenarios of the CMIP5 project from Michael Böttinger (2015)

The Paleoclimate Modelling Intercomparison Project (PMIP) studies the response of the climate system to different forcings and feedbacks by combining model simulations and paleoclimate reconstruction data. From the available relatively well-documented time periods (the last millennium prior to the industrial epoch, the mid-Holocene, the Last Glacial Maximum, the Last Interglacial and the mid-Pliocene Warm Period), the focus of this thesis will be on the Last Glacial Maximum (LGM, 21,000 years ago) and the mid-Holocene (6,000 years ago) (Pascale Braconnot, 2015). The individual model specifications of the periods are summarized in the following table Table 3.2.

3.2 Methods

In the following, the used mathematical and statistical methods are described. The Table 7.2 lists the relevant variables with a description and their resolution.

[1] only the SSP3-7.0 scenario was created to close the gap between the RCP6.0 and RCP8.5 scenarios.

Table 3.2: Specifications for the CMIP6 paleoclimate models for the mid-Holocene and LGM from Kageyama (2017a) and Kageyama (2017b)

Specification	mid-Holocene	LGM
Orbital Configurations	eccentricity = 0.018682	eccentricity = 0.018994
	obliquity = 24.105°	obliquity = 22.949°
	perihelion-180° = 0.87°	perihelion-180° = 114.42°
	Date of vernal equinox: March 21 at noon	
Trace Gases	CO_2 = 264.4 ppm	CO_2 = 190 ppm
	CH_4 = 597 ppb	CH_4 = 375 ppb
	N_2O = 262 ppb	N_2O = 200 ppb
	Chlorofluorocarbons = 0	
	O_3 same as in piControl	
Solar Activity	Same as in piControl[2]	
Ice Sheets	Same as in piControl	Modified
Topography and Coastlines	Same as in piControl	Modified
Aerosols/Vegetation	Modification depend on model complexity and configuration of historical experiments	

3.2.1 Analysis of the Large-Scale Climatic Conditions

To get a better idea of the climate conditions in the different time periods and to quantify changes, some descriptive variables were analyzed. Details on them can be found in Table 7.2. From the data of the individual time periods, the DJF months were selected and a temporal mean was calculated.

3.2.2 Strength of the Thermohaline Circulation

To calculate the strength of the thermohaline circulation, the meridional streamfunction for the Atlantic and Arctic oceans was used. The available data was a longitudinal average over the individual basins. From this, the maximum value over the entire depth of 4000 m at 45.5°N was located. The original unit of $\mathrm{kg\,s^{-1}}$ was transformed into Sv (1 Sv = $10^6\,\mathrm{m^3\,s^{-1}}$). Since the here used indicator only describes the situation in the North Atlantic, the term AMOC (Atlantic Meridional Overturning Circulation) will be used to describe the oceanic circulation.

3.2.3 Calculation of the Storm Tracks

There are two conventional ways to devise the storm track. One is to identify and track each cyclone path (the so-called Lagrangian method) and the other is to identify the variance of certain atmospheric variable(s) at each local grid point (Eulerian method). While the former gives precise information on individual storms, it is computationally demanding. An easier and more efficient but less detailed way was employed here by using the mean sea level pressure (MSLP) data. For the following analysis, the CMIP6 data was first merged and then the relevant geographical area

was selected (here 100°W to 60°E and 20° - 80°N). After deleting the 29th of February, the data was detrended. Then, a 2-6-day bandpass filter was applied to the December to February (DJF) period, which covers the synoptic time range (Ulbrich et al., 2009). Finally, the standard deviation is calculated, to show the most often taken path of the cyclones.

3.2.4 Relationship between the Atlantic Meridional Overturning Circulation (AMOC) and the Storm Tracks

To investigate the connection between the AMOC and the storm tracks both a composite analysis and a linear regression were employed. The linear regression was only possible for the periods since the pre-industrial times because the climate of the long past exhibited no long-term trend and there was only one model available with the required 6 hourly pressure data for the storm tracks. Therefore the composite analysis was added to investigate the relation for all four time period.

Composite Analysis

To carry out the Composite analysis, the available data has to be split into multiple parts. For this thesis, the timeline of the monthly AMOC was first converted into yearly averages and then separated into three parts by the 66th and 33rd quantile. As an example, the historical period is shown in Figure 3.2 with colored lines indicating the quantile. Based on the tertile, the years with a strong (above the red line in Figure 3.2), weak (green colored in Figure 3.2), and in-between circulation strength were chosen. Afterwards, the corresponding storm track years were selected and a mean over the upper, middle, and lower tertile were calculated. The result shows the mean behavior of the storm tracks during strong and weak AMOC years and the difference (33rd-66th tertile) indicates the regional changes of the storm tracks for a weakening of the circulation.

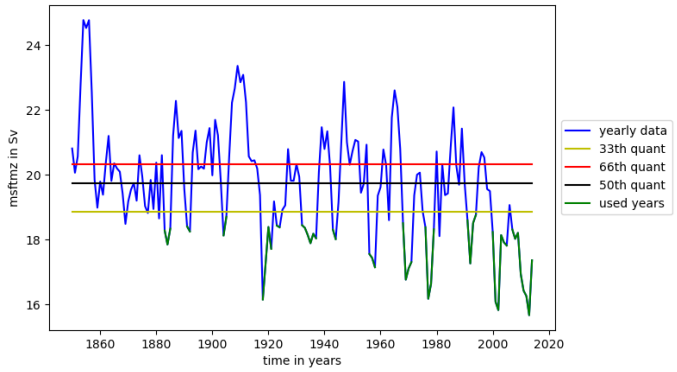

Figure 3.2: Plot showing the AMOC strength for the historical period as an example to illustrate the composite method. Additionally shown are the 33rd (yellow line), the 66th (red line) and the 50th (black line) quantile, and the data used for the weak-AMOC years (green).

Linear Regression

To visualize the correlation between the change of AMOC and the change of the storm tracks, a linear regression was performed. First, the difference of the AMOC between a period of the historical (1980-2000) and a period of the future times (2080-2100) was calculated. Then, the independent variable (here the oceanic streamfunction maximum) was normalized to create patterns

linked to one standard deviation (std) of the spread between the models. Afterward, the storm track response pattern (2080-2100 minus 1980-2000) was calculated. This was carried out for the models with available 6-hourly sea surface pressure data, which are highlighted in Table 7.1 with bold letters. For each grid point, a linear regression between the mean AMOC and storm tracks over the multiple models are calculated and the slope quantifies this ocean–atmosphere relationship.

By replacing the storm-track variable with the SAT, the atmospheric changes impacted by the SST, and similarly, with the sea ice coverage due to the atmosphere-ocean interactions are depicted. Finally, the eastward winds in 850 hPa were analyzed similarly to investigate the impact of a changing AMOC on low-level latitudinal winds.

4 Results

Here the obtained results of the large-scale climate conditions, the characteristics of the Atlantic Meridional Overturning Circulation and the European storm tracks, and their connection are presented.

4.1 Depiction of the Atlantic Meridional Overturning Circulation

4.1.1 Latitudinal Position of the Atlantic Meridional Overturning Circulation

In the literature, Atlantic Meridional Overturning Circulation strength is conventionally defined as the maximum meridional streamfunction at a fixed latitude between 25°N and 45°N. To decide which latitude is the suitable choice, the circulation strength was first computed for the most northern and southern latitudes. In this thesis, before further analyses are employed, a comparison between the oceanic strength at these two locations is examined. Figure 4.1 depicts the development of the AMOC in the historical period until 2014, followed by the projection under the Shared Socioeconomic Pathway5-8.5 scenario until the end of the century. Especially in the first half of the shown years, the data values are similar, despite a greater variability at 45°N. Under the SSP5-8.5 future scenario, a larger difference becomes obvious, with the more southern-defined AMOC showing a smaller weakening compared to its northern counterpart. Possible reasons for the differences are the greater influence of the stronger ice melting at high latitudes, affecting the 45°N AMOC more effectively. With a weaker oceanic circulation, the STG will probably become stronger, additionally dampening the reduction in the oceanic meridional overturning mass flow at 25°N (Menary et al., 2020). However, since the differences are relatively small, the AMOC strength will be derived at 45°N for the remainder of this thesis. An exception is the LGM, where a large ice sheet cover precludes using this latitude. Therefore will the analysis of this period be performed with the AMOC results from 25°N.

To better visualize the AMOC and its changes, a vertical cross-section at 45°N is produced in Figure 4.2. This cut of the Atlantic Ocean shows the vertical structure of the AMOC, which can mostly be found in the upper 2 km and has its greatest mean strength at approximately 1000 m. Close to 40°N the maximum overturning of the AMOC can be found, supporting the above-made decision to calculate the circulation strength at 45°N. The right plot displays the projected changes under the SSP5-8.5 scenario. Especially in the mid-latitudes the greatest change takes place and could result in a mean AMOC reduction of 14 Sv.

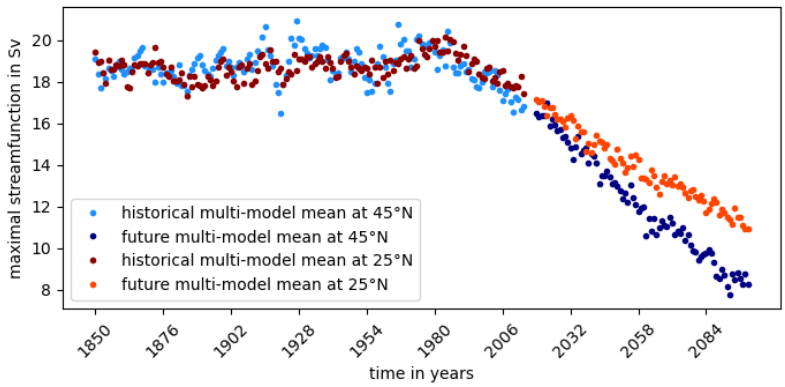

Figure 4.1: Development of the AMOC strength at 45°N (red and orange) and 25°N (light and dark blue) for the historical (dark red and light blue) and future (orange and dark blue) periods. The spin-up period of 2015-2020 is masked.

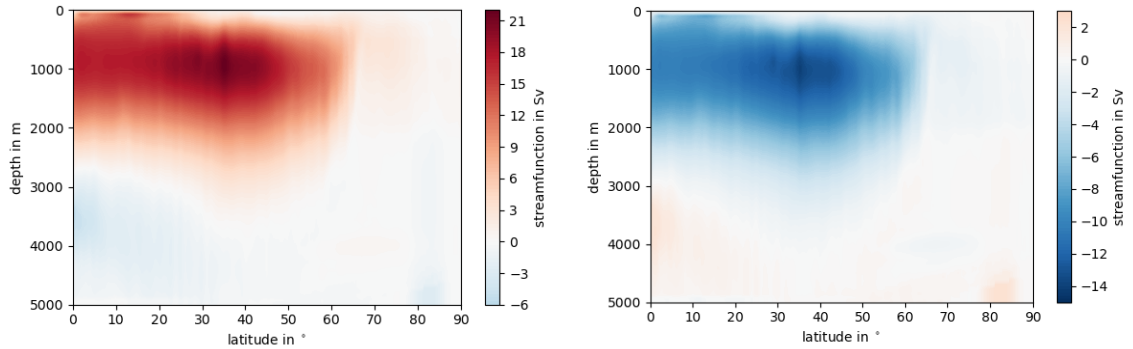

Figure 4.2: Vertical structure of the AMOC in the North Atlantic for the historical period (left) and predicted changes under the SSP5-8.5 scenario at the end of the century (right).

4.1.2 Comparison of the Employed Models

All the employed models simulated Atlantic Meridional Overturning Circulations (AMOCs) of different strengths and the historical mean of this quantity is depicted in Figure 4.3. Red dots are models that contain the 6-hourly mean sea level pressure data needed for the storm track analysis. Some models (FGOALS-g3) have a stronger than average and other models (INM-CM4-8 and INM-CM5-0) have a weaker than average AMOC. However, the remaining models show similar strengths.

The single model used for the paleoclimate analysis (red cross) seems to have a moderate oceanic circulation strength and should therefore produce relatively meaningful results.

4.2 Description of the Historical Conditions

The term "historical times" encompasses the time since the pre-industrial in 1850 until the year 2014. To better understand the changing climate, the conditions in the past 165 years shall be presented first.

The plots in Figure 4.4 show the mean near-surface air temperatures (left) and the sea surface temperatures (right) between 1850-2014. In the left plot, the influence of the ocean on the air temperatures can be seen. For regions at the same latitude, temperatures are warmer over the

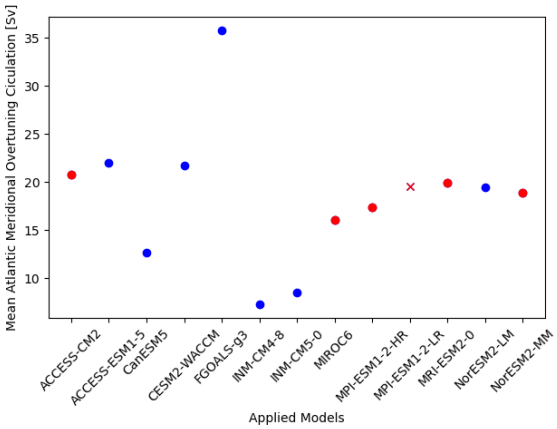

Figure 4.3: Mean AMOC strength of different models used for the historical period, which contained monthly near-surface air temperature and eastward wind data for the linear regression. Models with 6-hourly mean sea level pressure data, needed for the calculation of the storm tracks, are distinguished in red. The red cross is the model used for the paleoclimate analysis.

ocean than over the continents due to the higher heat capacity of the water and the atmosphere experiences less cooling during the night and in winter. Tropical heat being transported through the AMOC also leads to higher air temperatures over Europe compared to North America. This is additionally supported by the Sea Surface Temperatures (SSTs). Comparing the higher sea temperatures with the path of the AMOC in Figure 2.2 reveals the footprint of the AMOC is characterized by warmer ocean surface waters strongest visible east of southern North America and west of Europe.

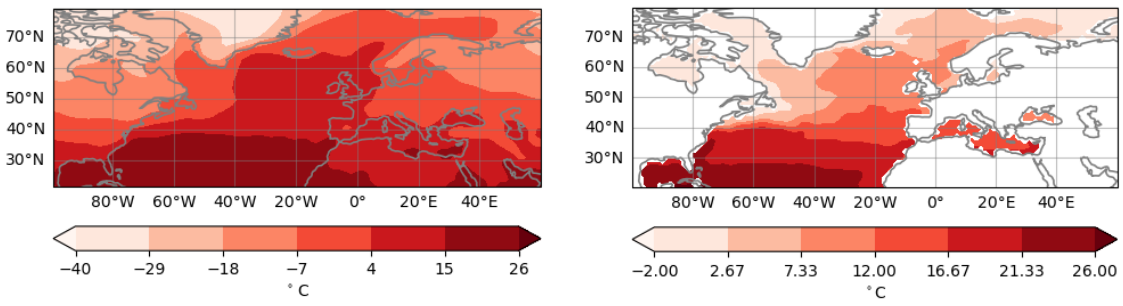

Figure 4.4: DJF mean of the near-surface air temperatures (left) and sea surface temperatures (right) in the historical time period.

Evaporation and precipitation (shown in Figure 4.5) are also influential to and influenced by the current climate. Both are the strongest over the oceans, mainly because of the higher moisture availability and both have their maximum east of the North American coast.

For the evaporation, wind speed and surface temperatures play an important role. Because of lower friction values and fewer obstacles (like buildings, trees, and mountains), the wind is generally stronger over the ocean parts. On top of the wind effect, the warmer SSTs associated with the Gulf Stream's heat transport also contribute to the high evaporation in the North Atlantic.

Strong and heavy precipitation is mostly linked to storms, including tropical and extratropical cyclones. These stormy systems generate rain, as can be seen in the precipitation maximum.

Comparing the precipitation region with the historical storm tracks (right plot in Figure 4.7) reveals that the central to northern North Atlantic high precipitation area coincides with the storm tracks. This suggests that the cyclonic systems strongly influence the precipitation. Since orography plays an additional role, the precipitation is slightly higher in coastal regions like Greenland, Norway, Great Britain, and Portugal.

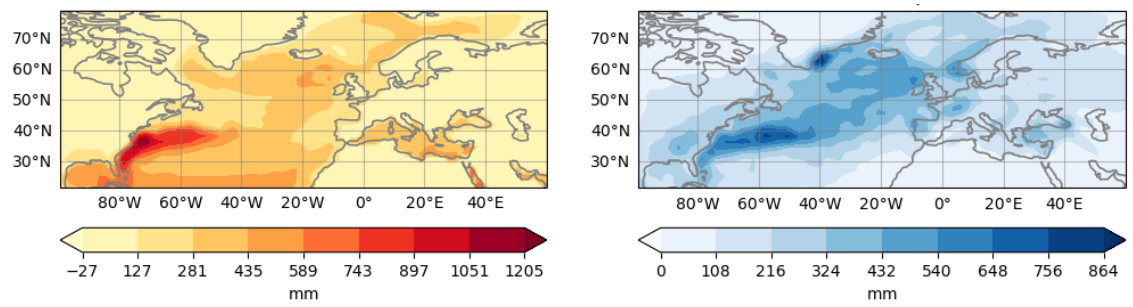

Figure 4.5: DJF mean of the evaporation (left) and precipitation (right) in the historical time period in mm.

Sea Surface Salinity (SSS) is of great importance for the ocean density and therefore for the deep water formation of the AMOC. Inland seas like the Baltic Sea, Mediterranean Sea, the Black Sea, or the Hudson Bay are more subjected to the regional climate. In the subtropical regions, strong evaporation leads to a reduction in the SSS, while higher latitude inland seas experience a freshening due to glacial melting and river runoff. The left figure in Figure 4.6 shows this difference the most clearly between the very salty Mediterranean (SSS $\approx$ 38 PSU) and the much fresher Baltic Sea (SSS $\approx$ 10 PSU). The salinity values of the open ocean are relatively uniform, ranging from 30 to 35 PSU. Around the still ice-covered continents, the ocean surface is fresher. Examples are the northeastern and western coasts of Greenland and the northeastern coast of North America.

The jet stream can be expressed in terms of the eastward winds in 250 hPa, and the historical conditions are shown on the right in Figure 4.6. In the mean, the polar jet is split over the eastern North Atlantic, with high wind speeds over the eastern coast of North America. These larger wind speeds in addition to the land-sea contrast at the North American coast and the oceanic heat and moisture reservoir are ingredients for a cyclone formation and some of the reasons, why the North Atlantic storm tracks have their greatest strength over this region.

In this historical climate, the AMOC experienced no clear trend but instead depicted some short-term (ocean-wise, meaning variability of years to decades) variability. From 1850 to 1990 the overall trend was slightly positive, with some greater changes in between. Around 1920 for example a stronger weakening of 2.5 Sv can be seen, but in 1933 the AMOC was more intense than the average by 2 Sv. Larger trends are the ongoing warming from the 1940s to 1985, followed by the circulation weakening trend, expected to continue into the future.

The historical North Atlantic storm tracks have their maximum on the northern tip of North America and extend over the North Atlantic towards Great Britain and Scandinavia. This indicates that most storms form off the western coast of North America, where warm and moist SSTs combined

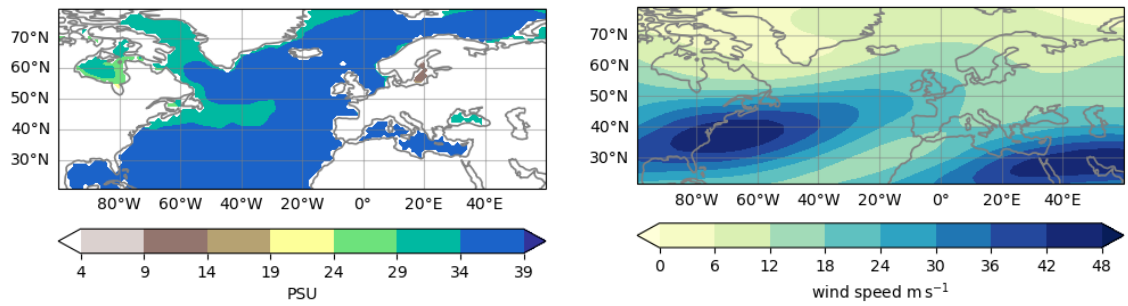

Figure 4.6: DJF mean of the Sea Surface Salinity in PSU (left) and eastward winds in 250 hPa in m s^{-2} (right) in the historical time period.

with strong baroclinicity. Additional effects like reduced friction and orographic instability play a secondary role. After their formation, most cyclonic systems travel northeastward towards Europe.

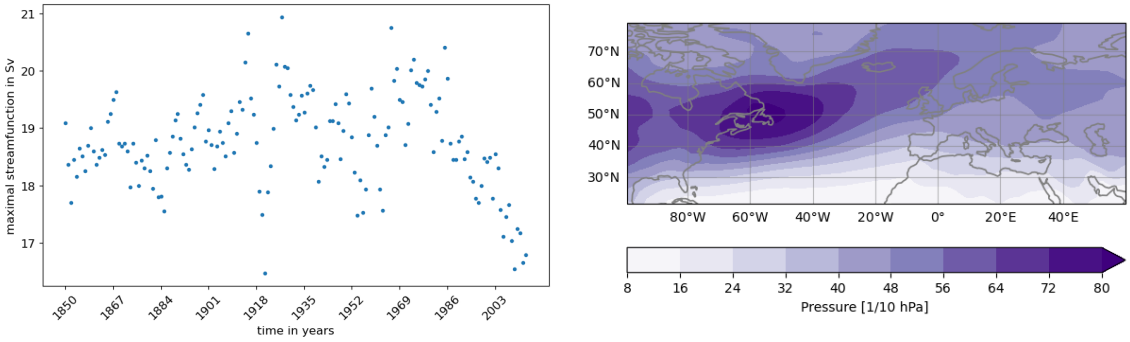

Figure 4.7: Maximum meridional overturning streamfunction at 45°N and standard deviation of the 2-6-day bandpass filtered mean sea level pressure data resulting in the AMOC (left) and the storm tracks (right) respectively for the historical period. For the method of calculation, see 3.2.2 and 3.2.3.

4.3 Analysis of the Future

4.3.1 Climate Change Impacts

With increasing evidence, the warming of the earth's climate becomes harder to dispute. This change will impact various parts of the climate system, some collected here.

The most well-known change is the near-surface air temperature, shown in the left plot in Figure 4.8. Over large parts of the North Atlantic Ocean, weaker warming in temperatures is projected, while stronger warming is predicted over the continents. Reasons for this are the larger heat capacity and greater inertia of the water, meaning that the ocean takes longer to reflect atmospheric temperature changes. With the stronger high latitude warming due to the polar amplification, the meridional temperature gradient between the tropics and the polar regions will weaken. This reduces the northward heat transport by the ocean, adding to the smaller warming over the North Atlantic region.

The atmospheric water vapor capacity is closely linked to the temperature via the Clausius-Clapeyron equation and suggests a vapor increase of 7 % per °C warming (Lee et al., 2021). With the expected warming of the future atmosphere, the aforementioned equation predicts an

increase in the water vapor content that the atmosphere can contain. The higher moisture content is depicted in the right plot in Figure 4.8 with the greatest increase over the Gulf Stream south of North America.

The eastward winds in 250 hPa describe the jet stream, and the left plot in Figure 4.9 shows the

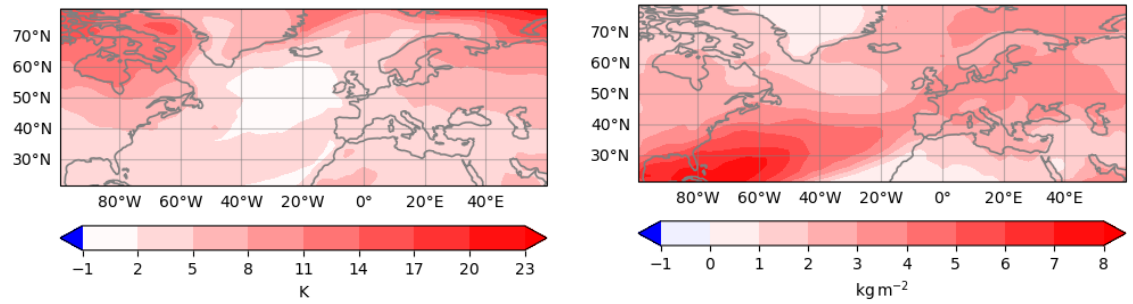

Figure 4.8: Changes of the near-surface air temperature in K (left) and the atmospheric water vapor content in $\mathrm{kg\,m^{-2}}$ (right) compared to the pre-industrial period by the end of the century under the SSP5-8.5 scenario.

probable changes by the end of the century. It can be seen that the mid-latitude jet stream will experience a strengthening over the Gulf of Mexico and the central North Atlantic. Compared to the pre-industrial conditions, this suggests a latitudinal narrowing of the jet and a shift toward Europe.

For the oceanic circulation, the density and therefore the sea surface temperature and salinity are of great importance. The change in SST in the future (not shown here) mostly depicts an increased warming trend in the high latitudes. Predicted salinity changes are shown in the right plot in Figure 4.9. Especially around Greenland and in the eastern North Atlantic the salt content will likely be reduced. One reason is the stronger ice melting, another cause is the weaker northward salt transport from the saline subtropics.

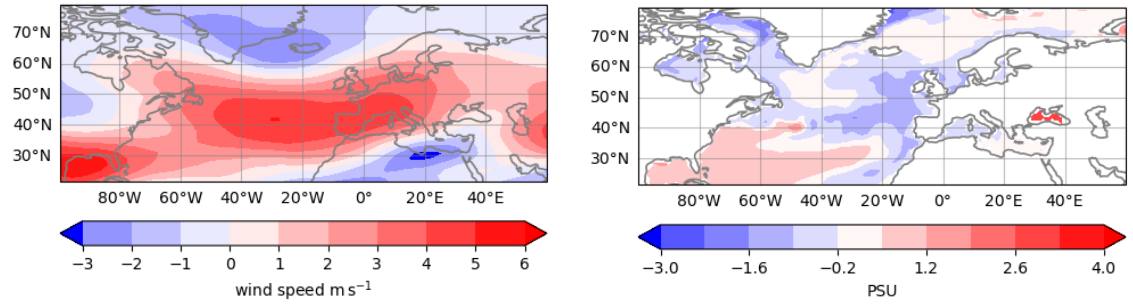

Figure 4.9: Changes of the eastward wind in 250 hPa in $\mathrm{m\,s^{-2}}$ (left) and the Sea Surface Salinity in PSU (right) compared to the pre-industrial period by the end of the century under the SSP5-8.5 scenario.

4.3.2 Climate Change Impact on the Storm Tracks and the Atlantic Meridional Overturning Circulation

The described climate change impacts influence both the AMOC and the European storm tracks. Their projected differences are depicted in the following plots.

Northward Oceanic Heat Transport

The ocean plays an important role in the northward transport of the greater solar energy of the tropics to the polar regions. Especially in the subtropics, this process is of importance, as can be seen in Figure 4.10. In the figure, the strength of the oceanic transport is depicted for the four relevant time periods, and in the NH the greatest transport takes place between 20° and 30°N.

The right plot in Figure 4.10 depicts the difference in strength compared to the pre-industrial. When analyzing the historical (blue line) and the future (orange line) changes, it becomes visible, that the energy transfer reduction on the NH is strongest under the SSP5-8.5 scenario with the largest reduction around 25°N. This is caused by the reduced meridional temperature gradient in the warmer climate, which weakens the northward heat transport.

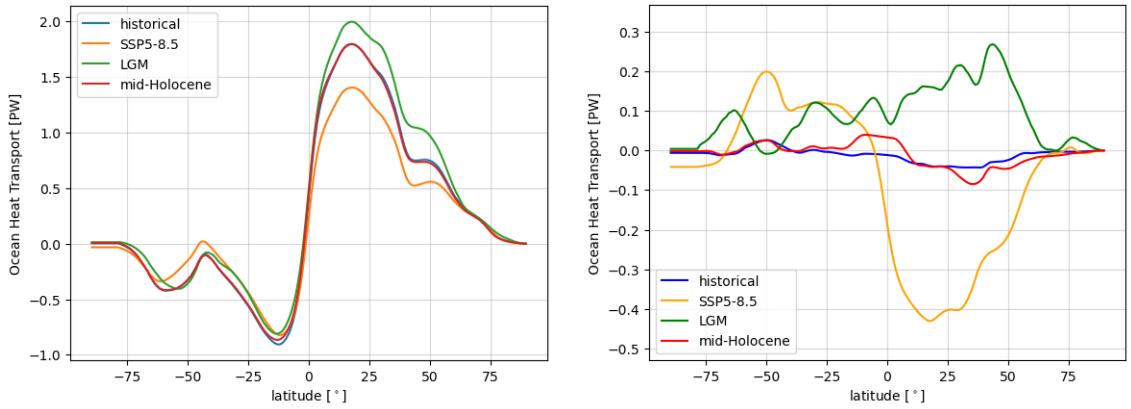

Figure 4.10: Latitudinal cut of the total oceanic northward heat transport (left) and difference to the pre-industrial (right) in PW for the historical (blue line), the SSP5-8.5 (orange line), the mid-Holocene (red line), and the LGM (green line).

Atlantic Meridional Overturning Circulation

To show the temporal development, a multi-model mean of the models in Table 7.1 is created and can be found in Figure 4.11. There it can be seen, that the AMOC showed little variability in the historical period. A strengthening occurred around 1918, followed by a strong weakening and a return to larger values afterward. Then in the 1990s, another increase in AMOC strength was observed, continued by a still ongoing weakening trend. This temporal evolution continues into the future period, where an almost linear decline is predicted. Compared to the historical strength between 17 and 21 Sv, the model mean shows a weakening trend and a projected maximal AMOC mass flow of 8 Sv by the end of the century.

The small strengthenings during the 20th century were probably caused by some long-term natural variability, but they cannot explain the negative trend that became obvious in the late 1990s. There are multiple reasons for the weakening of the AMOC. On the one hand, the high-latitude temperatures are increasing, both in the sea and the air. On the other hand, the melting of the ice sheets, sea ice, and glaciers leads to a freshening of the waters. These two developments decrease the deep water formation by reducing the surface densities and enhancing the vertical stratification. With less dense water sinking, a smaller amount of subtropical water can flow northward, resulting in a weaker AMOC. The polar amplification means a smaller meridional temperature gradient

which reduces the required northward heat transport. Therefore this branch of the AMOC is also weakened.

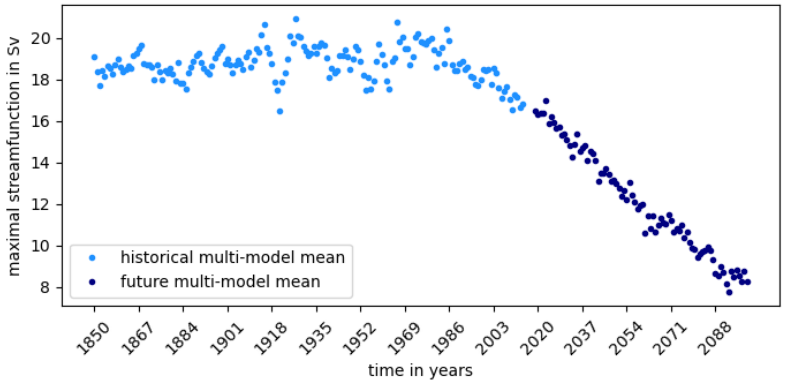

Figure 4.11: Development of the AMOC strength at 45°N for the historical (light blue) and future (dark blue) periods. Only the 6 models, which also have the 6-hourly pressure data available, were used for this multi-model mean. The spin-up period is masked. For more information on the models see Figure 4.3

Storm Tracks

As previously described, the storm tracks will most likely experience large-scale changes with the warming climate. By using the above-mentioned methods (chapter 3), these developments are depicted in Figure 4.12. Here the left side shows the storm track during the pre-industrial period in the years 1850-1880, and the right plot displays changes by the end of the century under the SSP5-8.5 scenario. In the pre-industrial time, the strongest cyclone density could be found near the northeastern edge of North America, extending to the east towards Iceland. At the end of the historical period (see Figure 7.5), a slight southeastward shift of the storm tracks over the North Atlantic Ocean took place. Additionally, the track was intensified north of Scandinavia and Eastern Europe. The pattern for the future projects an even stronger strengthening over the central North Atlantic and a further southeast intrusion into Europe. Over the entire European continent, an increased storm track is simulated. To the north and south, the storm track might be reduced, indicating a weak latitudinal narrow.

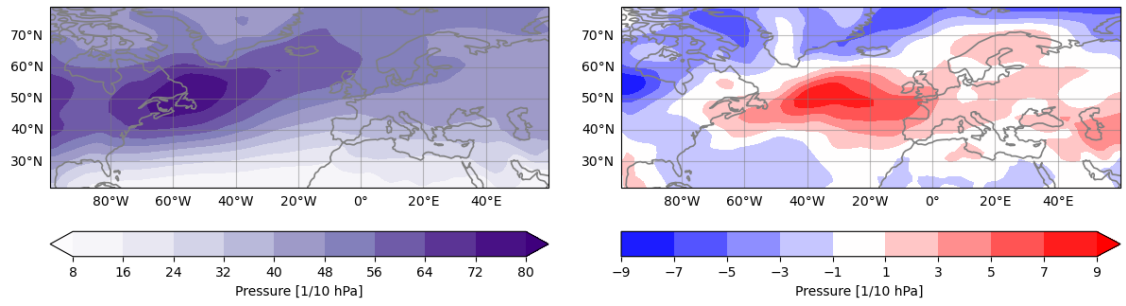

Figure 4.12: Storm track for the pre-industrial period (left) and change of the storm tracks at the end of the century for the SSP5-8.5 scenario compared to the pre-industrial storm tracks (right). For further information on how the storm tracks were calculated, see 3.2.3.

4.3.3 Linear Regression

To characterize the expected changes of the storm tracks caused by a changing AMOC, a linear regression was performed. Details for this method can be found in chapter 3.2.4 and the resulting plots are depicted in Figure 4.13. The hatched regions indicate areas with a higher significance.

The upper figure shows the regression slope between the development of the AMOC and the change of storm track. They suggest a strengthening and northeastward shift of the storm tracks over the eastern North Atlantic and Europe in response to a weakening of the AMOC.

The plot on the left side of the second line shows the regression slope of the near-surface air temperatures in a changing climate. Here a warming over the North American continent can be seen. However, of greater interest is the cooling trend over the northern part of the North Atlantic Ocean because of the reduced northward oceanic heat transport with a weaker AMOC.

Finally, the third plot depicts the results of the linear regression of the eastward winds in 850 hPa, to show the impacts of the storm tracks onto the low-level westerlies. This analysis indicates an increase in wind speed of the winds over Europe as expected from the stronger storm tracks above. Over the Mediterranean, a weakening of the low-level westerlies is probably linked to the weaker reduction of the storm track in this region.

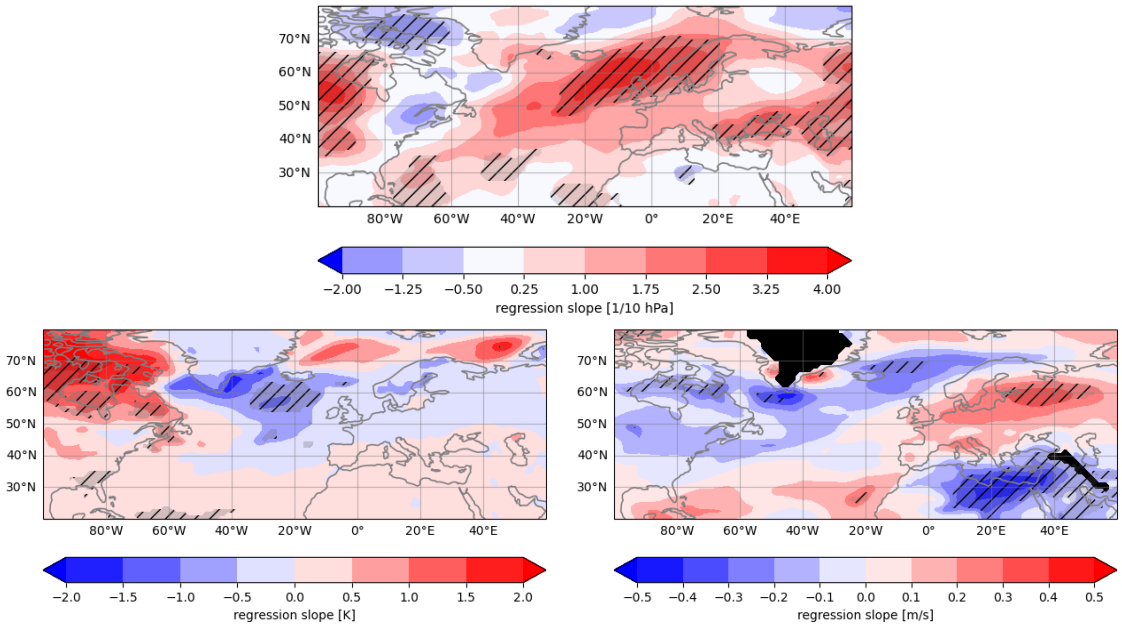

Figure 4.13: Plot of the multi-model regression slope between the negative changes of the AMOC and changes of the storm track (top), near-surface air temperatures (bottom left), and eastward wind in 850 hPa (bottom right) over the North Atlantic and Europe. The black shading indicates regions with a high topography, which created problems in the plotting of the 850 hPa winds. The hatched regions indicate a 90% statistical significance resulting from a Student's t-test. For further information on how the linear regression was performed, see 3.2.4.

4.4 Paleoclimatology

The climates of the mid-Holocene and the LGM were partly very different than the current climate conditions. To get a better overview of the settings, first, the oceanic and atmospheric conditions of

the paleoclimate periods are described and the states of the AMOC and storm tracks are analyzed. The plots showing the pre-industrial conditions can be found in the Appendix.

4.4.1 Large-Scale Climate Conditions

The first plots in Figure 4.14 show the difference of the incident shortwave radiation at the top of the atmosphere for the mid-Holocene and the LGM compared to the pre-industrial times. Incoming solar radiation during the LGM was similar to the amount in 1850-1880. But in the mid-Holocene period, the high latitudes received more energy. The tropical regions meanwhile experienced a strong reduction in solar forcing by 15 $\mathrm{W\,m^{-2}}$ similar to the description in subsection 2.5.2.

When comparing the near-surface air temperature of the paleoclimate periods to 1850-1880, dif-

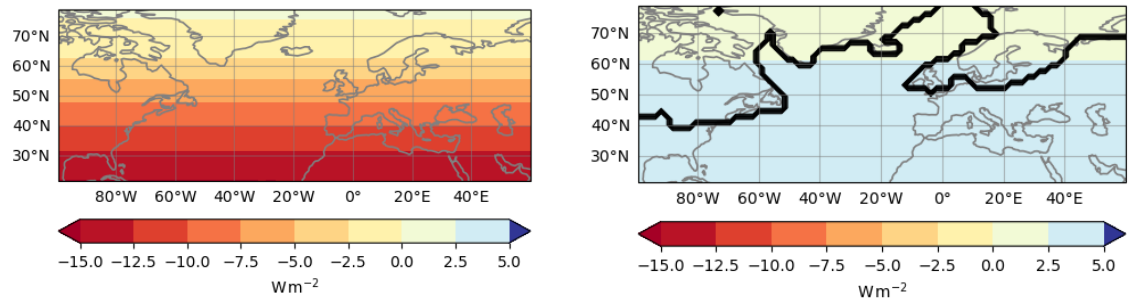

Figure 4.14: Top of the atmosphere incident shortwave radiation difference of the mid-Holocene (left) and the LGM (right) compared to the pre-industrial period for DJF in $\mathrm{W\,m^{-2}}$. The black line indicates the ice edge during the LGM.

ferences become visible as can be seen in Figure 4.15. While the mid-Holocene experienced only a slightly colder climate with some locally larger deviations, the changes during the LGM were more pronounced. During the last glacial maximum, air temperature reductions up to -39°K were possible.

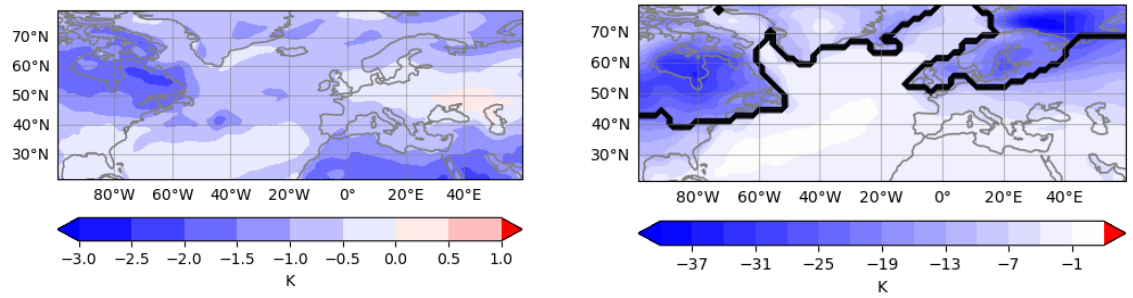

Figure 4.15: Near-surface air temperature difference of the mid-Holocene (left) and the LGM (right) compared to the pre-industrial period in Kelvin. Note the different value ranges between the plots. The black line indicates the ice edge during the LGM.

In the following plots in Figure 4.16, the changes of the eastward wind in 250 hPa are shown. The mid-Holocene experienced a slight intensification of the jet stream, stronger over the North American and European continents. During the LGM, winds in the upper troposphere were more

strongly enhanced, especially over the northwestern North Atlantic, meaning an intensification of the jet stream.

During the cooler mid-Holocene and much colder LGM, the water vapor content in the atmo-

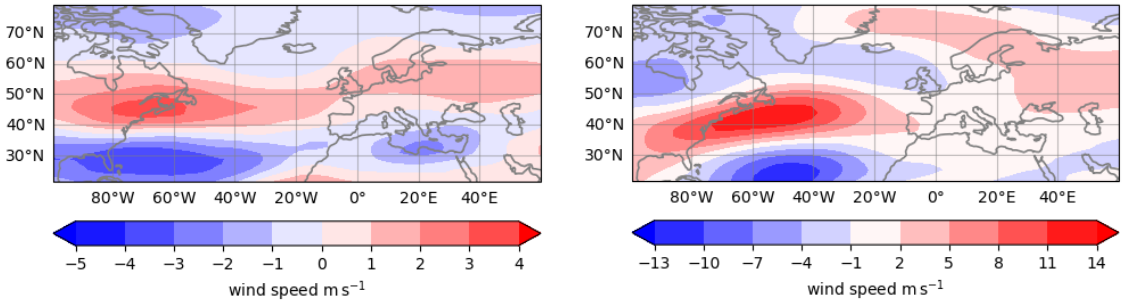

Figure 4.16: Eastward wind at 250 hPa depicting difference of the jet stream during the mid-Holocene (left) and the LGM (right) period compared to the pre-industrial time in $\mathrm{m\,s^{-2}}$. The black line indicates the ice edge during the LGM.

sphere was (much) lower according to the Clausius-Clapeyron-equation. Figure 4.17 shows the differences compared to the pre-industrial for the two periods. Especially, the LGM experienced a large-scale atmospheric drying, meaning that storms contained less moisture and could therefore transport less heat poleward.

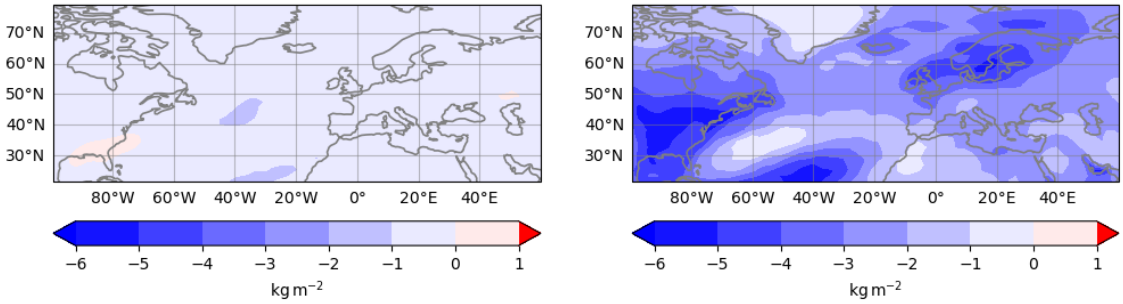

Figure 4.17: Atmospheric water vapor content difference of the mid-Holocene (left) and the LGM (right) compared to the pre-industrial period in $\mathrm{kg\,m^{-2}}$. The black line indicates the ice edge during the LGM.

4.4.2 Aspects of the Storm Tracks and the Atlantic Meridional Overturning Circulation

Northward Oceanic Heat Transport

The Northward Oceanic Heat Transport is an important part of the AMOC and can both influence and is influenced by the climate conditions. Figure 4.10 depicts the absolute transport (left) and projected changes relative to 1850-1880 (right). The mid-Holocene energy transfer was strongest at 20°N and had a strength very similar to the pre-industrial time, as can be seen in the left plot in the figure. During the LGM period, the oceanic northward heat transport was greatly increased and almost 15 % stronger than under the pre-industrial conditions.

Atlantic Meridional Overturning Circulation

Unlike the historical and future oceanic circulation, the paleoclimate AMOC shows no discernible trend. The Figure 4.18 shows the yearly variations during the mid-Holocene and the LGM. In the colder period, the AMOC had a stronger mean overturning circulation of 23.3 Sv compared to the mid-Holocene strength of 19.8 Sv.

During the LGM the sea and air temperatures were significantly lower than present conditions. In combination with the higher salinity because of the more extensive ice sheet cover, the deep water formation in the polar regions was likely greatly enhanced. In addition, the larger difference between high and low-latitude temperatures required a stronger northward heat transport and therefore a strengthening of the oceanic overturning circulation. The mid-Holocene has similar temperatures and ice cover to the pre-industrial time, resulting in an AMOC with comparable strength to the beginning of the historical period.

To ease comparing the AMOC for the different time periods, a long time series for all investi-

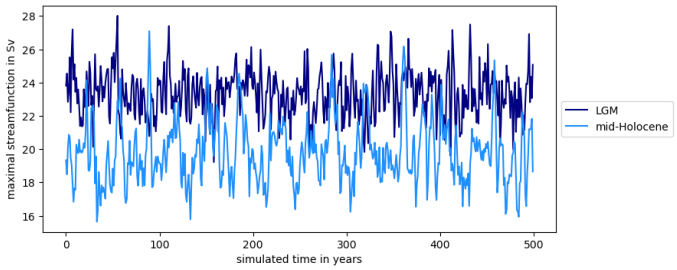

Figure 4.18: Temporal Development of the AMOC during the mid-Holocene (light blue) and the LGM (dark blue). The mid-Holocene circulation is depicted at 45°N and the LGM one at 25°N.

gated periods (LGM, Mid-Holocene, historical, and SSP5-8.5) has been created. When analyzing the mean streamfunction for all the periods (see Figure 4.19), the stronger overturning circulation during the LGM stands out most. The mid-Holocene and the beginning of the historical period have similar strengths with 19.8 Sv and 19.7 Sv water transport, respectively. But in the current time period, there is a circulation reduction towards its end which continues in the future. Under the SSP5-8.5 scenario, the AMOC will be reduced further, resulting in a circulation strength of approximately 8 Sv by the end of the century and have a resulting period mean value of 11.2 Sv.

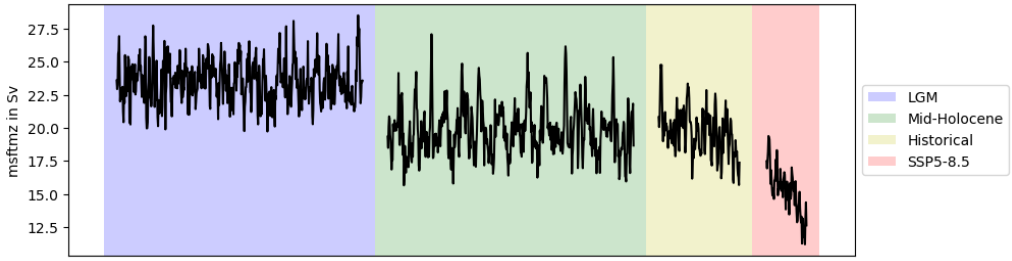

Figure 4.19: Yearly AMOC development for the four relevant time periods, each highlighted by a different color.

Storm Tracks

Under different climate conditions, the storm tracks were also different. Plots in Figure 4.20 show the respective differences between the mid-Holocene and the LGM to the pre-industrial year.

The mid-Holocene storm tracks (left plot) show a strengthening over northern North America, the central North Atlantic, and northern Europe and a weakening over Iceland and the west of Greenland.

During the LGM the ice sheets covered large parts of the continents and influenced the storm tracks. The greatest storm track changes can be found over the central North Atlantic, reaching along the southern edge of the FSIS ice sheet over the Mediterranean towards eastern Europe.

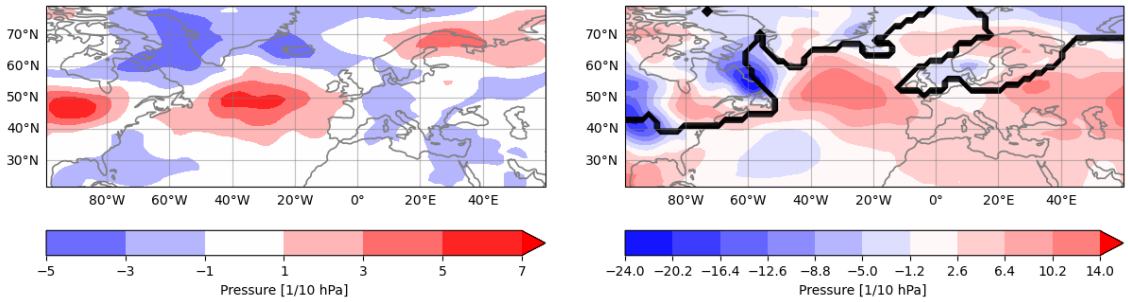

Figure 4.20: Storm track differences of the mid-Holocene (left) and the LGM (right) compared to the pre-industrial period. Note the different color bars between the two plots. The black line indicates the ice edge during the LGM.

4.5 Composite Analysis of the Connection between the Storm Tracks and the Atlantic Meridional Overturning Circulation

In this section the results of the composite analysis (see Figure 4.21) shall be presented. For further information on how the evaluation was performed see subsubsection 3.2.4.

The composite analysis does not assume a linear relationship between the variables, unlike the linear regression. This promises more reliable results especially for the paleoclimate because here the AMOC has no long-term trend. Additionally, the storm tracks and AMOC are not linearly coupled, but instead influence each other via multiple in-between variables. The linear regression from Figure 2.15 and Figure 4.13 is also not doable for the past climates because only one model with the required sea level pressure data was available. Therefore, a multi-model analysis was impossible for paleo periods. With the composite analysis, the different behaviors of storm tracks between weaker and stronger AMOC years within the same period of time are to be examined. The goal is to see if the signal remains physically consistent despite the changes in the background states. Since the lower (below the 33rd) tertile was subtracted from the upper (above the 66th tertile), the plots show the storm track changes due to a weakening of the AMOC.

Both the historical and the future composite show (moderate-) strong positive values over the North Atlantic between 45-60°N. The paleo periods show both a weaker trend and a greater variability, but display the same positive region over the northern North Atlantic. The main reason for

this difference in the paleoclimate is probably the greater uncertainty. But all periods indicate a strengthening of the storm track over the central North Atlantic during times of a weaker AMOC.

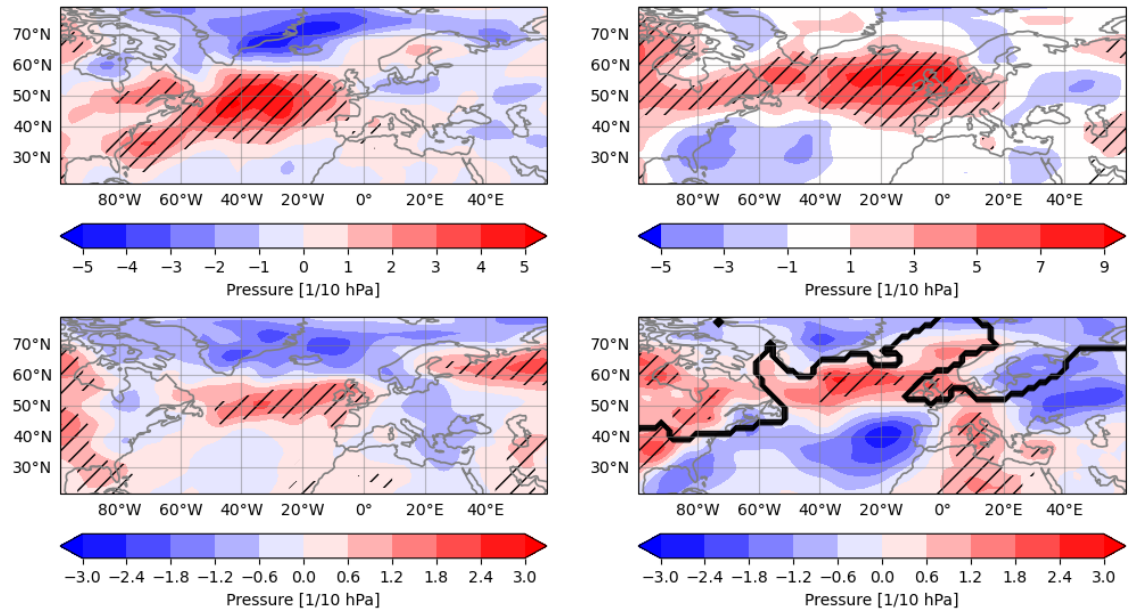

Figure 4.21: Difference of the lower and upper tertile (33rd-66th tertile) for the historical (top left), the SSP5-8.5 future (top right), the mid-Holocene (bottom left) and the LGM (bottom right) periods. The analysis was performed with the AMOC at 45°N for all but the LGM, where the ice sheet cover incites the usage of the oceanic circulation strength at 25°N. The black line indicates the ice edge during the LGM and the hatched area have a significance above 90% based on a Student's t-test. Note the different ranges of the colorbars. For further information on how the composites were calculated, see 3.2.4.

5 Discussion

In the following chapter, the above-presented results will be put into a larger context and compared to previous studies.

5.1 Climatic conditions

5.1.1 Climate Conditions in the Future under the SSP5-8.5 Scenario

Currently, the yearly carbon emissions are increasing, a trend predicted to continue into the future (Fox-Kemper et al., 2021a). With a larger Greenhouse Gas (GHG) concentration, the radiative balance is changed and less outgoing longwave radiation will impact the atmospheric temperatures. The above-performed analysis (left plot in Figure 4.8) indicates a possible local maximum warming by the end of the century compared to the pre-industrial period of 1850-1880 in the near-surface air temperatures up to 16°C. In higher latitudes, the warming is greater due to the polar amplification[1]. A weakening of the Atlantic Meridional Overturning Circulation (AMOC) will reduce the northward transport of warm waters also impacting the air temperatures. This results in much weaker warming over the path of the Gulf Stream from the North American coast into the North Atlantic. The strongest effect can be seen in the open ocean, where the reduced oceanic northward heat transport could even lead to an absolute cooling of the lower atmosphere.

The current Intergovernmental Panel on Climate Change (IPCC) report (Fox-Kemper et al. (2021a), Figure 4.41) shows a plot of the global surface air temperature changes estimate under the SSP5-8.5 scenario for the end of the 21st century relative to 1994-2014. Predicted are temperature increases up to 8°C in the high latitudes over continents. In the central North Atlantic, a region of much weaker warming (below 2°C) is located similar to the here-found results. The lower extreme warming temperatures in the Assessment report (AR)6 are likely because the report uses a CMIP6 multi-model annual mean, while the presented results only show the winter months.

Catto et al. (2011) followed the approach to double and quadruple the atmospheric CO_2 concentration and the resulting temperature changes can be found in their Figure 4 as a difference to the control run (no CO_2 concentration changes). The continental warming is stronger than over the ocean and the polar temperature increase is also greater. In the middle of the North Atlantic, both simulations of increased CO_2 concentrations show reduced warming. The magnitude of warming at the lower end spectrum indicates a regional warming up to 6°C, while the more extreme simulation predicts a warming up to 16°C.

Compared to the results presented herein (Figure 4.8), the stronger carbon increase scenario bears

[1] A combination of different processes which accelerate the warming in the polar regions. Examples are the reduced albedo caused by ice melting and the changed vertical temperature gradient (Fox-Kemper et al., 2021a).

a greater similarity in magnitude despite it being run with a larger CO_2 concentration[2]. The discrepancies support the above-theorized seasonal influence, however, the similarities indicate the correct representation of the physical processes.

The temperature changes in the future under a weakening of the AMOC were also investigated with the linear regression. Figure 4.13 (first plot in the second row) shows the changes caused by linear processes of the SAT with a weakened ocean circulation. This analysis displays the protruding region over the North Atlantic as a region of strong cooling, supporting the theory, that the reduced AMOC is responsible for the reduced warming.

Despite some differences in magnitude, the pattern of continental warming due to climate change and a reduced temperature increase over the central North Atlantic due to the reduced AMOC is very similar between the here-presented results, the paper by Catto et al. (2011) and the IPCC report.

The atmospheric water vapour content is linked to the temperature and with global warming, the amount of evaporated water in the atmosphere is expected to increase. A higher water vapour content influences the latent heat release by cyclones and can impact the effectiveness of the northward heat transport by the atmosphere and the severity of the storms.

In the considered area, the temperature increases with a mean of 4.3 °C indicating a water vapour mean uptake of roughly $3\,\mathrm{kg\,m^{-2}}$. The simulation results depicted in the right plot in Figure 4.8 indicate a slightly lower mean water vapour increase. Possible explanations are an underestimation by the model of the water vapour increase or the not considered dynamic processes by the Clausius-Clapeyron equation could have a greater impact (Oueslati et al., 2019). However, the plot correctly reproduces the higher atmospheric water vapour content in a warming climate and is in qualitative agreement with the sixth IPCC report.

Especially for the storm tracks the position of the jet stream is of importance, because the jet modulates the path of cyclones. In the left plot in Figure 4.9 the changes by the end of the century compared to the pre-industrial time are shown. The modifications are linked to the weaker meridional temperature gradient. This temperature difference is a relevant forcing for the jet stream and baroclinic instability, a dominant driver for extratropical cyclone development. Changes in the jet stream in a warmer climate have been investigated, however, especially in the Northern Hemisphere, and during the winter the changes are smaller and uncertain compared to the SH (Lee et al., 2021). Harvey et al. (2020) produced in their figure 3 a plot showing the difference between the ERA5 reanalysis DJF eastward wind in 250 hPa compared to the SSP2-4.5 scenario. Because of the more conservative scenario, the here-found values are higher. However, the pattern is very similar, with both plots depicting a "squeezing" (Fox-Kemper et al., 2021a) of the jet which reduces its latitudinal width and an eastward extension towards Europe. This matches with the jet weakening to the south and north in the here-produced plots. The strengthening over Europe also supports the intrusion of the jet into Europe.

[2] The SSP5-8.5 scenario projects a carbon concentration of 1150 ppm (Michael Böttinger, 2015) by 2100, putting the above-described simulations roughly between the doubled and quadrupled scenarios.

Salinity trends in the ocean are mostly controlled by freshwater input or removal by the atmosphere or cryosphere. Evaporation and sea ice formation for example lead to an increase in the salt content, while precipitation and ice melting reduce the salinity. In the North Atlantic, the AMOC is also of importance for the salt content of the water by transporting salty subtropical waters into higher latitudes. The warming of the climate will change the atmospheric impact, by strengthening both the precipitation and evaporation regions, meaning more precipitation and therefore freshening in the polar regions. Stronger evaporation in the subtropics will increase the salinity in this region, however, a weaker AMOC will no longer transport this salty water so far to the north. The melting of the glaciers of Greenland and the sea ice will reduce the salt content of the high-latitude ocean waters further. In general, the salinity change can be summarized as "salty becomes saltier and fresh becomes fresher", meaning that the salty subtropical regions are prone to a higher salinity content and the fresher polar region's salt content will reduce further in a warming climate (Bindoff et al., 2021). The right plot in Figure 4.9 presents the predicted salinity change by the end of the century.

Comparing these results to estimates from the 5th AR (their Figure 12.34 (Collins et al., 2013)) reveals that both plots show a salinity increase east of southern North America in the Gulf Stream region of approximately 1.5 PSU. The rest of the North Atlantic experiences a freshening, which is strongest (about 2 Sv) to the west/east in the AR5/here-presented results.

Especially near Greenland, the stronger ice melting strongly freshens the SSS. With a weaker AMOC circulation, less salty water is transported northward, additionally freshening the higher latitudes. The large salinity reduction west of Great Britain is probably caused by the changed position of the storm tracks leading to more precipitation and the change in the AMOC and gyre circulation (Fox-Kemper et al., 2021b).

5.1.2 Climate Conditions of the Paleoclimate

The climate of the past was significantly different from our present-day conditions. The climate of the past could be significantly different from today's conditions, in particular during the periods when the incoming shortwave insolation deviated from the current one (resulting from the so-called Milankocitch cycle) Examples of alternate paleoclimate states are the LGM and mid-Holocene.

The incoming insolation during these periods is shown in Figure 4.14. Especially in the mid-Holocene (left plot), solar insolation was very different from the pre-industrial time. Changes in the earth's orbit around the sun lead to an energy reduction of 15 $\mathrm{W\,m^{-2}}$ in the subtropical region, more pronounced in the winter months. Shi et al. (2020) also analyzed this period and created the insolation plot in Figure 2.16. Comparing this figure with the results from this thesis reveals similarities. Both show weaker insolation in winter, with negative values at 30°N of -15 $\mathrm{W\,m^{-2}}$ and slightly positive values around 5 $\mathrm{W\,m^{-2}}$ north of 60°N.

During the LGM the Milankovitch cycle was in a similar mode to today's climate, therefore, shows the comparison of the LGM insolation to the pre-industrial time very little differences as predicted in subsection 2.5.3.

During the mid-Holocene, a notable change in insolation led to the development of different climate systems as an intermediary period between the glacial time of the LGM and the relatively warm pre-industrial conditions. The time was characterized by higher near-surface air temperatures than the LGM and large-scale ice melting.

Despite the smaller incoming solar radiation in low latitudes the predicted temperature by proxies and model simulations is very close to the pre-industrial situation. Shi et al. (2020) found a regional cooling of 2°C over continents with a small warming over the central North Atlantic. The IPCC report (Gulev et al., 2021) presents varying temperature trends relative to the pre-industrial period. Some papers found a cooling of 0.03°C, while others detail a warmer average temperature of 0.7°C concurring with Brayshaw et al. (2010). The left plot in Figure 4.15 shows the outcomes for this thesis and displays a cooling of 0.8°C over the here-shown part of the NH. This mean surface temperature change is lower than any projections, however consulting Figure 2.17 indicates that geographical regions outside of the considered area have a different temperature trend. Therefore, the smaller cutout could be responsible for the lower near-surface temperatures and imply that the here-presented results are in broad agreement with the scientific consensus.

The LGM was part of the last time period with a large glacial ice cover of the polar earth and had the corresponding much lower air temperatures. According to the AR6, the glacial world was 5-7°C colder at the surface compared to the pre-industrial time (Gulev et al., 2021). Here a mean temperature reduction of -10°C was calculated. In the right plot in Figure 4.15 the here-found temperature pattern is displayed. Comparing these results to the left plot in Figure 2.19 reveals some differences. The most notable is the magnitude, which is almost double in the here-employed model. Additional sources (e.g. Tierney (2020)) support the more moderate cooling, suggesting that the Figure 4.15 simulates lower surface air temperatures. A probable cause is, that Cauquoin et al. (2023) and Tierney (2020) evaluated annular data, while the analysis for this thesis is based on the winter months of DJF. That would explain the lower minimal temperature and the colder mean temperature reduction compared to the other studies. The different figures however agree on the maximum cooling trend being situated above the North American and northern European continent. These are caused by the large FSIS and LIS reducing the temperatures above the ice sheets.

A change in the meridional temperature gradient has an impact on the jet stream, defined here as the eastward winds in 250 hPa. With a stronger gradient, the meridional circulation described in 2.3.1 will be strengthened and the mid-latitude westerlies experience an increase in wind speed.

The weak colder temperatures in the atmosphere between high and low latitudes during the mid-Holocene induced a northward shift of the jet stream (Repschläger et al., 2017). A comparison of this expectation to the left plot in Figure 4.16 shows good agreement as the northward shift is confirmed.

During the LGM the temperature gradient between the tropics and the high latitudes was much larger, leading to a strengthening of the mid-latitude jet stream. Additional projections include a shift to the south, a meridional narrowing, and a stronger intrusion into Europe (Ludwig et al., 2016). The right plot in Figure 4.16 shows the analytical result, which does not display a southward shift. Instead, it depicts the reduction in the meridional extent and a greater presence over Europe.

Comparing this plot with the Figure 2.20 reveals a greater strengthening of the jet stream in the here-used model. However, both the climatology (black lines in Figure 2.20 and Figure 7.1) and the predicted changes in the LGM compared to the pre-industrial period (Figure 2.20 and right plot in Figure 4.16) have overall a good overlap.

5.2 Characteristics of the Atlantic Meridional Overturning Circulation

5.2.1 Oceanic Northward Heat Transport

The strength of the meridional temperature gradient has an impact on the oceanic northward heat transport and one major component in this heat exchange between low and high latitudes is the AMOC. With a greater north-south temperature gradient, more heat is transferred northward in the NH by the ocean. Since the oceanic energy transport is more pronounced in the subtropical regions, the strongest transfer can be found at $\approx 25^{\circ}$ (see the left plot in Figure 4.10). The right plot in the same figure shows the difference of each period relative to the pre-industrial period. Here especially, the large positive change in the LGM (green line) and the strong reduction in the warmer future climate stand out.

During the glacial maximum, the meridional temperature gradient was the largest from all analyzed time periods, suggesting the greatest heat transport via a strong AMOC (compare to Figure 4.19). Kageyama et al. (2021) also investigated the LGM and found a stronger northward heat transport in both the atmosphere and the ocean during the period, with the greatest difference in the oceanic transfer being either in the subtropics (around 30°N) or the mid-latitudes (50°N).

In a warming climate, the temperature difference between the low and high latitudes is expected to reduce due to polar amplification (Forster et al., 2021), explaining the much weaker northward energy transport. Figure 4.10 projects a maximum weaker transport of 0.4 PW at 25°N and a slight positive change of northward heat transport at the high latitudes. The reduced transport value is close to the results from Mecking und Drijfhout (2023), which noted a reduced transport at 26.5°N of 0.3 PW mostly due to the weakened AMOC. Also, the enhanced northward transport into the Arctic region is supported by Mecking und Drijfhout (2023) which strengthens the polar amplification. Reasons are higher Sea Surface Temperature (SST) to the north and an enhancement of the wind-driven gyre transport (Lee et al., 2021).

The current IPCC report (Fox-Kemper et al. (2021b), their Figure 9.8) depicts a northward heat transport of 1-1.3 PW at 26.5°N for the historical period with an AMOC strength comparable to the pre-industrial time. Similar magnitudes are given by Clark et al. (2002). These values are lower than the here plotted 1.67 PW, probably because the IPCC report also reported a weaker oceanic circulation strength. The AMOC weakening alone causes an oceanic heat transport reduction of 0.17 PW in the recent decades (Fox-Kemper et al., 2021b), however, other mitigating factors lessen this change. Influences by other oceanic circulations (like the gyre transport (Fox-Kemper et al., 2021b)) could implicate a heat transport difference closer to the here shown 0.05 PW. In summary, other studies also find a stronger northern hemispheric ocean heat transport during the LGM and project for the future that a weakening of the AMOC will cause a reduction in transport.

5.2.2 Atlantic Meridional Overturning Circulation in the Historical Time Period

The historical time period encompasses the years from the pre-industrial 1850 to the year 2014. Before the year 2000, the AMOC showed no definite weakening trend and instead seemed to be controlled by natural variability and other factors. Throughout the entire 20th century the oceanic circulation depicted a weak positive anomaly compared to the pre-industrial reference period. The anomalies can be seen in Figure 2.4 and coincide with the here-found results (anomaly plot is not shown).

Different external influences on the circulation likely caused the changes. For example, the overall positive trend from 1940 to 1985 is probably a result of aerosol forcing. The short-term minima around the 1960s could be explained by the weaker deep convection in the Labrador Sea, reducing the AMOC intensity (Fox-Kemper et al. (2021a), Weaver et al. (1999)). After the turn of the century, the AMOC in the left plot in Figure 4.7 started to decline, a trend that is still ongoing and expected to continue in the warmer climate of the future. This is supported by the IPCC report (Fox-Kemper et al., 2021b) and the Figure 2.4. The most current AR finds an AMOC weakening of 2.5 Sv in the 14 years of the 21st century, same as the two aforementioned figures.

5.2.3 Atlantic Meridional Overturning Circulation in the Future Time Period

The climate until the end of the century is expected to warm, which will both increase the high-latitude SSTs and reduce the salinity content from glacial and ice sheet melting. These changes, especially in the deep-water formation areas, will likely lead to impacts on the ocean and the AMOC, decreasing its overturning strength. Most papers (e.g. Vellinga und Wood (2002), Caesar et al. (2018), Caesar et al. (2021)) agree, that the North Atlantic circulation will continue to slow down, however, the amount of reduction is still an ongoing topic of debate. Weakening is expected to be between 25-40 % (Fox-Kemper et al., 2021b), with the most current IPCC report suggesting an anomaly of approximately 9 Sv under the SSP5-8.5 scenario compared to 2014 (see Figure 2.4). The here created multi-model mean in Figure 4.11 shows within the same time period a reduction by 8 Sv, showing good agreement with the IPCC AR6 report.

5.2.4 Atlantic Meridional Overturning Circulation in the Paleoclimate

The literature research revealed no coherent picture of the past AMOC. Past studies investigating the circulation during the LGM and the mid-Holocene showed that the relative changes of the circulation strength compared to pre-industrial time depends on the used models, proxies, and/or resolution. The here-used model and resolution revealed a strengthening of the oceanic circulation in both time periods, with a greater difference to the historical during the LGM. Since the papers indicate a greater deviation during the glacial time, the results in Figure 4.18 are qualitatively consistent with some of the literature findings.

5.3 Evaluation of the Composite Analysis

This part of the discussion will review the composite analysis results to see if they show consistent results as to the difference in the here-calculated averaged storm track changes between the four

periods and the pre-industrial years. Additional studies will be consulted to support the outcomes. Because the upper percentile was subtracted from the lower percentile, the resulting plots show the change of the storm track in response to a weakening of the AMOC. Positive values mean that storm tracks strengthen when the ocean circulation transitions from a strong to a weak state or that a strengthening of the AMOC weakens the storm tracks.

The theory described in section 2.4 suggests, that a reduced AMOC will locally enhance the meridional temperature gradient. This change influences the baroclinicity, an important factor for cyclone formation and storm track strengthening.

5.3.1 Outcomes of the Composite Analysis

Evaluating the composite analysis (see Figure 4.21) indicates a qualitative consistent picture for all four analyzed time periods. A weakening of the AMOC corresponds to a strengthening of the storm tracks over the central North Atlantic and a reduction to the north, east of Greenland (more during the historical and mid-Holocene), and the south near Florida and Spain (more in the SSP5-8.5 and the LGM). This pattern indicates a very weak southward shift, latitudinal narrowing, and increased strength of the storm tracks over the central North Atlantic, reaching toward Great Britain.

For the future scenario, the absolute changes are the greatest compared to the other times. The probable explanation is, that the AMOC experienced a large reduction by the end of the century, causing considerable differences in the storm tracks and most clearly depicting the storm track changes. Weaker overall trends for the paleoclimates are probably partly instigated by the fact that these results are based on only one model and cannot reflect the model uncertainty. The non-existence of an AMOC trend additionally prevents the storm track response from crystallizing out more distinctly.

5.3.2 Comparison of the Composite Analysis to Model Outcomes and Scientific Studies

The Historical Period

The storm track during the historical period is shown in the right plot in Figure 4.7. Since the AMOC experiences a weakening, especially towards the end of the historical period, the positive values in Figure 4.21 indicate a strengthening of the storm track.

Comparing the changes of the storm tracks in the historical period (see Figure 7.5 in chapter 7) to the composite plot reveals a very similar region of storm track strengthening due to AMOC weakening over the central North Atlantic. The weakening to the north is less pronounced, a storm track intensification over Scandinavia and northern Europe is on the other hand more notable.

The Future Period

The changes of storm tracks in the future under the SSP5-8.5 scenario from the pre-industrial period are shown in the right plot in Figure 4.12. A comparison to the second composite prediction in Figure 4.21 shows many similarities. Both depictions have southward extensions of the storm

tracks over the central and eastern North Atlantic and predict a strengthening of the tracks by 9 (1/10 hPa). And even though the composite is further to the north, especially in the western North Atlantic, the results have a good resemblance. Because future climate exhibits a clear weakening of the oceanic circulation compared to pre-industrial time, the results show a good agreement with the suggested physical processes of the response of storm tracks to a weakening of AMOC.

As an additional tool for the data analysis for this period, the linear regression is also available. The first plot in Figure 4.13 depicts the results of this examination. A weakening of the oceanic circulation is followed by a north-eastward shift of the storm tracks. This line of investigation shows a southward shift over the North Atlantic, a strong poleward component near Europe, and the storm track is only strengthened by 4 (1/10 hPa), however, all analyses show an eastward shift of the storm track resulting in higher cyclone activity over the central and eastern North Atlantic and Great Britain. The regression analysis however depicts the linear correspondence of the storm tracks to the AMOC changes, while the composite analysis does not assume the type of connection of the variables. Therefore, the linear regression indicates that the AMOC weakening leads linearly to an eastward shift in the eastern North Atlantic and over Europe, with lesser impact on western North Atlantic changes.

Subsection 2.3.5 summarized the current scientific consensus and described that the storm tracks will most likely experience large-scale changes with the warming climate.

Harvey et al. (2020) employed the same method (2-6-day bandpass filter of mean sea level pressure data) and project (CMIP6) and used a similar forcing (SSP2-4.5 and SSP5-8.5, respectively) as the current thesis. Figure 2.11 from the paper projects an intensification, a southward shift and eastward extension of the tracks with the strongest change being over the central North Atlantic and the British Isles. Comparing these results to the here-found outcomes shows a great overlap. Albeit the Figure 4.12 has a greater magnitude in change, there is an agreement with the slight southward shift over the western North Atlantic and eastwards towards Europe, additionally to the strengthening of the storm track.

The Mid-Holocene

The left plot in Figure 4.20 depicts the changes in the mid-Holocene compared to the pre-industrial. Over the central North Atlantic and central Europe, the here used model predicts a weak strengthening. In papers, mixed results have been found for the mid-Holocene, and the development of the storm track compared to the pre-industrial is unsure. Arguments for a weakening (e.g., changes in insolation, cooler SSTs) and a strengthening (e.g., greater land-sea contrast, cyclones triggering cyclogenesis) of the track can be made.

The Last Glacial Maximum

For the glacial period, the ice sheet has a large impact and moves the storm tracks southwards over the eastern North Atlantic and Europe. In the right plot in Figure 4.20, the storm track is strengthened along the ice edge over the open ocean and is then pushed to the south by the FSIS. These results are supported by scientific research, like Raible et al. (2021) and Ludwig et al. (2016).

Figures 2.22 and 2.23 also predict a shift of the storm track south or southeastward and a strengthening near the North American coast, south of the FSIS in Europe, and over the Mediterranean.

For the past period of the mid-Holocene and the LGM, the composite analysis predicts a similar change compared to the other periods. The employed model however sees no strong long-term changes in the AMOC and it is therefore not possible to validate the results with a long-term storm track trend. A comparison as above with the mean storm track changes relative to the pre-industrial time reveals contrasting results. Both of the paleoclimate periods display a stronger storm track over the area, where a reduction is expected from the composite analysis. This indicates, that a comparison between drastically different climate conditions is not scientifically sound. Other factors than the AMOC probably played a bigger role during the past climates. Examples herefore are the different insolation during the mid-Holocene and the greater meridional temperature gradient during the LGM, affecting the baroclinicity and therefore modulating the storm tracks. In other words, storm tracks can still strengthen due to the notably strengthened baroclinicity, despite the strengthened AMOC.

5.4 Comparison of Linear Regression Results between the CMIP6 and CMIP3 Models

The linear regression in 4.3.3 was based on the analysis by Woollings et al. (2012) in the year 2012 within the CMIP3 project. Here the results with the CMIP6 models (see Figure 4.13) shall be compared to the previous outcomes (see Figure 2.15).

Comparing the results with each other, similar patterns become obvious. Especially the AMOC-induced storm track changes (top in Figure 4.13 and first in Figure 2.15) both show a stronger track north-west from Great Britain and Scandinavia. The near-surface temperatures (first in the second row in Figure 4.13 and second in Figure 2.15) both display a cooling over the middle North Atlantic Ocean but have also greater differences between them. Not only does Woollings et al. (2012) figure show a greater cooling up to 4°C while the CMIP6 shows a cooling of only 1.8°. The newer plot also indicates warming over the North American continent and over the Norwegian and Barents Seas. Comparing the eastward winds in 850 hPa (on the right in the second row in Figure 4.13 and third in Figure 2.15) reveals some comparable structures. Both figures depict a similar strength in response to the low-level eastward winds with a changing AMOC of $\pm$ 0.5 m s^{-1}. The plots both show a positive change over northern Europa and a weakening in the Mediterranean area. However, over the ocean, the CMIP3 project indicates a reduction in the south and a wind speed increase to the north. The CMIP6 project on the other hand shows a strengthening to the south and slower wind speeds over the northern North Atlantic. Despite having employed a different method, the left plot in Figure 2.12 agrees well with these findings.

A possible cause for these discrepancies might be the differences between the new SSP pathways and the former Special Report on Emissions Scenarios (SRES). The CMIP3 analysis was based on

the A1B scenario[3], which assumed an atmospheric carbon dioxide concentration of 700 ppmv by the end of the century. In the year 2100, this scenario predicted a carbon emission of 15 GtC/year (Michael Mann, 2015). This would result in a global surface temperature increase by 2.8 °C (Solomon et al., 2007). Under the CMIP6 SSP5-8.5 scenario, the models indicate an atmospheric CO_2 concentration of 1150 ppm and a carbon emission of 130Gt/year by 2100 (Brian O'Neill, 2015) causing a global warming of almost 5°C. These CMIP6 values are significantly higher than the ones for the CMIP3 scenario, impacting the temperature, wind, and storm track changes. Also, improved model capabilities, the consideration of more subsystems of the climate system, and a better resolution may play roles of varying importance.

To sum up, especially the storm track plots of the different linear regression analyses show a large qualitative agreement in position and magnitude. The different projects predict an eastward shift of the storm track and a definite strengthening. When comparing the near-surface air temperature, a general cooling trend over the North Atlantic can be seen. There are differences in magnitude and geographical spread, however, overall the results are similar. The low-level winds have a greater consensus again than the SATs. Over the north European continent, an increase in wind speed is predicted and the Mediterranean and North African regions will likely experience a weakening.

[3] This scenario assumes rapid economic growth, an increasing world population until the middle of the next century followed by a decrease, and the introduction of new technologies using energy equally from fossil and renewable sources. It is assumed that no additional climate protection measures are taken (Solomon et al., 2007).

6 Summary

In this master thesis, the relationship between the Atlantic Meridional Overturning Circulation (AMOC) and the European storm tracks was investigated and tested if this link is consistent for historical, future, and paleoclimate times. First, the current climate conditions were evaluated, and afterward changes in the future under the SSP5-8.5 scenario and during the mid-Holocene and the LGM in the paleoclimate were investigated. After confirming a broad congruence with climatic conditions in other papers, the behavior of the AMOC and the European storm tracks was studied. Results indicated a (slightly) stronger oceanic circulation during the paleoclimate times of the mid-Holocene and the LGM and a steep decline in strongly warming climate. The storm tracks during the mid-Holocene experienced a weak strengthening and a eastward shift. During the LGM the mean cyclone path was greatly influenced by the ice sheets, were shifted to the northeast and exhibited a intensification south of Greenland and over the southern European continent. In the warmer climate of the future, the storm tracks are projected to be strengthened and have a stronger extension into Europe.

To study the connection between the two climate components, a composite analysis was applied. This method aimed to identify the different characteristics of storm tracks between times with strong and weak AMOC, which would be applicable for multiple time periods in the paleoclimate and for future scenarios. The main result is that a weakening of the AMOC is associated with a strengthening and north-eastward shift of the storm tracks over the central and northern North Atlantic reaching Great Britain. A comparison to the linear regression and the literature research shows good agreement on both the storm track and AMOC changes for the future and supports the here-found results. For the paleoclimate, the non-existent AMOC trend, the lack of available models for the analysis, and the different climate conditions hinder direct validation with simulated storm tracks. Nevertheless, the agreement for the historical and future periods between the composites and the predicted changes instills confidence that the outcomes of this analysis can also be applied to the paleoclimate period.

The AMOC is only a small part of the global Thermohaline Circulation (THC), but unlike the branches in the Pacific and the Indian Ocean, it is predicted to experience the most changes in the future. The above-conducted research highly suggests a weakening of the Atlantic circulation with a weaker overturning in the future. This indicates less Atlantic waters reaching the Southern Ocean and therefore less water becomes part of the ACC. The THC branches in the other ocean basins therefore receive a reduced amount of cold and dense bottom water and cool surface flows from the Antarctic, indicating a similar weakening of the THC in the Pacific and Indian Ocean like in the Atlantic. With no influenced deep water formation regions and with the less poleward extension, the expected changes of the THC are smaller, but probably still large enough to cause impacts on the individual ocean basin and the surrounding atmosphere.

This thesis focused on the response of the storm tracks to a change in the oceanic circulation. However, as already indicated above, the climate system is large and complex with many interacting components. Concentration on just two parts guarantees some missed influences. For example, the subtropical and subpolar gyres (STG/SPG) in the ocean and the surface density in the deep-water formation regions are important in impacting the AMOC. The storm tracks are, next to the ocean, affected by the phase of the North Atlantic oscillation (NAO), Artic Ocean (AO), and the Atlantic Multidecadal Oscillation (AMO). These additional influences are not discussed in this study to simplify the work and allow its completion within the given time frame of a year. To increase the reliability of this study, more models especially for the paleoclimate periods are needed. It could also be considered to add the effects of the NAO or the STG/SPG onto the storm tracks and AMOC respectively, to allow a further investigation of the variability of the relationship between the AMOC and the storm tracks.

7 Appendix

7.1 Employed Models

Table 7.1: Nominal resolution and vertical level number for the used models. Bold models contain 6-hourly sea surface pressure data from WCRP (2015)

Institution ID	Source ID	nominal resolution		vertical levels	
		atmosphere	ocean	atmosphere	ocean
CAS	FGOALS-g3	250 km	100 km	26	30
CCCma	CanESM5	500 km	100 km	49	45
CSIRO	ACCESS-ESM1-5	250 km	100 km	38	50
CSIRO-ARCCSS	**ACCESS-CM2**	250 km	100 km	85	50
INM	INM-CM4-8	100 km	100 km	21	40
INM	INM-CM5-0	100 km	50 km	73	40
MIROC	**MIROC6**	250 km	100 km	81	63
MPI-M	**MPI-ESM1-2-HR**	100 km	50 km	95	40
MPI-M	**MPI-ESM1-2-LR**	250 km	250 km	47	40
MRI	MRI-ESM2-0	100 km	100 km	80	61
NCAR	CESM2-WACCM	100 km	100 km	70	60
NCC	**NorESM2-MM**	100 km	100 km	32	70
NCC	NorESM2-LM	250 km	100 km	32	70

7.2 Evaluated Variables

Table 7.2: Analyzed variables with description, unit and temporal resolution. The shortages for the temporal resolution represent the monthly (mon) data from the Atmosphere (A), the Ocean (O), or the Sea Ice (SI) region. Outliers are the fixed (time-invariant) field (fx) and the 6 hourly sampled data, at a specified time point within the time period on pressure levels (6hrPlevPt) from DKRZ (2023).

Variable Shortage	Description	Unit	Temporal Resolution
evspsbl	Evaporation Including Sublimation and Transpiration	$\mathrm{kg\,m^{-2}s^{-1}}$	Amon
hfbasin	Northward Ocean Heat Transport	W	Omon
msftmz	Ocean Meridional Overturning Mass Streamfunction	$\mathrm{kg\,s^{-1}}$	Omon
pr	Precipitation	$\mathrm{kg\,m^{-2}\,s^{-1}}$	Amon
prw	Water Vapor Path	$\mathrm{kg\,m^{-2}}$	Amon
psl	Sea Level Pressure	Pa	6hrPlevPt
rsdt	TOA Incident Shortwave Radiation	$\mathrm{W\,m^{-2}}$	Amon
siconca	Sea-Ice Area Percentage (Atmospheric Grid)	%	SImon
sos	Sea Surface Salinity	0.001	Omon
sftgif	Land Ice Area Percentage	%	fx
tas	Near-Surface Air Temperature	K	Amon
tos	Sea Surface Temperature	°C	Omon
ua	Eastward Wind[1]	$\mathrm{m\,s^{-1}}$	Amon

7.3 Climate Conditions for the Pre-industrial time

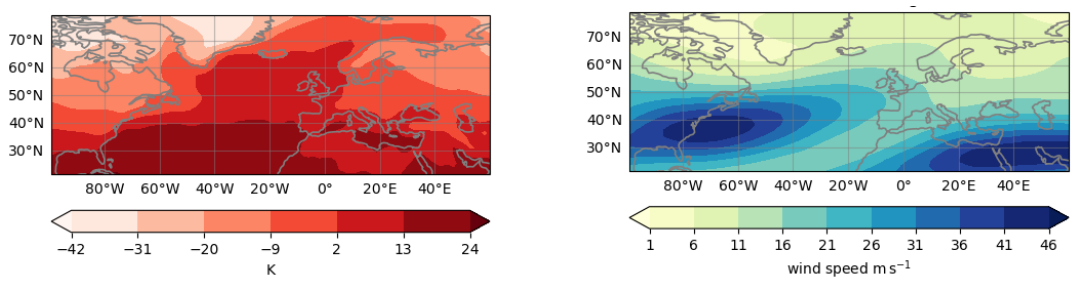

Figure 7.1: Near-surface air temperature (left) and eastward wind at 250 hPa (right) in the pre-industrial in $\mathrm{W\,m^{-2}}$ and $\mathrm{m\,s^{-2}}$ respectively.

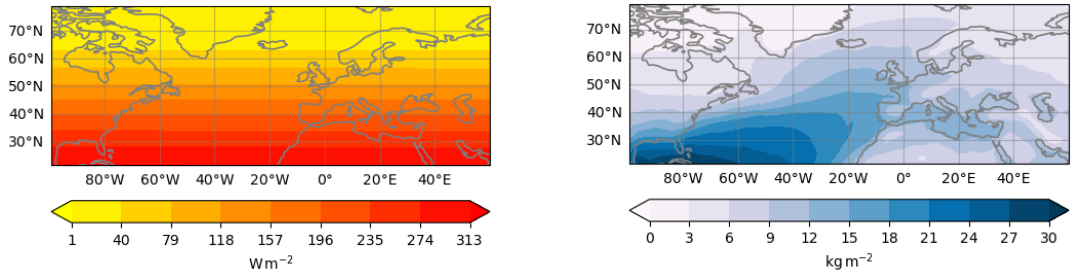

Figure 7.2: Top of the atmosphere incident shortwave radiation (left) and atmospheric water vapor content (right) in the pre-industrial in $\mathrm{W\,m^{-2}}$ and $\mathrm{kg\,m^{-2}}$ respectively.

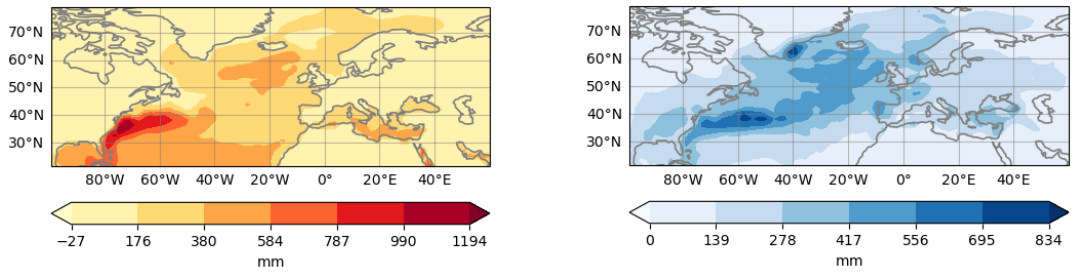

Figure 7.3: Mean of the evaporation (left) and precipitation (right) in the pre-industrial in mm.

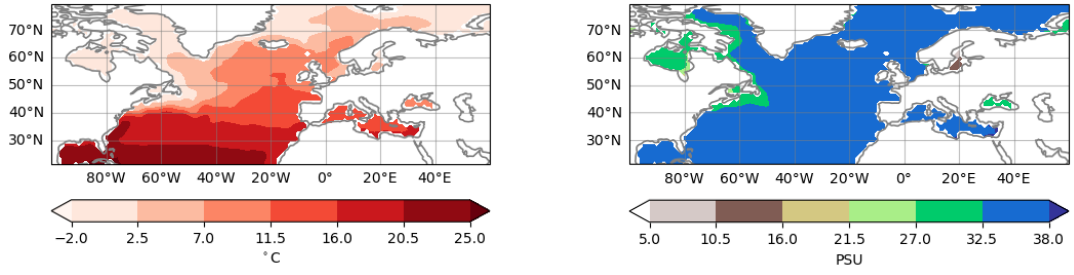

Figure 7.4: Mean of the sea surface temperature (left) and sea surface salinity (right) in the pre-industrial in °C and PSU respectively.

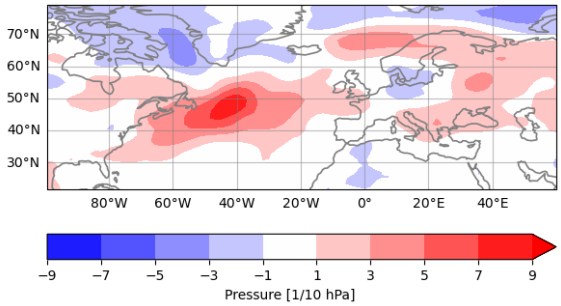

Figure 7.5: Mean storm track changes from the historical to the pre-industrial era.

7.4 Ice Cover

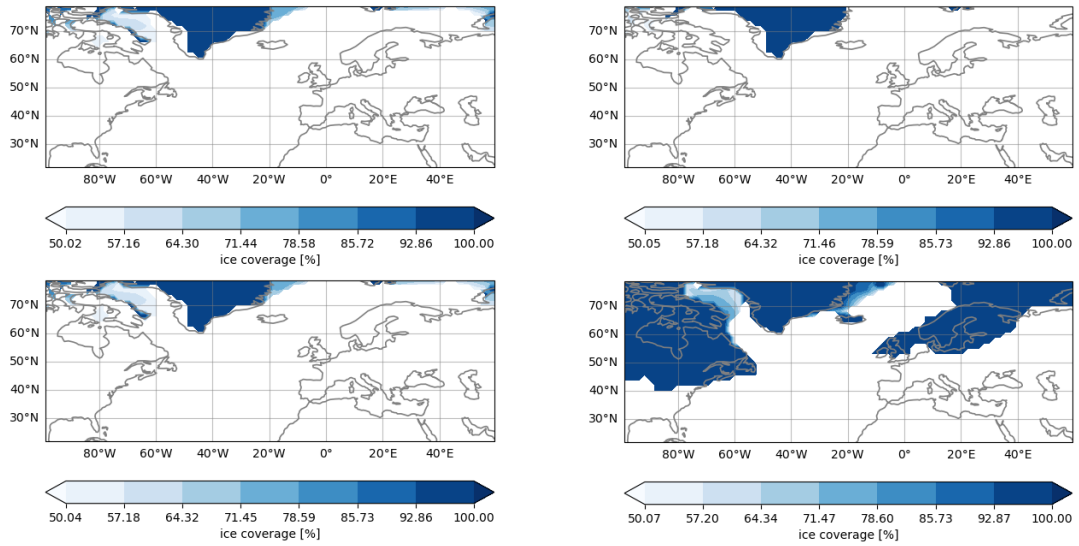

Figure 7.6: Sea and land ice cover during the historical, future, mid-Holocene, and LGM periods in % with the cover exceeding 50 %.

Bibliography

Aken, H. M. v., 2007: The Oceanic Thermohaline Circulation: An Introduction. *Atmospheric and oceanographic sciences library*, doi:10.1007/978-0-387-48039-8.

Barker, P. und E. Thomas, 2004: Origin, signature and palaeoclimatic influence of the Antarctic Circumpolar Current. *Earth-Science Reviews*, **66 (1)**, 143–162, doi:https://doi.org/10.1016/j.earscirev.2003.10.003, URL https://www.sciencedirect.com/science/article/pii/S0012825203001272.

BBC, 2023: URL https://www.bbc.co.uk/bitesize/guides/zpykxsg/revision/1.

Bellomo, K., M. Angeloni, S. Corti, und J. Hardenberg, 2021: Future climate change shaped by inter-model differences in Atlantic meridional overturning circulation response. *Nature Communications*, **12**, 3659, doi:10.1038/s41467-021-24015-w.

Bellomo, K., V. Meccia, R. D'Agostino, F. Fabiano, S. Larson, J. Hardenberg, und S. Corti, 2023: Impacts of a weakened AMOC on precipitation over the Euro-Atlantic region in the EC-Earth3 climate model. *Climate Dynamics*, 1–20, doi:10.1007/s00382-023-06754-2.

Bengtsson, L., K. I. Hodges, und N. Keenlyside, 2009: Will Extratropical Storms Intensify in a Warmer Climate? *Journal of Climate*, **22 (9)**, 2276 – 2301, doi:10.1175/2008JCLI2678.1, URL https://journals.ametsoc.org/view/journals/clim/22/9/2008jcli2678.1.xml.

Bengtsson, L., K. I. Hodges, und E. Roeckner, 2006: Storm Tracks and Climate Change. *Journal of Climate*, **19 (15)**, 3518 – 3543, doi:10.1175/JCLI3815.1, URL https://journals.ametsoc.org/view/journals/clim/19/15/jcli3815.1.xml.

Bindoff, N., W. Cheung, J. Kairo, J. Arístegui, V. Guinder, R. Hallberg, N. Hilmi, N. Jiao, M. Karim, L. Levin, S. O'Donoghue, S. P. Cuicapusa, B. Rinkevich, T. Suga, A. Tagliabue, und P. Williamson, 2021: *Changing Ocean, Marine Ecosystems, and Dependent Communities*, 447–587. Cambridge University Press, Cambridge, United Kingdom and New York, NY, USA, URL https://doi.org/10.1017/9781009157964.007.

Brayshaw, D., B. Hoskins, und E. Black, 2010: Some physical drivers of changes in the winter storm tracks over the North Atlantic and Mediterranean during the Holocene. *Philosophical transactions. Series A, Mathematical, physical, and engineering sciences*, **368**, 5185–223, doi:10.1098/rsta.2010.0180.

Brayshaw, D. J., B. Hoskins, und M. Blackburn, 2009a: The Basic Ingredients of the North Atlantic Storm Track. Part I: Land–Sea Contrast and Orography. *Journal of the Atmospheric Sciences*, **66 (9)**, 2539 – 2558, doi:10.1175/2009JAS3078.1, URL https://journals.ametsoc.org/view/journals/atsc/66/9/2009jas3078.1.xml.

Brayshaw, D. J., T. Woollings, und M. Vellinga, 2009b: Tropical and Extratropical Responses of the North Atlantic Atmospheric Circulation to a Sustained Weakening of the MOC. *Journal of Climate*, **22 (11)**, 3146–3155, doi:10.1175/2008JCLI2594.1, URL https://journals.ametsoc.org/view/journals/clim/22/11/2008jcli2594.1.xml.

Brian O'Neill, D. v. V., Claudia Tebaldi, 2015: URL https://view.es-doc.org/index.html?renderMethod=id&project=cmip6&id=707142bb-67d6-44c0-966b-92deb1164851&version=1.

Brovkin, V., S. Lorenz, T. Raddatz, T. Ilyina, I. Stemmler, M. Toohey, und M. Claussen, 2019: What was the source of the atmospheric CO_2 increase during the holocene? *Biogeosciences*, **16 (13)**, 2543–2555, doi:10.5194/bg-16-2543-2019, URL https://bg.copernicus.org/articles/16/2543/2019/.

Caesar, L., S. Rahmstorf, A. Robinson, G. Feulner, und V. Saba, 2018: Observed fingerprint of a weakening Atlantic Ocean overturning circulation. *Nature*, **556**, 191–196, doi:10.1038/s41586-018-0006-5, URL https://doi.org/10.1038/s41586-018-0006-5.

Caesar, L. M., G. D. Thornalley, D. J. R. Cahill, und S. N. Rahmstorf, 2021: Current Atlantic Meridional Overturning Circulation weakest in last millennium. *Nature Geoscience*, **14**, 118–120, doi:10.1038/s41561-021-00699-z, URL https://doi.org/10.1038/s41561-021-00699-z.

Cao, J., B. Wang, und J. Liu, 2019: Attribution of the Last Glacial Maximum climate formation. *Climate Dynamics*, **53**, 1661–1679, doi:10.1007/s00382-019-04711-6, URL https://doi.org/10.1007/s00382-019-04711-6.

Catto, J. L., L. C. Shaffrey, und K. I. Hodges, 2011: Northern Hemisphere Extratropical Cyclones in a Warming Climate in the HiGEM High-Resolution Climate Model. *Journal of Climate*, **24 (20)**, 5336–5352, doi:10.1175/2011JCLI4181.1, URL https://journals.ametsoc.org/view/journals/clim/24/20/2011jcli4181.1.xml.

Cauquoin, A., A. Abe-Ouchi, T. Obase, W.-L. Chan, A. Paul, und M. Werner, 2023: Effects of last glacial maximum (lgm) sea surface temperature and sea ice extent on the isotope–temperature slope at polar ice core sites. *Climate of the Past*, **19 (6)**, 1275–1294, doi:10.5194/cp-19-1275-2023, URL https://cp.copernicus.org/articles/19/1275/2023/.

Clark, P. U., A. S. Dyke, J. D. Shakun, A. E. Carlson, J. Clark, B. Wohlfarth, J. X. Mitrovica, S. W. Hostetler, und A. M. McCabe, 2009: The last glacial maximum. *Science*, **325 (5941)**, 710–714, doi:10.1126/science.1172873, URL https://www.science.org/doi/abs/10.1126/science.1172873, https://www.science.org/doi/pdf/10.1126/science.1172873.

Clark, P. U., N. G. Pisias, T. F. Stocker, und A. J. Weaver, 2002: The role of the thermohaline circulation in abrupt climate change. *Nature*, **415**, doi:10.1038/415863a, URL https://doi.org/10.1038/415863a.

Collins, M., R. Knutti, J. Arblaster, J.-L. Dufresne, T. Fichefet, P. Friedlingstein, X. Gao, W. Gutowski, T. Johns, G. Krinner, M. Shongwe, C. Tebaldi, A. Weaver, und M. Wehner, 2013: *Long-term Climate Change: Projections, Commitments and Irreversibility*, 1029–1136. Cambridge University Press, Cambridge, United Kingdom and New York, NY, USA, doi: 10.1017/CBO9781107415324.024.

Dey, D. und K. Döös, 2020: Atmospheric freshwater transport from the atlantic to the pacific ocean: A lagrangian analysis. *Geophysical Research Letters*, **47 (6)**, doi:10.1029/2019GL086176, URL https://agupubs.onlinelibrary.wiley.com/doi/abs/10.1029/2019GL086176, https://agupubs.onlinelibrary.wiley.com/doi/pdf/10.1029/2019GL086176.

Disasters, T. S. A. N., June 15, 2021: URL https://appliedsciences.nasa.gov/our-impact/story/remembering-mt-pinatubo.

DKRZ, August 2023: URL https://esgf-data.dkrz.de/projects/esgf-dkrz/.

Eyring, V., 2015: URL https://view.es-doc.org/index.html?renderMethod=id&project=cmip6&id=713f15b6-e289-44e9-ba74-0d0e827e42ac&version=1.

Fichefet, T., S. Hovine, und J.-C. Duplessy, 1994: A model study of the Atlantic thermohaline circulation during the last glacial maximum. *Nature*, **372**, 252–255, doi:10.1038/372252a0, URL https://doi.org/10.1038/372252a0.

Forster, P., T. Storelvmo, K. Armour, W. Collins, J.-L. Dufresne, D. Frame, D. Lunt, T. Mauritsen, M. Palmer, M. Watanabe, M. Wild, und H. Zhang, 2021: *The Earth's Energy Budget, Climate Feedbacks, and Climate Sensitivity*, 923–1054. Cambridge University Press, Cambridge, United Kingdom and New York, NY, USA, doi:10.1017/9781009157896.009.

Fox-Kemper, B., H. Hewitt, C. Xiao, G. Aðalgeirsdóttir, S. Drijfhout, T. Edwards, N. Golledge, M. Hemer, R. Kopp, G. Krinner, A. Mix, D. Notz, S. Nowicki, I. Nurhati, L. Ruiz, J.-B. Sallée, A. Slangen, und Y. Yu, 2021a: Ocean, Cryosphere and Sea Level Change. In Climate Change 2021: The Physical Science Basis. Contribution of Working Group I to the Sixth Assessment Report of the Intergovernmental Panel on Climate Change . *Cambridge University Press, Cambridge, United Kingdom and New York, NY, USA*, 1211–1362, doi:doi:10.1017/9781009157896.011., URL https://www.ipcc.ch/report/ar6/wg1/downloads/report/IPCC$_$AR6$_$WGI$_$Chapter09.pdf.

Fox-Kemper, B., H. Hewitt, C. Xiao, G. Aðalgeirsdóttir, S. Drijfhout, T. Edwards, N. Golledge, M. Hemer, R. Kopp, G. Krinner, A. Mix, D. Notz, S. Nowicki, I. Nurhati, L. Ruiz, J.-B. Sallée, A. Slangen, und Y. Yu, 2021b: *Ocean, Cryosphere and Sea Level Change*, 1211–1362. Cambridge University Press, Cambridge, United Kingdom and New York, NY, USA, doi: 10.1017/9781009157896.011.

Garcia-Soto, C., L. Cheng, L. Caesar, S. Schmidtko, E. B. Jewett, A. Cheripka, I. Rigor, A. Caballero, S. Chiba, J. C. Báez, T. Zielinski, und J. P. Abraham, 2021: An Overview of Ocean

Climate Change Indicators: Sea Surface Temperature, Ocean Heat Content, Ocean pH, Dissolved Oxygen Concentration, Arctic Sea Ice Extent, Thickness and Volume, Sea Level and Strength of the AMOC (Atlantic Meridional Overturning Circulation). *Frontiers in Marine Science*, **8**, doi:10.3389/fmars.2021.642372, URL https://www.frontiersin.org/articles/10.3389/fmars.2021.642372.

Griffin, D., C. González Martín, C. Hoose, und D. Smith, 2017: *Global-Scale Atmospheric Dispersion of Microorganisms*. John Wiley & Sons, Ltd, 155-194 pp., doi:10.1002/9781119132318.ch2c, URL https://onlinelibrary.wiley.com/doi/abs/10.1002/9781119132318.ch2c.

Gulev, S., P. Thorne, F. D. J. Ahn, C. Domingues, S. Gerland, D. Gong, D. Kaufman, H. Nnamchi, J. Quaas, J. Rivera, S. Sathyendranath, S. Smith, B. Trewin, K. von Schuckmann, und R. Vose, 2021: *Changing State of the Climate System*, 287–422. Cambridge University Press, Cambridge, United Kingdom and New York, NY, USA, doi:10.1017/9781009157896.004.

Harvey, B. J., P. Cook, L. C. Shaffrey, und R. Schiemann, 2020: The Response of the Northern Hemisphere Storm Tracks and Jet Streams to Climate Change in the CMIP3, CMIP5, and CMIP6 Climate Models. *Journal of Geophysical Research: Atmospheres*, **125 (23)**, e2020JD032 701, doi:https://doi.org/10.1029/2020JD032701, URL https://agupubs.onlinelibrary.wiley.com/doi/abs/10.1029/2020JD032701, e2020JD032701 2020JD032701, https://agupubs.onlinelibrary.wiley.com/doi/pdf/10.1029/2020JD032701.

Hu, A., G. A. Meehl, und W. Han, 2007: Role of the Bering Strait in the thermohaline circulation and abrupt climate change. *Geophysical Research Letters*, **34 (5)**, doi:10.1029/2006GL028906, URL https://agupubs.onlinelibrary.wiley.com/doi/abs/10.1029/2006GL028906, https://agupubs.onlinelibrary.wiley.com/doi/pdf/10.1029/2006GL028906.

Kageyama, M., 2017a: URL https://pmip4.lsce.ipsl.fr/doku.php/exp_design:mh.

———, 2017b: URL https://pmip4.lsce.ipsl.fr/doku.php/exp_design:lgm.

Kageyama, M., S. P. Harrison, M.-L. Kapsch, M. Lofverstrom, J. M. Lora, U. Mikolajewicz, S. Sherriff-Tadano, T. Vadsaria, A. Abe-Ouchi, N. Bouttes, D. Chandan, L. J. Gregoire, R. F. Ivanovic, K. Izumi, A. N. LeGrande, F. Lhardy, G. Lohmann, P. A. Morozova, R. Ohgaito, A. Paul, W. R. Peltier, C. J. Poulsen, A. Quiquet, D. M. Roche, X. Shi, J. E. Tierney, P. J. Valdes, E. Volodin, und J. Zhu, 2021: The PMIP4 Last Glacial Maximum experiments: preliminary results and comparison with the PMIP3 simulations. *Climate of the Past*, **17 (3)**, 1065–1089, doi:10.5194/cp-17-1065-2021, URL https://cp.copernicus.org/articles/17/1065/2021/.

Kang, Y. und H. Yang, 2023: Quantifying effects of earth orbital parameters and greenhouse gases on mid-holocene climate. *EGUsphere*, **2023**, 1–18, doi:10.5194/egusphere-2023-380, URL https://egusphere.copernicus.org/preprints/2023/egusphere-2023-380/.

Kostov, Y., K. C. Armour, und J. Marshall, 2014: Impact of the Atlantic meridional overturning circulation on ocean heat storage and transient climate change. *Geophysical Research Letters*, **41 (6)**, 2108–2116, doi:10.1002/2013GL058998, URL https://agupubs.onlinelibrary.wiley.com/doi/abs/10.1002/2013GL058998, https://agupubs.onlinelibrary.wiley.com/doi/pdf/10.1002/2013GL058998.

Kuhlbrodt, T., A. Griesel, M. Montoya, A. Levermann, M. Hofmann, und S. Rahmstorf, 2007: On the driving processes of the Atlantic meridional overturning circulation. *Reviews of Geophysics*, **45 (2)**, doi:10.1029/2004RG000166, URL https://agupubs.onlinelibrary.wiley.com/doi/abs/10.1029/2004RG000166, https://agupubs.onlinelibrary.wiley.com/doi/pdf/10.1029/2004RG000166.

Kuhlbrodt, T. R., S. Zickfeld, K. Vikebø, F. B. Sundby, S. Hofmann, M. Link, P. M. Bondeau, A. Cramer, W. Jaeger, und Carlo, 2009: An Integrated Assessment of changes in the thermohaline circulation. *Climatic Change*, **96**, 489–537, doi:10.1007/s10584-009-9561-y, URL https://doi.org/10.1007/s10584-009-9561-y.

Lan, X., K. Thoning, und E. Dlugokencky, 2023: Trends in globally-averaged CH4, N2O, and SF6 determined from NOAA Global Monitoring Laboratory measurements. doi:https://doi.org/10.15138/P8XG-AA10, URL https://gml.noaa.gov/ccgg/trends$_$ch4/.

Laîné, A., M. Kageyama, D. Salas-Mélia, A. Voldoire, G. Rivière, G. Ramstein, S. Planton, S. Tyteca, und J. Y. Peterschmitt, 2009: Northern hemisphere storm tracks during the last glacial maximum in the PMIP2 ocean-atmosphere coupled models: energetic study, seasonal cycle, precipitation. *Climate Dynamics*, **32**, 593–614, doi:10.1007/s00382-008-0391-9, URL https://doi.org/10.1007/s00382-008-0391-9.

Lee, J.-Y., J. Marotzke, G. Bala, L. Cao, S. Corti, J. Dunne, F. Engelbrecht, E. Fischer, J. Fyfe, C. Jones, A. Maycock, J. Mutemi, O. Ndiaye, S. Panickal, , und T. Zhou, 2021: *Future Global Climate: Scenario-based Projections and Near-term Information*, 1211–1362. Cambridge University Press, Cambridge, United Kingdom and New York, NY, USA, doi:10.1017/9781009157896.011.

Ludwig, P., E. J. Schaffernicht, Y. Shao, und J. G. Pinto, 2016: Regional atmospheric circulation over Europe during the Last Glacial Maximum and its links to precipitation. *Journal of Geophysical Research: Atmospheres*, **121 (5)**, 2130–2145, doi:10.1002/2015JD024444, URL https://agupubs.onlinelibrary.wiley.com/doi/abs/10.1002/2015JD024444, https://agupubs.onlinelibrary.wiley.com/doi/pdf/10.1002/2015JD024444.

Luetscher, M., R. Boch, H. Sodemann, C. Spötl, H. Cheng, R. L. Edwards, S. Frisia, F. Hof, und W. Müller, 2015: North Atlantic storm track changes during the Last Glacial Maximum recorded by Alpine speleothems. *Nature Communications*, **6**, 2041–1723, doi:10.1038/ncomms7344, URL https://doi.org/10.1038/ncomms7344.

Mecking, J. V. und S. S. Drijfhout, 2023: The decrease in ocean heat transport in response to global warming. *Nature Climate Change*, **13**, 1229 – 1236, URL https://api.semanticscholar.org/CorpusID:264085015.

Menary, M. B., J. Robson, R. P. Allan, B. B. B. Booth, C. Cassou, G. Gastineau, J. Gregory, D. Hodson, C. Jones, J. Mignot, M. Ringer, R. Sutton, L. Wilcox, und R. Zhang, 2020: Aerosol-forced amoc changes in cmip6 historical simulations. *Geophysical Research Letters*, **47 (14)**, e2020GL088 166, doi:https://doi.org/10.1029/2020GL088166, URL https://agupubs.onlinelibrary.wiley.com/doi/abs/10.1029/2020GL088166, e2020GL088166 2020GL088166, https://agupubs.onlinelibrary.wiley.com/doi/pdf/10.1029/2020GL088166.

Menviel, L., J. Yu, F. Joos, A. Mouchet, K. J. Meissner, und M. H. England, 2017: Poorly ventilated deep ocean at the last glacial maximum inferred from carbon isotopes: A data-model comparison study. *Paleoceanography*, **32 (1)**, 2–17, doi:10.1002/2016PA003024, URL https://agupubs.onlinelibrary.wiley.com/doi/abs/10.1002/2016PA003024, https://agupubs.onlinelibrary.wiley.com/doi/pdf/10.1002/2016PA003024.

Menviel, L. C., P. Spence, L. C. Skinner, K. Tachikawa, T. Friedrich, L. Missiaen, und J. Yu, 2020: Enhanced mid-depth southward transport in the northeast atlantic at the last glacial maximum despite a weaker amoc. *Paleoceanography and Paleoclimatology*, **35 (2)**, e2019PA003 793, doi:10.1029/2019PA003793, URL https://agupubs.onlinelibrary.wiley.com/doi/abs/10.1029/2019PA003793, e2019PA003793 10.1029/2019PA003793, https://agupubs.onlinelibrary.wiley.com/doi/pdf/10.1029/2019PA003793.

Michael Böttinger, D. D. K., 2015: URL https://www.dkrz.de/en/communication/climate-simulations/cmip6-en/the-ssp-scenarios?set_language=en.

Michael Mann, B. G., 2015: URL https://www.e-education.psu.edu/meteo469/node/145.

Oueslati, B., P. Yiou, und A. Jézéquel, 2019: Revisiting the dynamic and thermodynamic processes driving the record-breaking January 2014 precipitation in the southern UK. *Scientific Reports*, doi:10.1038/s41598-019-39306-y.

Pascale Braconnot, S. H., 2015: URL https://airtable.com/appYNLuWqAgzLbhSq/shrxlyZ2IeTGEil9Z/tblRtvvOrcEsbketW.

Peltier, W., 2007: Rapid climate change and Arctic Ocean freshening. *Geology*, **35 (12)**, 1147–1148, doi:10.1130/focus122007.1, URL https://doi.org/10.1130/focus122007.1, https://pubs.geoscienceworld.org/gsa/geology/article-pdf/35/12/1147/3533871/i0091-7613-35-12-1147.pdf.

Pinto, J. G. und P. Ludwig, 2020: Extratropical cyclones over the North Atlantic and western Europe during the Last Glacial Maximum and implications for proxy interpretation. *Climate of the Past*, **16 (2)**, 611–626, doi:10.5194/cp-16-611-2020, URL https://cp.copernicus.org/articles/16/611/2020/.

Priestley, M. D. K., D. Ackerley, J. L. Catto, K. I. Hodges, R. E. McDonald, und R. W. Lee, 2020: An Overview of the Extratropical Storm Tracks in CMIP6 Historical Simulations. *Journal of Climate*, **33 (15)**, 6315 – 6343, doi:10.1175/JCLI-D-19-0928.1, URL https://journals.ametsoc.org/view/journals/clim/33/15/JCLI-D-19-0928.1.xml.

R. J. Stouffer, S. M., 2003: Equilibrium response of thermohaline circulation to large changes in atmospheric CO2 concentration. *Climate Dynamics*, **20**, 759–773, doi:10.1007/s00382-002-0302-4, URL https://doi.org/10.1007/s00382-002-0302-4.

Rahmstorf, S., 2003: Thermohaline circulation: The current climate. *Nature*, doi:10.1038/421699a, URL https://doi.org/10.1038/421699a.

———, 2006: Thermohaline Ocean Circulation. *Encyclopedia of Quaternary Sciences*, URL http://www.pik-potsdam.de/$\sim$/Publications/Book$_$chapters/rahmstorf$_$eqs$_$2006.pdf.

Raible, C. C., J. G. Pinto, P. Ludwig, und M. Messmer, 2021: A review of past changes in extratropical cyclones in the northern hemisphere and what can be learned for the future. *WIREs Climate Change*, **12 (1)**, e680, doi:https://doi.org/10.1002/wcc.680, URL https://wires.onlinelibrary.wiley.com/doi/abs/10.1002/wcc.680, https://wires.onlinelibrary.wiley.com/doi/pdf/10.1002/wcc.680.

Repschläger, J., D. Garbe-Schönberg, M. Weinelt, und R. Schneider, 2017: Holocene evolution of the north atlantic subsurface transport. *Climate of the Past*, **13 (4)**, 333–344, doi:10.5194/cp-13-333-2017, URL https://cp.copernicus.org/articles/13/333/2017/.

Repschläger, J., M. Weinelt, H. Kinkel, N. Andersen, D. Garbe-Schönberg, und C. Schwab, 2015: Response of the subtropical north atlantic surface hydrography on deglacial and holocene amoc changes. *Paleoceanography*, **30 (5)**, 456–476, doi:10.1002/2014PA002637, URL https://agupubs.onlinelibrary.wiley.com/doi/abs/10.1002/2014PA002637, https://agupubs.onlinelibrary.wiley.com/doi/pdf/10.1002/2014PA002637.

Routson, C. C., N. P. McKay, D. S. Kaufman, M. P. Erb, H. Goosse, B. N. Shuman, J. R. Rodysill, und T. Ault, 2019: Mid-latitude net precipitation decreased with Arctic warming during the Holocene. *Nature*, **568**, 83 – 87, doi:10.1038/s41586-019-1060-3, URL https://doi.org/10.1038/s41586-019-1060-3.

Schultz, D. M., D. Keyser, und L. F. Bosart, 1998: The Effect of Large-Scale Flow on Low-Level Frontal Structure and Evolution in Midlatitude Cyclones. *Monthly Weather Review*, **126 (7)**, 1767–1791, doi:10.1175/1520-0493(1998)1262.0.CO;2, URL https://journals.ametsoc.org/view/journals/mwre/126/7/1520-0493$_$1998$_$126$_$1767$_$teolsf$_$2.0.co$_$2.xml.

Shi, X. und G. Lohmann, 2016: Simulated response of the mid-holocene atlantic meridional overturning circulation in echam6-fesom/mpiom. *Journal of Geophysical Research: Oceans*, **121 (8)**, 6444–6469, doi:10.1002/2015JC011584, URL https://agupubs.onlinelibrary.wiley.com/doi/abs/10.1002/2015JC011584, https://agupubs.onlinelibrary.wiley.com/doi/pdf/10.1002/2015JC011584.

Shi, X., G. Lohmann, D. Sidorenko, und H. Yang, 2020: Early-holocene simulations using different forcings and resolutions in awi-esm. *The Holocene*, **30 (7)**, 996–1015, doi:10.1177/0959683620908634, URL https://doi.org/10.1177/0959683620908634, https://doi.org/10.1177/0959683620908634.

Society, N. G., October 19, 2023: URL https://education.nationalgeographic.org/resource/atmosphere/.

Society, R. M., 04 August, 2020: URL https://www.rmets.org/metmatters/global-atmospheric-circulation.

Solomon, S., D. Qin, M. Manning, Z. Chen, M. Marquis, K. Averyt, M. Tignor, und H. Miller, 2007: IPCC AR4 WG1 Climate Change 2007: The Physical Science Basis, Contribution of Working Group I to the Fourth Assessment Report of the Intergovernmental Panel on Climate Change. *Cambridge University Press, Cambridge, United Kingdom and New York, NY, USA*, URL https://www.ipcc.ch/report/ar4/wg1/.

Stouffer, R. J., J. Yin, J. M. Gregory, K. W. Dixon, M. J. Spelman, W. Hurlin, A. J. Weaver, M. Eby, G. M. Flato, H. Hasumi, A. Hu, J. H. Jungclaus, I. V. Kamenkovich, A. Levermann, M. Montoya, S. Murakami, S. Nawrath, A. Oka, W. R. Peltier, D. Y. Robitaille, A. Sokolov, G. Vettoretti, und S. L. Weber, 2006: Investigating the Causes of the Response of the Thermohaline Circulation to Past and Future Climate Changes. *Journal of Climate*, **19 (8)**, 1365 – 1387, doi:10.1175/JCLI3689.1, URL https://journals.ametsoc.org/view/journals/clim/19/8/jcli3689.1.xml.

Thomas F. Stocker, A. S., 1997: Influence of CO2 emission rates on the stability of the thermohaline circulation. *Nature*, **388**, 862–865, doi:10.1038/42224, URL https://doi.org/10.1038/42224.

Thornalley, D. J. R., H. Elderfield, und I. N. McCave, 2009: Holocene oscillations in temperature and salinity of the surface subpolar North Atlantic. *Nature*, **457**, 711–714, doi:10.1038/nature07717, URL https://doi.org/10.1038/nature07717.

Tierney, J., August 2020: URL https://www.usgs.gov/media/images/last-glacial-maximum-surface-air-temperature.

Ulbrich, U., G. C. Leckebusch, und J. G. Pinto, 2009: Extra-tropical cyclones in the present and future climate: a review. *Theoretical and Applied Climatology*, **96 (1)**, 117–131, doi:10.1007/s00704-008-0083-8.

Umling, N. E., D. W. Oppo, P. Chen, J. Yu, Z. Liu, M. Yan, G. Gebbie, D. C. Lund, K. R. Pietro, Z. D. Jin, K.-F. Huang, K. B. Costa, und F. A. L. Toledo, 2019: Atlantic Circulation and Ice Sheet Influences on Upper South Atlantic Temperatures During the Last Deglaciation. *Paleoceanography and Paleoclimatology*, **34 (6)**, 990–1005, doi:10.1029/2019PA003558, URL https://agupubs.onlinelibrary.wiley.com/doi/abs/10.1029/2019PA003558, https://agupubs.onlinelibrary.wiley.com/doi/pdf/10.1029/2019PA003558.

Vellinga, M. und R. A. Wood, 2002: Global Climatic Impacts of a Collapse of the Atlantic Thermohaline Circulation. *Climatic Change*, **54**, 251–267, doi:10.1023/A:1016168827653, URL https://doi.org/10.1023/A:1016168827653.

Vellinga, R. A., Michael Wood, 2008: Impacts of thermohaline circulation shutdown in the twenty-first century. *Climatic Change*, **91**, 43–63, doi:10.1007/s10584-006-9146-y, URL https://doi.org/10.1007/s10584-006-9146-y.

Waelbroeck, P. und M. P. Members, 2009: Constraints on the magnitude and patterns of ocean cooling at the Last Glacial Maximum. *Nature Geoscience*, **9**, 127–132, doi:10.1038/NGEO411.

Wang, Z. und L. A. Mysak, 2000: A Simple Coupled Atmosphere–Ocean–Sea Ice–Land Surface Model for Climate and Paleoclimate Studies. *Journal of Climate*, **13 (6)**, 1150–1172, doi:10.1175/1520-0442(2000)0132.0.CO;2, URL https://journals.ametsoc.org/view/journals/clim/13/6/1520-0442$_$2000$_$013$_$1150$_$ascaos$_$2.0.co$_$2.xml.

WCRP, 2015: URL https://wcrp-cmip.github.io/CMIP6_CVs/docs/CMIP6_source_id.html.

Weaver, A., C. Bitz, A. Fanning, und M. Holland, 1999: Thermohaline circulation: High-latitude phenomena and the difference between the Pacific and Atlantic. *Annual Review of Earth and Planetary Sciences - ANNU REV EARTH PLANET SCI*, **27**, doi:10.1146/annurev.earth.27.1.231.

Woollings, T., J. M. Gregory, J. G. Pinto, M. Reyers, und D. J. Brayshaw, 2012: Response of the North Atlantic storm track to climate change shaped by ocean–atmosphere coupling. *Nature Geoscience*, **5**, 313–317, doi:10.1038/ngeo1438, URL https://doi.org/10.1038/ngeo1438.

Wunsch, C., 2002: What Is the Thermohaline Circulation? *Science*, **298 (5596)**, 1179–1181, doi:10.1126/science.1079329, URL https://www.science.org/doi/abs/10.1126/science.1079329.

Yin, J. und R. J. Stouffer, 2007: Comparison of the Stability of the Atlantic Thermohaline Circulation in Two Coupled Atmosphere–Ocean General Circulation Models. *Journal of Climate*, **20 (17)**, 4293–4315, doi:10.1175/JCLI4256.1, URL https://journals.ametsoc.org/view/journals/clim/20/17/jcli4256.1.xml.

Zappa, G., B. J. Hoskins, und T. G. Shepherd, 2015: The dependence of wintertime Mediterranean precipitation on the atmospheric circulation response to climate change. *Environmental Research Letters*, **10 (10)**, 104 012, doi:10.1088/1748-9326/10/10/104012, URL https://dx.doi.org/10.1088/1748-9326/10/10/104012.

Zhang, M., Y. Liu, J. Zhang, und Q. Wen, 2021: Amoc and climate responses to dust reduction and greening of the sahara during the mid-holocene. *Journal of Climate*, **34 (12)**, 4893–4912, doi:10.1175/JCLI-D-20-0628.1, URL https://journals.ametsoc.org/view/journals/clim/34/12/JCLI-D-20-0628.1.xml.

Zhang, M., Y. Liu, J. Zhu, Z. Wang, und Z. Liu, 2022: Impact of dust on climate and amoc during the last glacial maximum simulated by cesm1.2. *Geophysical Research Letters*, **49 (3)**,

e2021GL096 672, doi:10.1029/2021GL096672, URL https://agupubs.onlinelibrary.wiley.com/doi/abs/10.1029/2021GL096672, e2021GL096672 2021GL096672, https://agupubs.onlinelibrary.wiley.com/doi/pdf/10.1029/2021GL096672.

Zhu, J., Z. Liu, X. Zhang, I. Eisenman, und W. Liu, 2014: Linear weakening of the amoc in response to receding glacial ice sheets in ccsm3. *Geophysical Research Letters*, **41 (17)**, 6252–6258, doi:10.1002/2014GL060891, URL https://agupubs.onlinelibrary.wiley.com/doi/abs/10.1002/2014GL060891, https://agupubs.onlinelibrary.wiley.com/doi/pdf/10.1002/2014GL060891.

Acknowledgement

I would, first of all, like to thank Prof. Dr. Joaquim Pinto for allowing me to investigate my favorite oceanic circulation and its link to the atmosphere and for giving me the possibility to deepen my knowledge of these topics. Thank you also for all of your instructions and feedback on the data analysis and the written thesis.

My thanks go as well to Prof. Dr. Andreas Fink, who gave me my first introduction to oceanography and told me about the Thermohaline Circulation, my now favorite oceanic circulation.

Next, I would like to give thanks to Dr. Patrick Ludwig, who especially helped with the paleoclimate parts, but also with the rest of the work. Thank you for your advice to help with the programming and the structure.

I owe a lot of gratitude to Dr. Ting-Chen Chen, who worked intensely with me from the beginning on, gave me extensive and helpful feedback, was always ready to debug my code, and debated scientific practices with me. Thank you for all the time you put into this thesis with your help and your open ears.

I wish also to express my gratitude to Dr. Eleonora Cusinato, who gave me feedback on the written thesis and was a valuable contact person in all ocean questions.

And my final thanks go to my friend who helped to simplify convoluted sentences and improve my grammar.

Thank you all for your help over the past year!

Declaration of Authorship

I hereby declare that the thesis submitted is my own unaided work. All direct or indirect sources used are acknowledged as references. I am aware that the thesis in digital form can be examined for the use of unauthorized aid and to determine wether the thesis as a whole or parts incorporated in it may be deemed as plagiarism.
For the comparison of my work with existing sources I agree that it shall be entered in a database where it shall also remain after examination, to enable comparison with future theses submitted. Further rights of reproduction and usage, however, are not granted here. This paper was not previously presented to another examination board and has not been published.

Karlsruhe, 30.11.2023

Name